UNIVERSITY OF GAZİANTEP

GRADUATE SCHOOL OF

NATURAL & APPLIED SCIENCES

DEVELOPMENT OF NON-INVASIVE DIAGNOSTIC SYSTEM USING INFRARED THERMAL IMAGING FOR DEEP VEIN THROMBOSIS AND RAYNAUD'S PHENOMENON

Ph. D. THESIS

IN

ELECTRICAL AND ELECTRONICS ENGINEERING

BY

SEYDİ KAÇMAZ

SEPTEMBER 2018

DEVELOPMENT OF NON-INVASIVE DIAGNOSTIC SYSTEM USING INFRARED THERMAL IMAGING FOR DEEP VEIN THROMBOSIS AND RAYNAUD'S PHENOMENON

Ph. D. Thesis

in

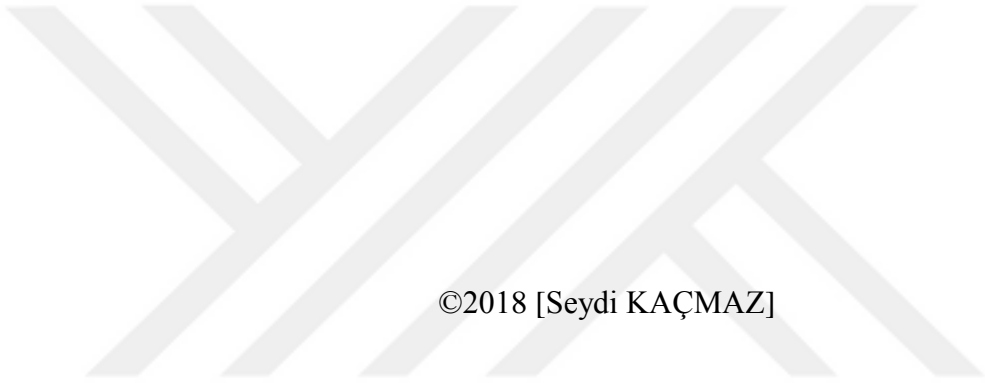**Electrical and Electronics Engineering**

University of Gaziantep

Supervisor
Prof. Dr. Ergun ERÇELEBİ

by

Seydi KAÇMAZ

September 2018

REPUBLIC OF TURKEY
UNIVERSITY OF GAZİANTEP
GRADUATE SCHOOL OF NATURAL & APPLIED SCIENCES
ELECTRICAL AND ELECTRONICS ENGINEERING

Name of the thesis: Development of non-invasive diagnostic system using infrared thermal imaging for deep vein thrombosis and raynaud's phenomenon

Name of the student: Seydi KAÇMAZ

Exam date: 13.09.2018

Approval of the Graduate School of Natural and Applied Sciences

Prof. Dr. A. Necmeddin YAZICI

Director

I certify that this thesis satisfies all the requirements as a thesis for the degree of Doctor of Philosophy.

Prof. Dr. Ergun ERÇELEBİ

Head of Department

This is to certify that we have read this thesis and that in our consensus opinion it is fully adequate, in scope and quality, as a thesis for the degree of Doctor of Philosophy.

Prof. Dr. Ergun ERÇELEBİ

Supervisor

Examining Committee Members: Signature
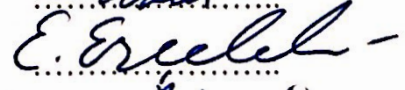
Prof. Dr. İlyas EKER
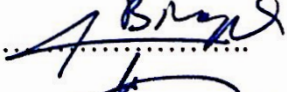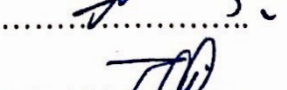
Prof. Dr. Ergun ERÇELEBİ

Assoc. Prof. Dr. Ahmet BİNGÜL

Asst. Prof. Dr. Murat FURAT

Asst. Prof. Dr. Taner İNCE

I hereby declare that all information in this document has been obtained and presented in accordance with academic rules and ethical conduct. I also declare that, as required by these rules and conduct, I have fully cited and referenced all material and results that are not original to this work.

Seydi KAÇMAZ

ABSTRACT

DEVELOPMENT OF NON-INVASIVE DIAGNOSTIC SYSTEM USING INFRARED THERMAL IMAGING FOR DEEP VEIN THROMBOSIS AND RAYNAUD'S PHENOMENON

KAÇMAZ, Seydi

Ph. D. in Electrical and Electronics Engineering

Supervisor: Prof. Dr. Ergun ERÇELEBİ

September 2018

129 pages

With the advent of the new generation of infrared detectors, infrared thermal imaging has become an alternative medical diagnostic tool by providing abnormal temperature pattern measurements. Studies have shown that many diseases are associated with heat. For this reason, examining observable abnormalities in thermograms and monitoring the heat exchange processes of the human body can provide information about the pathology of the underlying diseases. Accordingly, infrared thermal imaging may be useful for the early screening and detection of a wide variety of diseases. However, analysis of the infrared thermal images of the human body has become a difficult problem, due to the nature of the thermal images, the lack of expertise, and the lack of medical infrared thermal imaging databases. In addition, a fully automated system is needed to provide an objective assessment. In this study, automated computer aided softwares are developed for use in Deep Vein Thrombosis and Primary and Secondary Raynaud's diseases. In the first study, it is shown that infrared thermal imaging could be used as a pre-screening test to diagnose Deep Vein Thrombosis. The developed methodology can be used in other diseases that can occur in organs with symmetry in the body other than the disease concerned. In the second study, a method for diagnosis and follow-up of Primary and Secondary Raynaud's disease is proposed. These studies demonstrate the usability of infrared thermal imaging by providing support to medical specialists.

Key Words: Infrared Thermal Imaging, Computer Aided Diagnosis, Deep Vein Thrombosis, Raynaud Phenomenon

ÖZET

DERİN VEN TROMBOZU VE RAYNAUD FENOMENİ İÇİN KIZILÖTESİ TERMAL GÖRÜNTÜLEME KULLANARAK İNVAZİV OLMAYAN TANI SİSTEMİNİN GELİŞTİRİLMESİ

KAÇMAZ, Seydi

Doktora Tezi, Elektrik ve Elektronik Mühendisliği

Tez Yöneticisi: Prof. Dr. Ergun ERÇELEBİ

Eylül 2018

129 sayfa

Yeni nesil kızılötesi dedektörlerin ortaya çıkmasıyla birlikte, kızılötesi termal görüntüleme, anormal sıcaklık deseni ölçümleri sağlayarak alternatif tıbbi bir tanı aracı haline gelmiştir. Yapılan araştırmalarda birçok hastalığın ısı ile ilişkili olduğu gösterilmiştir. Bu nedenle, termogramlarda gözlemlenebilir anormalliklerin incelenmesi ve insan vücudunun ısı değişim süreçlerinin takip edilmesi altta yatan hastalıkların patolojisi hakkında bilgi sağlayabilir. Buna göre kızılötesi termal görüntüleme, tıpta çok çeşitli hastalıkların erken taranması ve saptanması için yararlı olabilir. Ancak insan vücudunun kızılötesi termal görüntülerinin analizi; termal görüntülerin özellikleri, ilgili uzmanın azlığı ve tıbbi kızılötesi termal görüntü veri tabanlarının eksikliğinden dolayı zor bir problem haline gelmiştir. Ayrıca objektif bir değerlendirme sağlamak için tam otomatik bir sisteme gerek duyulmaktadır. Bu çalışmada, Derin Ven Trombozu ile Birincil ve İkincil Raynaud hastalıklarında kullanılmak üzere otomatik bilgisayar destekli yazılım geliştirilmiştir. İlk çalışmada, Derin Ven Trombozu tanısında kızılötesi termal görüntülemenin bir ön tarama testi olarak kullanılabileceği gösterilmiştir. Geliştirilen yöntem yapısı itibariyle ilgili hastalığın dışında vücutta simetrisi bulunan organlarda oluşabilecek diğer hastalıklar içinde kullanılabilecektir. İkinci çalışmada ise Birincil ve İkincil Raynaud hastalığının teşhisi ve takibine yönelik bir yöntem önerilmiştir. Yapılan çalışmalar, tıbbi uzmanlara destek sağlayarak kızılötesi termal görüntülemenin kullanılabilirliğini göstermiştir.

Anahtar Kelimeler: Kızılötesi Termal Görüntüleme, Bilgisayar Destekli Tanı, Derin Ven Trombozu, Raynaud Fenomeni

"To my family"

ACKNOWLEDGEMENTS

TABLE OF CONTENTS

LIST OF FIGURES

LIST OF TABLES

LIST OF SYMBOLS/ABBREVIATIONS

ANS	Autonomic Nervous System
APMs	Active Appearance Models
ART	Adaptive Resonance Theory
AUC	Area Under Curve
BC	Before Chris
CAD	Computer Aided Detection
CAD	Coronary Artery Disease
CDF	Cumulative Distribution Function
CDUSG	Color Doppler Ultrasonography
CLAHE	Contrast Limited Adaptive Histogram Equalization
COM	Co-occurrence Matrix
CT	Computer Tomography
CTS	Computerized Thermographic System
CTS	Carpal Tunnel Syndrome
DVT	Deep Vein Thrombosis
DWT	Discrete Wavelet Transform
EB-USG	Emergency Bedside Ultrasonography
FPA	Focal Plane Array
FTFPs	Facial Thermal Points
GA	Genetic Algorithm
H1N1	Swine Flu
HCS	Healthy Controls
HT	Heart Plant
IEC	International Electrochemical Commission
IR	Infrared
IRT Images	Infrared Thermal Images

ISO	International Organization for Standardization
LoG	Laplacian of Gaussian
MFT	Mean Foot Temperature
MRI	Magnetic Resonance Imaging
MSE	Mean Square Error
NEC	Necrotizing Enterocolitis
OES	Open End Snake
PCA	Principal Component Analysis
PRP	Primary Raynaud's Phenomenon
PTV	Perception Threshold Values
RF	Raynaud's Phenomenon
ROC	Receiver Operator Characteristics
ROI	Region of Interest
R-USG	Radiology Ultrasonography
SAR	Specific Absorption Ratio
SARS	Severe Acute Respiratory Syndrome
SSc	Systemic Sclerosis
STREL	Structuring Element
TIVs	Thermal Intensity Values
TMT	Temporomandibular joint
USG	Ultrasonography

CHAPTER I

1.1. INTRODUCTION

Throughout history, it has been proven that temperature is a very good indicator of health and disease discrimination [1], [2]. Since 400 BC, the temperature has been used for clinical diagnosis in different forms [3]. As a homotherm, a person can maintain his body at a constant temperature, regardless of environmental temperature [4]. The body of the homotherms is divided into two parts as the core temperature and the outer wall temperature [5]. The core temperature is constantly maintained in a narrow range of about 33–42 °C [5]. Regulation of the inner core temperature is one of the most basic features of the normal human body. A few degrees of change in the core temperature are considered a clear indicator of possible disease [4].

Clinical infrared thermography is defined as recording temperature distribution using infrared radiation emitted from the surface of the human body (the skin) [4]. Since the beginning of the first fifty years, many studies have been done on thermal imaging evaluation for various medical applications. The results of these studies are not always favorable to the clinical use of the thermography because of poor protocols, poor quality control, poor training, and often a lack of understanding of the proper role and scope of the thermography [6]. Despite growing skepticism, interest in this technique was high and the development of quantitative infrared thermal imaging techniques helped to overcome many of the initial challenges. Today, medical infrared thermal imaging has been extensively investigated among various applications of oncology and especially breast cancer detection, and many new studies are still being studied [7]. Advances in computerized infrared thermal imaging, dynamic thermography and infrared camera technology now provide adequate means to re-evaluate the value of medical thermography.

The thermoregulation of the human body is influenced by a variety of factors including pathological abnormalities. Thus, recording the temperature distribution of the human body can provide valuable information about the underlying physiological processes that cause these abnormalities. Human skin plays an important role in thermoregulation by dissipating or protecting heat. The skin heat dissipation is essentially radiant and occurs in the infrared portion of the spectrum, allowing the use of infrared detectors to record skin temperature distribution, especially when the whole body core temperature is spread out [1], [8].

Abnormal thermal patterns, which can be easily recognized by infrared imaging, can allow early diagnosis. Thermographic findings are generally correlated with other clinical findings. Although it is often not specific and largely due to environmental factors, there is a range of reasons why this technique has been widely accepted in the medical world. Above all, infrared imaging is a remote, non-contact, non-invasive technique. It is possible to monitor a large area simultaneously and quickly. Also, it is easy and fast to interpret colored thermograms. In addition, this technique only records the natural radiation from skin surfaces and so does not have any harmful radiation effects. Therefore, it is suitable for long-term and continuous use. Finally, infrared imaging is a real- time imaging technique that can monitor dynamic changes in temperature. Because of these advantages, thermography is used as an effective alternative diagnostic tool. Table 1.1 shows contralateral temperature differences in various body parts (left and right sides) in normal individuals [4], [9].

Medical diagnosis is usually a challenging process. As disease symptoms are usually not specific, doctors tend to use a systematic diagnostic method to determine the cause of the disease. This is usually achieved through estimation, screening and testing based on the likelihood of a situation based on medical history or conditions. Many of today's applications involve invasive methods that can take time to obtain a diagnosis, cause discomfort to the patient, and cause complications. As a result, it is preferable to use non-invasive methods to get rid of the undesirable effects of the investigations.

Table 1. 1 Contralateral temperature differences in various body parts (left and right sides) in normal subjects

Body Parts	Average Temperature Difference (℃)
Forehead	0.12
Cheek	0.18
Chest	0.14
Abdomen	0.18
Neck (Posterior)	0.15
Lumber (Back)	0.25
Body Average	0.17
Arm (Biceps)	0.13
Palm	0.23
Thigh (Front)	0.11
Thigh (Rear)	0.15
Foot (Dorsal)	0.30
Average Fingertips	0.38
Average Foot Toe-Fingertips	0.50

1.2. THESIS AIMS AND OBJECTIVES

Infrared (IR) thermal imaging is widely used in a broad applications ranging from military applications to noninvasive diagnosis. As clinical imaging method, some clinical applications were first used between 1960 and 1980. Among the various clinical applications, early literature has reported promising results in pain assessment, breast cancer and rheumatoid arthritis cases [10]–[12]. Other studies point to some limitations of the technique for clinical purposes [13], [14]. Indeed, until recently, a number of topics have been identified that prevent the widespread use of IR imaging for medical applications: limitations of modalities, technological constraints of previous systems (size and weight, cooling requirements), subjective interpretation of thermograms, lack of precision and cost of IR systems. However, thanks to the technological developments and standardized protocols in IR imaging technology, it has led to a new trend in technology for medical applications.

On the other hand, the problem of interpreting IR images is still ongoing. Analysis of thermograms is still made visually by a clinical expert trained in thermography. The interpretation of the thermograms is based on the ability to distinguish subtle temperature changes and to identify typical patterns associated with a particular pathology or physiological problem. The ability to detect these changes in a gray level image, where each gray level corresponds to a temperature or a temperature range, is not very good. The ability to detect these changes in a gray level image, where each gray level corresponds to a temperature or a temperature range, is not very good. The use of Pseudocolours is not a good alternative because of the psychological effects of hot and cold colors [15]. A quantitative assessment of thermograms is the only way to achieve the most accurate assessment, exceeding the nature of the current evaluation method. At present, quantitative assessment consists of manual identification of potential areas of interest, identification of hot and cold spots, simple asymmetry analysis with statistics from the first order, and subtraction of images in a series [16].

Several attempts have been proposed in the literature to quantify the analysis of thermal images. However, no general strategy has been proposed to address the clinical infrared imaging features. In addition, some of the important building blocks of the automatic abnormality detection architecture for clinical IR imaging are still missing.

IR thermal imaging indirectly aggregates the surface temperature distribution of an object. For this reason, it depends not only on the object temperature, but also on the surface properties, the surface direction, the wavelength used, and the environmental conditions that can affect the collection of IR radiation in general. This typically results in a narrow density range and sometimes a strong overlap of the temperature distribution between the object and the background. In addition, IR thermal imaging tends to produce uniform image regions and no color information is available; this limits or prevents the use of tissue or color based segmentation techniques. Even segmentation of simple regions in an IR image can be difficult, for example, in the case of segmentation of cold extremities (hands and feet). Segmentation techniques developed for other imaging modalities or other IR applications typically do not work well when applied to IR images of the human body. Several automatic segmentation approaches have been proposed that work well with this modality. Proper evaluation of anomalies in IR images of the human body requires a robust segmentation approach.

The identification of potentially abnormal regions of the IR image of the human body may be attempted blindly if no information is available in advance about the problem at hand. However, if a specific clinical context is known, more focused research can be done by looking for specific anatomical structures or physiologically active regions. IR thermal images tend to be smooth and lack general texture and color information. Temperature changes in an object or body region are usually not indicative of structural regions such as bones in the X-rays or white matter for brain in the Magnetic Resonance Imaging (MRI). As a result, anatomical information is difficult to remove. This thesis suggests a new approach to the extraction of anatomical regions based on the detection of anatomical regions.

In this thesis, the two main aspects of digital processing of thermographic images are discussed, and the general purpose perspective such as automation and computerization of thermal images as much as possible in order to facilitate the physician's task is taken into consideration.

A general framework is proposed for the automatic detection of anomalies in clinical infrared images. Basically, two main problems are addressed: the separation of the main object from the background and the acquisition of the potentially abnormal region. The first step will involve preprocessing the thermal images to reduce the noise that occurs during the initial acquisition and storage of the images. In addition, for an optimal selection of regions of interest (ROI), removal of the unrelated background for subsequent analysis will be performed. And the second goal will be to identify areas of interest for thermal analysis of images.

In conclusion, examining the anomalies in the thermograms and monitoring the heat exchange processes of the human body provide important information about the pathology of the underlying diseases [17], [18]. Therefore, it is necessary to develop computer-aided diagnostic systems that automatically interpret thermograms for early detection of abnormalities by removing the subjectivity of human interpretation.

1.3. THESIS OUTLINE

This study is covered in seven chapters. The first chapter is evaluated as the introductory part, started with a preliminary presentation and continued with the aim and objectives of the thesis. In the second chapter, the basis of the infrared imaging is explained, then in the field of medicine infrared thermal imaging examples are given, followed by the data processing methods in the literature for the medical thermograms and finally the standard protocol used in the thermography is discussed.

An overview of the remaining chapters is as follows. In the third chapter, thermal image processing methodology is explained in detail. In this section, the methods used in this thesis are handled one by one. Then, in the fourth chapter, how infrared thermal imaging can be used to diagnose Deep Vein Thrombosis is explained and experimental results are shown. In the fifth chapter, thermal imaging system design for diagnosis and follow-up of the primary and secondary Raynaud Phenomenon is presented, but only the method and an example are given because the system was not tested on the patients. At the sixth chapter, a general summary of the thesis is explained and the way for future studies is discussed. In the seventh chapter, references to all publications mentioned in the thesis are shown.

CHAPTER II

2.1. INFRARED IMAGING

Thermography allows the non-contact measurement of the temperature of an object to be viewed and recorded. Thermal imaging was originally designed for military purposes in the 1950's, especially for night vision [19]. It was then used not only for night vision but also for military vehicle drivers to acquire targets, surveillance, target search and monitoring by increasing their visibility under smoke, dust, light fog and rain. However, thanks to technological developments and improvements in thermal imaging systems, over the last 60 years thermal imaging applications have been extended to engineering applications in a wide range of industries including building inspection, electrical and mechanical automation, petrochemical industries, veterinary medicine and medicine. In general, thermal imaging applications can be divided into four main categories: predictive maintenance, condition monitoring, problem diagnosis, research and development.

In IR thermal imaging, a thermal camera system converts IR radiation (approximately 0.9 μm to 14 μm in wavelength) into a visual image of thermal variation [19]. All objects at the temperature above the absolute zero emit IR radiation, and the amount of radiation emitted increases with temperature.

An IR camera system is designed very similar to a digital video camera system (Figure 2.1). It consists of a lens that focuses on focal plane array (FPA) camera detector, and electronics and software for processing and displaying signals and images. The FPA's resolution can range from about 160 × 120 pixels to 1024 × 1024 pixels.
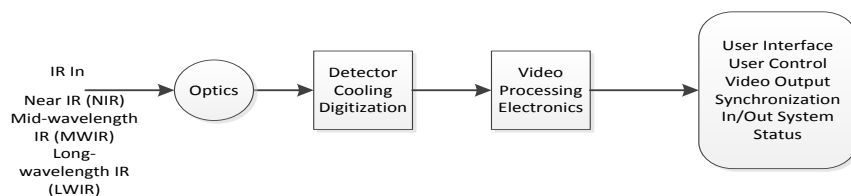
Figure 2. 1 Simplified block diagram of an IR camera system **[19]**

All objects on the absolute zero temperature (-273.15 °C) emit energy into their surroundings in the form of electromagnetic waves [20]. This natural process is known as thermal radiation. The amount of energy emitted by an object depends on the temperature of the object, the distribution of the radiation wave length, the surface area, and the type of surface [19], [21]. An ideal object called a perfect black body does not reflect or transmit radiation from the surface or from the body. It absorbs 100% of incoming radiation, which makes it a perfect absorbent.

The radial properties of a material are expressed by emissivity, ε. The global emissivity of a body is the ratio of the energy emitted by an isothermally emissive body over the energy emitted by a black body at the same temperature. It is a measure of the ability of the body to radiate the energy it absorbs. The perfect black body is the perfect radiator, so the value of the emissive is 1 [22]. The emission at frequency v, ε_v, is defined at similar intervals by considering radiation with frequencies in the range $[v, v + dv]$. In the thermal balance, the emitted energy must be balanced by the energy absorbed by the body periphery [4]. Kirchhoff's law states that for any uniform environment in the thermal equilibrium, the emissivity and absorption coefficient for any spectral range is equal to the ratio of the body's surface emissive power over emissive power a black body. This relationship helps to define the emissivity (ε_v) of a body [4] as

$$\varepsilon_v = \frac{E_v}{E_{bv}} \tag{2.1}$$

where E_v is the body's surface emissive power at frequency v, E_{bv} is the emissive power of a black body at frequency v, and ε_v measures the fraction of the incident radiation absorbed per unit time by a thin layer of unit thickness at the same frequency. Therefore, the emissivity, ε_v, is a number between 0 and 1. The higher the emissivity of the object means the better the radiation properties.

Planck's black body law defines the properties of an object's radiation, in terms of spectral radiant emission. The spectral radiant emitter is also known as the emission power. As a function of the wavelength, Planck's law is written as [23]–[25].

$$E_\lambda = \varepsilon_\lambda \frac{2\pi hc^2}{\lambda^5} \left[\exp\left(\frac{hc}{\lambda kT} \right) - 1 \right]^{-1} \tag{2.2}$$

or in terms of the number of emitted photons as

$$P_\lambda = \varepsilon_\lambda \frac{2\pi c}{\lambda^4} \left[\exp\left(\frac{hc}{\lambda kT}\right) - 1 \right]^{-1} \tag{2.3}$$

where

h (Planck's constant) = 6.6261×10^{-34} J s, c (speed of light) = 2.9979×10^8 ms^{-1}, k (Boltzmann's constant) = 1.3807×10^{-23} WsK^{-1}, λ = wavelength in μm, T = temperature in degrees Kelvin (K), ε_λ = the emissivity of the surface at a given wavelength, E_λ = spectral radiant emittance/emissive power per unit wavelength and unit area [$Wcm^{-2}\mu m^{-1}$].

Planck's equation describes the spectral properties of the source as a function of wavelength. The wavelength at which E_λ is maximized shifts to shorter wavelengths as the temperature of the object of interest increases. This peak wavelength is explained by Wien's displacement law [24].

$$\lambda_{max} T = 0.002898 \tag{2.4}$$

where λ_{max} is the wavelength of maximum emissive power (in meters) at temperature T (in degrees Kelvin). In accordance with Wien's displacement law, the emission power of a black body is exponentially reduced with temperature, and the wavelength at maximum emission power passes to longer wavelengths at lower temperatures [4] as shown in Figure 2.2. Since the black body is a perfect absorber and emitter, it shows that a black body absorbs and emits the maximum theoretically possible energy at a given temperature. The amount of radiation emitted by a black body, E_b, is proportional to the fourth power of the thermodynamic temperature (also called the absolute temperature, T, in Kelvin), as described by Stefan-Boltzmann's law [4], [20]

$$E_b = \sigma T^4 \tag{2.5}$$

where σ (the Stefan-Boltzmann constant) is 5.669×10^{-8} Wm^{-2} K^{-4}. The total emissive power from a black body, E_b (in Wm^{-2}) can also be obtained by integrating Planck's function over all wavelengths (from 0 to ∞) [26]. A grey body is an object that has a constant value for its emissivity for all wavelengths [19]. For a grey body, the total emissive power, E_g, defined by the Stefan-Boltzmann law, takes the form

$$E_g = \sigma T^4 \qquad\qquad (2.6)$$

which indicates that the total emissive power of a grey body, E_g, is the same as that of a black body, E_b, of the same temperature, reduced in proportion to the value of ε of the object [19]. However, most bodies are not black bodies or gray bodies, but more selectively radiators. A selective radiator is an object with strongly varying emissivity with wavelength. However, it is generally possible to treat objects as gray bodies as long as the thermography works only within limited spectral ranges.
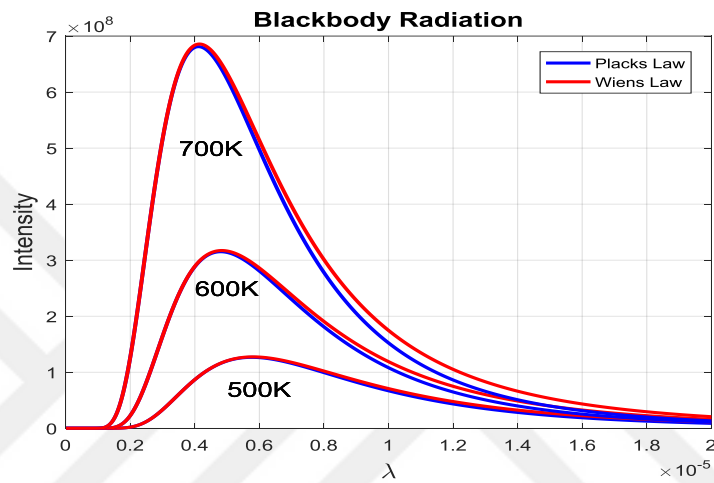
Figure 2. 2 Blackbody Radiation Spectrum from Wien's Law and Planck's law

The IR radiation emitted by human skin is mainly in the 2 - 20 μm wavelength and has an average peak at 9 - 10 μm. With Planck's equation and the implementation of Wien's Law, it was found that approximately 90% of the radiation emitted by humans is at longer wavelengths (6-14 μm) [18]. Also, there is no difference in emissivity of black, white and burnt skin. For this reason, the temperature distribution or measurements of the heat setting recorded on an IR thermograms come from the outer surface layer of the skin and are independent of the race [27].

For this reason, it is useful to use thermal imaging to investigate the underlying physiological changes associated with many diseases, such as inflammatory diseases, complex regional pain syndrome, and Raynaud's phenomenon. Thermal imaging allows objective measurement of temperature changes that are clinically important in some medical applications. With the critical use of technology and an accurate understanding of thermal physiology, thermal imaging can be a reliable and accepted diagnostic tool in medicine [28].

2.2. INFRARED THERMAL IMAGING IN MEDICINE

Abnormal thermal patterns, which can be easily recognized by infrared imaging, allow early diagnosis. Thermographic findings are generally correlated with other clinical findings. There is a range of reasons why this technique is widely accepted in the medical world, although it is often not specific and largely due to environmental factors. Above all, infrared imaging is a remote, non-contact, and non-invasive technique. It is possible to monitor a large area simultaneously and quickly. It is often easy and fast to interpret colored thermograms. In addition, this technique only records the natural radiation from skin surfaces and does not have any harmful effects. Therefore, it is suitable for long-term and continuous use. Finally, infrared imaging is a real-time imaging technique that can monitor dynamic changes in temperature. Because of these advantages, thermography is an effective alternative diagnostic tool.

2.2.1. Thermoregulation Studies

Muscle functioning during metabolism or exercise is a major source of body heat [4]. The resulting heat is transferred internally through the blood flow from the veins towards the outer surfaces. Blood picks up heat from the body and loses from the peripheral regions, especially the skin. This process is called thermoregulation. Surface temperature distribution is governed by a number of factors such as blood flow near the surface, heat conduction of deep blood vessels, and evaporation through the skin [29]. Thermography is an effective tool for monitoring thermoregulation processes. Gulyaev and colleagues found that in the majority of healthy individuals; observed an increase in temperature in hands, feet and face areas at rest [29]. Immobility is often accompanied by relaxation and redistribution of blood, thus increasing the temperature of the skin surface. It is also observed that the changes in the sympathetic system and the blood flow lead to temperature fluctuations in the hands and feet. Short-term fluctuations are associated with the capillaries, while long-term changes are due to the arteriovenous anastomosis. In the Vainer study, infrared imaging in short wavelength (about 3 μm) is used to study the skin sweating procedure [30]. In this study, it was found that the low temperature regions surrounded by the secretory channels of each sweat gland are asymmetric. In addition, studies have been carried out on the effect of central nervous system and the local superficial localization of hypertension resulting from metabolic or environmental overheating. On top of that,

it has started an important debate on the connection of sweating and thermoregulation system. Bouzida et al. has proposed two approaches as thermoregulation mechanism, blood flow modulation and cold stress [5]. In the first approach, blood pressure (systolic and diastolic values) are modulated with a suitable mechanical design, revealing a periodic change in temperature due to changes in blood volume in blood vessels. In the second approach, the left hand was placed on a cold metal surface and observed with infrared imaging of the temperature changes of the two hands after exposure to cold stress. When waited for a long time, it was seen that the temperature of the stimulated hand decreased while the temperature of the other hand increased. This is attributed to the response of the thermoregulation mechanism to the body heat to remain unchanged. Kargel observed warming of ear regions of subjects using different mobile phones [31]. Accordingly, it has been determined that mobile phones having a high specific absorption ratio (SAR) cause more temperature increase. It has been reported that the maximum temperature increase is towards the end of the talk and the warm-up time is increased by the speech duration [32].

2.2.2. Breast cancer detection

Breast cancer constitutes about 30% of all cancer cases, with cancer being the most common cancer in women [33]. Between 2003 and 2007, the mean age of death for breast cancer was 68 years. The mortality rates for 20 age groups below 20, 20-34, 35-44, 45-54, 55-64, 65-74, 75-84 and 85 in various age groups were approximately 0.0%, 0.9%, 6.0%, 15.0% 20.8%, 19.7%, 22.6% and 15.1%, respectively [34]. Diagnosis was not possible in the age group below 20 years, while it was 1.9%, 10.2%, 22.6%, 24.4%, 19.7%, 5.5% and 5.6%, respectively, in the other age groups [34]. Studies show that early diagnosis increases survival rate by 85%, while late diagnosis provides only a 10% survival [35]. For this reason, early diagnosis is an important factor for successful breast cancer treatment. In 1982, the US Food and Drug Administration (FDA) approved thermography as an aid to breast cancer diagnosis. Kennedy et al., in their study of thermography and other imaging techniques used in breast cancer, concluded that thermography could provide additional functional information about the thermal and vascular status of tissues [36]. Ng has provided an excellent review detailing the basic methodology, standard applications, image acquisition and analysis of thermography as a non-invasive breast tumor detection method [18]. He described the

abnormal breast thermogram as indicating a significant biological risk. Tumors have generally been shown to increase blood flow, resulting in increased metabolic rate and localized high temperature points that can be seen with infrared imaging. Apart from passive breast imaging, cold stimulus based imaging methods are practically applied [37]. Blood vessels produced by cancerous tumors are composed of simple endothelial tubes lacking a muscle layer. Such blood vessels fail to constrict in response to sympathetic impulses, such as sudden cold stress, and exhibit a hyperthermic pattern due to vasodilation. Deng and Liu have shown that tumors under the skin enhance thermographic contrast with induced sweating [38]. They sprayed the skin surface with water and 75% medical ethanol solution, then took the thermal images of the evaporating area and performed their work. This study has increased the accuracy of early diagnosis of tumors, especially those located farther from the surface. Spitalier et al. received thermographic images of 61,000 women and showed that 60% of breast cancer cases can be detected using early-stage thermography in their 10-year-long study [39]. In addition, they confirmed that abnormal temperature patterns in infrared images are the highest predictors of breast cancer risk in the future [40]. Gamagami studies on angiogenesis with thermography have shown that 15% of the cases, which can not be detected by mammography, can be detected by thermography [41]. Again, hypervascularity and hyperthermia have shown that apparent breast cancer can be seen in 86% of cases. Head et al. reported that prognostic markers of growth rate strongly correlated with thermograms [42]. He reports that thermovascular changes in the breasts are directly related to prognosis and aggression of the tumor. And hot cancer sites (the most active cancer cells) showed a low prognosis with a survival rate of 24% within 3 years, whereas cold cancer sites had a relatively better prognosis with a survival rate of 80% within 3 years [37]. Aweda et al. found that the average oxygen consumption and average metabolic heat output of the control group were higher than those of the breast, head, neck, cervical and other cancer groups [43].

There are many other techniques such as Mammography, MRI, CT, and Ultrasound in the detection of breast cancer separately from thermography. Among them, mammography is the most popular technique, but it contains some inherent problems such as exposure to X-ray radiation, relatively higher cost, difficulty in detecting small sized tumors in early stages, and low sensitivity due to chest structure in young ladies. Thermography has become a relatively new imaging tool in breast cancer research,

where such problems have not been experienced. According to Arora et al., Infrared imaging appears to be an effective alternative diagnosis in patients with particularly dense breast parenchyma [44].

In another typical study demonstrating the efficacy of thermography in early breast cancer detection, a lump was detected in the right chest of a female patient with a negative mammography report [45]. However, it is found that the lump region is at a higher temperature than normal tissues by using thermography. After the tests, the results of the biopsy confirmed that the skin was cancerous.

2.2.3. Diagnosis of diabetic neuropathy and vascular disorders

Almost half of diabetic patients are hospitalized because of the most common foot complications [46]. The main causes of such foot complications are reduced blood volume (vascular malfunction) and loss of sensation (neuropathy). A review of the role of infrared imaging in diabetic foot complications was performed by Bharara et al. [47]. Vascular disorders and diabetic neuropathy cause changes in skin surface temperature, making thermography an appropriate tool for diagnosis. Jiang et al. analyzed metabolic parameters of diabetic patients using thermography [48]. Branemark et al. working with a number of patients on diabetes subjects, they determined that all of them had abnormal heat patterns on their hands and feet (such as reduced heat in the hands, toes, and footbath areas) [49]. Sun et al. examined the relationship between foot floor skin temperature and sympathetic dysfunction in diabetic risky feet [50]. They found that mean foot temperatures were significantly higher in subjects with diabetic risk (30.2 ± 1.3 ºC) than subjects with normal subjects (26.8 ± 1.8 ºC). Their studies have indicated that the sweating disorder that occurs in the first stages of sympathetic disturbances in diabetic feet can be detected by thermography. Bagavathiappan et al. studied randomly selected type 2 diabetes patients and persons with no foot problems [51]. Those patients whose vibration perception threshold values (PTV) were over 20 were found to have a higher mean foot temperature (MFT). Neuropathic patients have higher MFT values than non-neuropathic patients, whereas PTV values correlate positively with right and left toes. Armstrong and colleagues have compared skin temperature in asymptomatic peripheral sensor neuropathy, neuropathic ulcers, and Charcots' arthropathies by

taking the opposite limb as control [52]. In subjects with asymptomatic peripheral sensor neuropathy, Charcots reported that there was a significant difference in people with arthropathy and neuropathic ulcer at these temperatures, although the contralateral parts of the feet did not have a significant temperature difference in skin temperatures.

One of the complications of diabetes in the early stages of arteriosclerosis obliterans is peripheral circulation. Hosaki et al. have investigated peripheral circulation in diabetic patients with infrared imaging [53]. In accordance with clinical findings, they observed that heat distributions were shaped according to abnormal blood flow in the affected areas.

Bagavathiappan et al. found that diabetic patients with vascular disease were more affected by affected area temperatures than unaffected areas [7], [54], [55].This abnormal temperature increase is based on slow blood circulation in the affected areas [54].

2.2.4. Fever Screening

Nguyen et al. have performed general fever screening over face and neck region thermograms using infrared thermal imaging [56]. The sensitivity of the thermal imaging method is similar to that of previously reported cases of fever. In this respect, it was concluded that the thermography was an effective tool for rapid, contactless and mass scanning of fever screening. Chamberlain et al. used thermometer-based infrared emission at various age groups for normal ear temperature determination [57]. Infrared imaging-based techniques, which can be used in epidemics such as severe acute respiratory syndrome (SARS) and avian influenza, have opened the way for mass use in fever screening [58]–[62]. In a recent study, for example, thermography was successfully used in mass screening in SARS patients, where highly contagious corona viruses were caused [63]. Chiang et al. reported similarly that the monitoring of potential patients was essential to prevent the spread of SARS [64]. Ng has studied the effectiveness of infrared imaging in fever mass screening [65]. In this work, he concluded that high body temperature is one of the most common syndromes common in many infectious diseases. Therefore, he argued that thermography is a powerful tool

for public health crises. Nishiura and Kamiya used infrared imaging to scan passengers entering Narita international airport in Japan during the swine flu (H1N1) outbreak in 2009 [66]. Bitar et al. has provided a detailed literature review on the potential use and effectiveness of the thermography during epidemics [67].

Ring et al. conducted studies on infrared imaging in detecting fever in children with the highest risk group [68]. They found that the underarm temperature (measured by a conventional thermometer) and the inner edge temperatures of the eyes (measured by infrared) are interrelated. In other studies, the temperature above 37.5 ºC ± 0.5 ºC was considered to be a possible indicator of fever. Diseases such as SARS, influenza, swine flu and tuberculosis are considered global threats and are thought to be the most effective way to screen fever to control the spread of these diseases. For this reason, a joint working group has been established by the International Organization for Standardization (ISO). In addition, the International Electrochemical Commission (IEC) has been established for the installation of thermography systems, the selection of thermal imaging systems, human temperature measurement and the development of procedural recommendations in international standards [58], [69]–[71]. Standards ISO (ISO / TR 13154: 2009) and SPRING (TR 15-1: Requirements and test methods and TR 15-2: Users' application guidelines) are recommended for reliable and repeatable infrared imaging in mass fever monitoring [72]–[74]

2.2.5. Dental diagnosis

Infrared imaging is widely used in dentistry [75]. In 1996, Gratt et al. developed a new classification system using chronic orofacial pain patient thermograms [76]. The thermograms are classified as normal (0-0.25 ºC), hot (0.35 over) and cold (0.35 below) according to the temperature difference values in the right and left anatomical regions. Cold thermograms have been reported to have a clinical diagnosis of peripheral nerve-induced pain or sympathetic nervous system-related pain, while hot thermograms have a clinical diagnosis of sympathetic nervous system pain, peripheral nerve-induced pain, temporomandibular joint (TMJ) arthropathy or sinusitis. Normal thermograms can be used to diagnose fracture dental syndrome, trigeminal neuralgia, pretrigeminal neuralgia, or psychogenic facial pain. This new method has been confirmed in 92% of cases. While asymptomatic TMJ patients exhibit thermal

symmetry with a mean of 0.1 ºC, patients with TMJ pain have an average of 0.4 ºC asymmetric thermal patterns [77], [78]. Canavan et al. reported that the mild to moderate temporomandibular joint disorder (TMJ) patients were associated with pain levels of right and left thermal differences [79]. Gratt et al. reported that infrared imaging of the chin is an effective method for diagnosing inferior alveolar nerve impairment [80].

2.2.6. Dermatological applications

Skin diseases generally begin with abnormal temperatures on the skin surface and then turn red. For this reason, infrared imaging can be considered a suitable technique for the investigation of skin diseases. Thermography has been used in the diagnosis of leprosy cases, and it has been reported that cold areas such as ear and nose edges are heavily affected [81], [82]. Vargas et al. developed a normalized thermography methodology (ratio of the measured mean temperature to the reference temperature) to diagnose the leprosy in a 50-year-old male patient with a 20-year hepatitis-C history [83]. Patients who were followed for 587 days could see the efficacy of the leprosy treatment only after 182 days, but could be detected after 87 days by thermal images. Benko et al. investigated the thermal effects of exposure to beta radiation using infrared images [84]. It has been observed that the average temperature of the area exposed to beta radiation is immediately increased.

Thomas et al. have demonstrated the use of thermography in laser-based skin treatments such as vascular lesions and epilation [85]. Mason et al. concluded that thermographic findings would be more accurate than clinical findings in evaluating the depth of burn injuries [86]. Cole et al. reported that infrared imaging would be helpful in selecting patients with early surgical need [87]. Schnell and Zaspel used thermography for cooling management of large burns [88]. Mercer et al. have used infrared imaging to monitor wound healing of patients with chronic venous stasis ulcers [89]. Weerd et al. indirectly monitored the skin blood perfusion thermography in preoperative planning and post-operative monitoring of autologous breast reconstruction [90]. Recently Flores-Sahagun et al. used thermography in the analysis and identification of basal cell carcinoma, the most common skin cancer malignancy

[91]. Costello et al. used infrared imaging to assess patients' skin temperature reduction following cryotherapy [92].

2.2.7. Blood Pressure Monitoring

Arterial blood pressure and related thermograms in hypertensive patients separated in two groups were obtained from Cesaris et al. [93]. The first group was treated with a combination of atenolol and chlorthalidone and the other group was treated with a combination of labetalol and chlorthalidone. Before the treatment, the hands of the subjects were monitored using thermography in both groups. There was no change in peripheral vascular flow in the first group after 1 month of treatment, but significant improvement in vascular flow in the second group.

2.2.8. Diagnosis of Rheumatic Diseases

Thermography has been successfully used to assess Raynaud's phenomenon [94]–[97], gout [98], and arthritis [10], [99] and post-treatment healing. Arnold et al. reported that infrared imaging is an excellent technique for measuring skin temperature in different joints [100]. Ring has shown that joints exhibit anomalous temperature distribution in patients with rheumatoid arthritis, juvenile arthritis, osteoarthritis, gout [101]. Collins et al. developed a thermography-based index to measure the degree of joint inflammation [10]. Ring et al. have demonstrated the use of thermography to measure the effects of non-steroidal anti-inflammatory drugs (aspirin, indomethacin and benorilate) on rheumatoid arthritis and gout. Based on their own work, they concluded that infrared imaging is a suitable tool for assessing the response of anti-inflammatory treatment. Paterson et al. used thermography to evaluate rheumatoid inflammation of the knee joint during anti-inflammatory steroid therapy. Frize et al. used thermography for the diagnosis of rheumatoid arthritis and found that metacarpal phalangeal joints, middle fingers, and knee joints were the most suitable locations [102]. Wu et al. reported that local skin temperature around the coccygeal region of coccidiosis patients significantly decreased after conservative treatment [103]. Their work has resulted in the use of thermography as an effective tool for assessing pain severity after coxsychiatric treatment. Park et al. reported the efficacy of infrared thermal imaging in patients with shoulder impingement syndrome [104]. The thermographic results

were compared with other clinical findings and it was found that decreasing movement limitation and hypothermic temperature distribution were related to each other. Inactivity in the shoulders causes localized muscle atrophy resulting in reduced blood flow to the capillaries. This results in hypothermic patterns [105]. Vecchio et al. observed abnormal temperature distribution in most patients with unilateral motionless shoulder complaints [106]. Jeracitano et al. have shown that cases with frozen shoulder syndrome show abnormal temperature [107]. Thomas et al. examined the unilateral and bilateral tennis elbow cases using thermography and found hot spots in unilateral with 94% and bilateral cases with 100% [108].

2.2.9. Diagnosis of Dry Eye Syndrome and Ocular Diseases

Morgan et al. recorded thermograms of normal subjects with dry eye syndrome using infrared thermography [109]. According to the results of the thermograms, ocular surface temperatures were found to be 32.38 ± 0.69 ºC in patients with dry eye syndrome and 31.94 ± 0.54 ºC in healthy volunteers. Tan et al. examined manual, semi-automated, and fully automated methods using thermography to determine eye surface temperatures [3], [110]. Chang et al. used infrared imaging for the diagnosis of inflammatory status of Graves' ophthalmopathic patients [111]. For people with Graves' ophthalmopathy, the temperature differences between the reference point and other regions are significantly higher than the control group. It has also been found that thermography is very useful for investigating the effects of methylprednisolone pulse therapy. Brunsmann et al. laser cornea used infrared imaging to evaluate the thermal load during refractive surgery [112]. Ng et al. suggest that increased eye temperatures may be a possible sign of fever [113].

2.2.10. Diagnosis of Liver Diseases

Mansfield et al. have used thermography to detect liver metastases that cause abnormal temperature patterns on the skin surface [114]. Knobel et al. have used infrared imaging to examine the relationship between body temperature and necrotizing enterocolitis (NEC) in premature newborn infants in the incubator [115]. The mean abdomen-breast temperature difference was more prevalent in premature infants with NEC disease. Milonov et al. have used thermography with electrothermometry in

persons with parasitic liver disease [116]. In this study, (unilocular echinococcosis caused by Echinococcus granulosus) unilocular hydatid disease and multilocular cyst hydatic (multilocular echinococcosis caused by Echinococcus multilocularis) were detected. Their work shows that thermography is a tool for detecting pus cysts. Bhatia et al. found an abnormality in abdominal thermograms of 96% in a study of thermograms of infants and children with acute and chronic liver disease [117].

2.2.11. Kidney Treatment

In various studies it has been shown that infrared imaging allows real-time imaging of flow distribution of hemofiltration [118]. Kopsa et al. have concluded that thermographic evaluation may be complementary in the diagnosis of pathologic intrarenal or perirenal disorders in patients with renal transplantation and in assessing graft function [119]. Oosterlinck and De have reported that the thermography can be used to detect different arterial sites in the kidney, which may help at least remove avascular nephrotic fields without damaging bleeding and kidney tissue [120].

2.2.12. Heart Operations

Manginas et al. have studied the applicability of thermography in patients with coronary artery disease (CAD) or with heart transplant (HT) [121]. Sixteen patients with CAD in the study were evaluated with thermography with 19 patients with heart transplantation and 6 patients without structural heart disease (control). When the right and left ventricular temperatures were compared, there was a significantly higher temperature difference between subjects with CAD (0.19 ± 0.11 ºC), those with HT (0.10 ± 0.06 ºC) and those with control group (0.07 ± 0.04 ºC). In addition, thermography is able to detect early signs of atherosclerosis and it is possible to use heart attack as an early indicator [122]. Infrared imaging is used as an additional imaging technique in a number of heart operations [123]. Madjid et al. have used intracoronary thermography to detect high-risk sensitive plaques [124].

2.2.13. Gynecology

Thermography is also used extensively in the field of gynecology [125], [126]. Birnbaum and Kliot found that the increase in the number and size of blood vessels during pregnancy and the increase in uterine volume can be detected by thermography [127]. Menczer and Eskin performed thermography experiments involving monitoring breast nipples, nipple and upper parts of pregnants for four weeks before and after birth [128]. Women with postpartum aches were reported to have higher breast temperatures than those without pain.

2.2.14. Personality Tests and Brain Imaging

Gulyaev et al. observed that the personality and psychological state of the subjects affected thermographic patterns [29]. According to them, temperature distributions vary depending on the level of stress, concentration and psychological activities. Shevelev has developed a new method called thermoencephaloscopy for thermal imaging of the brain cortex [129]. Neural activity is considered as the primary mechanism by which local metabolism and local cerebral blood flow lead to temperature changes. This technique reveals the active (hot) and inactive (cold) regions of the cerebral cortex. It has also been observed that this technique can detect the activation sequences of certain cortical regions. Studies show that 0.5-2.0 $^{\circ}$C is higher than normal tissues around glial brain tumors [130].

2.2.15. Results

With the development of new generation infrared detectors, infrared thermal imaging becomes a better alternative diagnostic tool due to the extraction of abnormal temperature thermograms. In addition to better temperature accuracy, high-resolution two-dimensional image acquisition and contactless measurement, thermography is absolutely innocuous imaging. Thermal images can be stored digitally and thermograms can be interpreted in more detail using various software packages. Interpretation of thermograms that can be converted into colors is relatively easy and fast. When working up to today, thermography has been successfully used in diseases such as breast cancer, diabetes, dentistry, diabetic neuropathy, and so on. Over the years the use in medical literature is likely to increase even more.

2.3. DATA PROCESSING METHODS FOR MEDICAL THERMOGRAMS

In medical thermal data analysis, two main approaches have been used in various studies; one is physical model based approach and the other is image processing based approach. The physical model based approach includes the anatomy and geometry of the skin tissue structure, the blood vessels, the heat exchange processes in the body. This method is used to determine the location and depth of the heat source, to find the thermal parameters for skin identification, and so on. It has also been used in some studies to calculate physiological information such as localized blood flow, heart rate and breath velocity [54], [131]–[141]. At the core of this approach are the bioheat transfer model, a geometric model and various assumptions. However, in this thesis study, the approach based on the bioheat transfer model has not been given in detail because an image processing based approach is proposed.

The second approach usually involves processing and analysis of images obtained from thermal data. Unlike the first approach, in such studies, there is no need to know the underlying physical mechanism of human physiology. Only the thermogram images and the correlations between the diseases are detected and the related markers are obtained. In many studies using this approach, early diagnostic techniques to detect various diseases have been discussed [17], [28], [142]–[147].

Identification of correlations between disease and image features is assessed using image processing in two main categories as segmentation of thermal images and removal of related regions (ROI). Techniques used in the extraction of indicators in medical thermograms is given in the following.

2.3.1. Image Segmentation and ROI determination

ROI detection is done manually in some studies or automatically in others. Due to undefined and indefinite boundary lines in thermal images, segmenting ROIs in a fully automatic manner is not always possible. The most common approaches to segmentation are edge based techniques, threshold based techniques, and region growing techniques [148], [149]. In this section, we first give examples from the

manual studies in the literature and then describe fully automated ROI segmentation applications.

Herry and Frize [150] performed ROI segmentation both manually and automatically, using the results from the hot spot and cold spot analysis for pain detection. The analysis of high and low regions at abnormal grade was made based on the indices of isothermal regions and density profile lines. The noise in the thermograms was removed using a wavelet technique as it could maintain sharpness. Then, the thermograms were separated into body parts (such as face, fore leg, upper back, etc.) by edge detection, simple morphological operations and contour extraction based on template matching. In addition, ROIs were segmented by right and left symmetry for the detection of contralateral parts.

Zhu et al. [151] presented another method for manual ROI detection. They performed extraction of supraorbital veins in the thermal forehead images using the Open End Snake (OES) segmentation method. In this method, vessels were first automatically identified using the top hat and Hough Transforms [152] method. Then an automatic localization of the central lines of the vessels was performed using an active contour model. Finally, a special operator was used to quickly determine vessel boundaries to investigate the maximum temperature gradient along the radial direction of a vessel at each point of the active contour. It has been reported that the method can segment vessels with high noise levels and perform better than other vessel segmentation methods according to two performance criteria (Accuracy and Hausdorff distance). However, the method was both dependent on the manual selection of the number of vessels in the ROI as well as the selection of the right ROI by the expert operator. Additionally, the performance of the method has been found to decrease with decreasing image quality.

Koay et al. [153] developed semi-automatic image segmentation and ROI identification methods for breast thermograms. First, they performed image enhancement using a disk with a five-pixel radius as the configuration element and top and bottom hat morphological operators. In this view, the contours and edges in the image were highlighted. ROI was defined using the ellipse fitting algorithm. The nipples were determined to be closest to the eccentricity value of the region 1. The

segmented breasts were divided into four quadrants and statistical parameters were calculated for each breast and quadrant.

Many researchers have encountered the problem of fully automatic segmentation of ROIs. The solution of this problem is very important in order for an algorithm to be reproducible and stable. In clinical trials, the mass scanning of a disease can only be made possible by removing the user subjectivity.

Qi et al. [146] obtained four property curves with the Hough transform [152] to automatically separate the left and right breast segments in the thermograms for breast cancer detection. These curves consisted of left and right body boundary curves and two parabolic curves showing the lower limits of the breasts. Unlike the left and right borders of the breasts, it was difficult to determine the lower bounds of the breasts with the edge operator. The adapted Hough transformation was used to detect parabolic curves to find the lower bounds of the breasts. Breast borders were found in this study, but some parts of the breast, especially in the border regions, have disappeared. This, of course, would jeopardize the validity of any automated diagnostic method based on left-right comparisons due to lack of symmetry [154]. Also, the possibility of containing lesions in the discarded areas would leave doubt [154].

In a face recognition study, facial segment thermograms were divided into sections by using a series of approaches such as horizontal and vertical profile analysis, Sobel edge detection and ellipse fitting method [155]. Initially, the portrait was subtracted from the gray scale image due to the high contrast between the front and the background. Then, using the thermal property of the skin, the head was segmented. From the segmented image, the neck region was also removed by using horizontal and vertical profile analysis. The vertical profile was obtained by summing the densities at each row, while the horizontal profile was obtained using the sum of the densities at each column. Analysis of both profiles was done to define the ROI on the head. Within this ROI, Sobel edge detection was used to obtain edge data for use in adapting an ellipse around the face. The adapted ellipse was then used as a mask to remove the face region.

Palfy and Papez identified the main outlines of the hand for thermal analysis of Carpal tunnel syndrome (CTS) using a simple edge detection algorithm [156]. They put a cold towel under the hand during the taking of the thermogram to increase the hand's contrast and make it easy to distinguish it from the backplane. After the baseline segmentation, the hand was divided into 12 ROIs by the calculation of the center of mass and the determination of the characteristic points between the fingers and tips. The local maxima and minima were subtracted to determine the fingertips and points between the fingers by calculating the distances between each edge and the center of mass. Finally, these points were combined to define different hand parts, including carpal and wrist parts.

In another study involving hand and arm segmentation, a combination of techniques such as Otsu global threshold, Canny edge detector and morphological operations were used [157]. Initially, the noise in the IR thermal images was subtracted using a fixed wavelet transform [158], which preserved fine detail in the image. Then, by using Canny edge detector, hand boundaries were determined. The binary image obtained by the Otsu thresholding method was combined with the edge-detected image. The resulting image was subjected to a series of morphological operations such as opening and closing [158]. Finally, the important points in the segment image (fingers, wrist, thumb and elbow intersection points) were defined using profile lines. The success rate of the tested segmentation technique was found to be 78.8% in the thermal hand images with 658 frontal and 1216 left and right, back and palm views. However, the method had some weaknesses. When two fingers were close to each other and there was a cold finger on the fingertip, the algorithm was not found sufficient.

Alternatively, Zhang et al. [159] developed a method that includes Genetic Algorithm (GA) and Otsu thresholding to segment the thermograms. In this study, the genetic algorithm was started with randomly selected probable solutions as much as possible, and with the help of the logistic mapping equation, an initial population with the maximum population was allowed to be produced. The fitness function was calculated by taking the distance between the background class and the object class as the measurement function of the dispersion matrix. The dispersion matrix was formulated on the basis of the threshold calculated by the Otsu thresholding method. An adaptive mutation rate based on the maximum value of the fitness function in the current

population was also used to improve the performance of the GA method. This approach yielded better segmentation than the Otsu method alone, providing rapid application and good stability.

Chang et al. [160] incorporated wavelet transform into multi-level automatic thresholding algorithms due to its multiresolution nature. In this transformation, a series of extended wavelets at different scales were convolved with the histogram of the thermogram. This was followed by the definition of zero crossings and the identification of the local extremities in the modified histogram set, respectively, to define the thresholds and the gray levels. The best threshold value for multi-level image segmentation was determined by lowering a cost function to the lowest value. The obtained results were compared with those obtained with the plane curve approach and found to be superior. The planar curve approach has been used to locate potential thresholds using the cumulative distribution function (CDF) curve of the histogram for multilevel segmentation [160], [161].

Edge detection and global thresholding methods can cause some information or fine detail to be lost, especially in areas with low contrast. Motta et al. [154] recovered undetected low-contrast regions in a segmented image. In this method, Otsu thresholding, which detects a contour on the segmented image, was used to search the region with the smallest gray level variance. The reason for this was that the region with the largest contour was the region with the lowest contrast pixels at the same time. The average gray level value in this area was then used as the new threshold value for an input image. Left and right segmentation of a mammal was then performed in thermograms using automatic boundary detection, mathematical morphology and curve subtraction and interpolation. Good results were obtained in the images obtained in this study. However, in breast thermogram analysis, this method could only be used with frontal imaging. The validity of the method was confirmed only by medical experts.

Selvarasu et al. [162], [163] compared region growing based approaches with combinations of edge detection and morphological based approaches in arthritis and stress fracture segmentation. In the previous approach, the first pixels in the region, having sharp transitions (above the threshold value), was identified using Sobel masks

and marked as edge pixels. Morphological operations such as dilation, area filling, and erosion were performed on images where edges were detected to identify abnormal areas. In the region growing approach, thermogram was divided into subimages consisting of pixels with values within a certain range tolerance. The pixel with the median density was selected as the seed pixel and the tolerance value of 0.04 was selected as the similarity criterion to identify the abnormal regions. The regional growth approach has identified the anomalies effectively and standardized for all disease types that show themselves as hot spots on thermograms. It was also claimed that this approach was independent of parameters and fast.

Then Selvarasu et al. [163] compared the region growing approach with a wavelet-based approach to performing thermogram segmentation of arthritis and stress fractures. In the wavelet-based approach, the thermograms were converted from color to gray to reduce processing time and computational complexity. Subsequently, discrete wavelet transform (DWT) using Haar wavelets was applied to gray scale thermograms to obtain vertical, horizontal, and diagonal detail images as well as the approximation image. As the researchers observed that the anomaly always appeared as a low-resolution region, the detailed coefficients adjusted to zero while the approximation image was preserved. The thermograms were then reconstructed and hot spots were isolated using thresholds. Each hot spot was then quantitatively characterized. Both techniques could successfully identify and measure the abnormality. Because of its multiresolution nature, the wavelet transform was very useful if the anomaly was in a different resolution than the normal tissue. However, only one level of resolution was used. If all the detail coefficients were not equal to 0, as mentioned in the study, this wavelet-based method could be used for low-pass filtering the image.

Herry and Frize [164] identified potential ROIs using dermatomal subdivisions of the body, isothermal analysis, and segmentation techniques. Firstly, in the ROI segmentation, the background was subtracted from the thermogram by a combination of Tsai's optimal thresholding method [165] and additional morphological operations. After these steps, specific reference points in the body were identified by analyzing the profiles and contours on the image. Landmarks known as dermatomes of the body, were the areas around shoulders and hips for the chest and back, hip splits for the back,

and the knee for the legs. More specific regions from dermatomes were identified based on isothermal analysis (hot and cold regions). In order to obtain the most important regions, they performed operations such as merging the regions, throwing small regions at 10 pixels, thresholding, and removing artifacts from the boundaries of the segmented ROIs.

Tang and Ding [147] detected ROIs in breast thermograms using mathematical morphology. In this work, the thermal pattern in a thermogram was defined as a cluster of peaks and ridges on a topographic surface. Based on this, the authors performed a series of morphological operations to perform the breast segmentation. During rough segmentation, opening and closing with different lengths and oriented structural elements have been carried out. The so-called positive power of the pixel was calculated by the difference between the maximum and minimum values of the pixels from the images obtained after the opening. They did the same after closing to calculate the so-called negative power of the pixel. When the positive power of the pixel was larger than the negative power, it was determined that this pixel had a positive direction. The positive direction of a pixel was used to determine the pattern of heat in the rough segmentation stage. In order to narrow the result of coarse segmentation, a marker image was obtained by first calculating the difference between the image and the image after opening. A refined heat pattern was then obtained by performing a logical "AND" operation between the marker image and the roughly segmented image to remove unwanted heat patterns (along the outer borders of the breasts). Then, using the extended maxima transformation, another marker image was formed which consisted of a series of pixels representing the desired heat arrangements in the breast area. This marker image was then used to determine the locations of the remainder of the desired heat settings in the refined image.

Herry et al. [166] performed segmentation of abnormal regions with a simple translation to calculate the absolute difference between the two contralateral knees. Then, thresholding was performed using the 90% point of the total scatter function on the absolute difference image to obtain the set of interest showing asymmetry anomalies. Then the clusters were mirrored and turned back to their equivalent in the contralateral knee.

Most of the improved methods in the thermogram analysis discussed in this section require a preliminary knowledge of the ROIs developed and investigated for a particular type of disease. Herry et al. [166] developed an alternative approach to derive abnormal regions from a wide variety of clinical thermogram images. Accordingly, no specific information was required on the underlying thermal dysfunctions. This approach consisted of feature images and adaptive resonance theory (ART) applied to thresholded linear composites clustered neural network. Feature images were obtained by combining normalized global contrast, entropy filter and Laplacian Gaussian (LoG) and Sobel operators. When ART was applied directly to the body region, it allocated clusters to the region with a matching-based learning method. The ART network consisted of a layer of cluster nodes and two layers of input data from each layer. Based on unsupervised learning, the existing cluster-matching nodes in the ART network were searched to match the input data to the network. If no matching node was found, a new node was added. To do this, the signals and inputs from the feedback links were compared and then bridged by a parameter that determines whether the input will assign a new one to the existing cluster. The results from ART and feature detectors were combined with a logical "AND" operation. Experimental results have shown that the approach could detect abnormalities in the thermograms. However, only two images with known anomalies were tested.

2.3.2. Asymmetry based approaches

In medical field, thermograms are known to exhibit symmetry in temperature patterns [17], [142], [144], [167]. Based on this information, it is assumed that small asymmetries in temperature patterns show abnormal conditions. This is the basic principle in detecting lesions in breast cancer studies and in detecting abnormalities in other parts of the human body [144]. In the case of an asymmetric thermogram, this asymmetry may be indicative of a physiological abnormality such as pathological (cancer, infection, vascular disease, fibrotic disease) or an anatomic variant [17], [28], [144], [167]. Since it is difficult to be detected by the human eye for these small asymmetries, it is extremely important to automate detection. Another important aspect of such an approach is the elimination of the individual and environmental factors of temperature changes [17], [142] because they can disrupt the structure of the thermogram in the image.

Most asymmetry studies in thermogram analysis use the differences in the first and second order statistical parameters in the contralateral images. The first order statistical parameters are obtained using the image histogram and the second order statistical parameters are calculated from the gray-level co-occurrence matrices [28]. Second-order parameters have been successful in distinguishing almost all malignant tumors. Fujimasa [17] and Mabuchi et al. [142] presented a computerized thermographic system (CTS) that performs thermogram analyzes based on asymmetry and thermographic index. In these studies, the body region was divided into two symmetrical parts, the affected side and the healthy side on the opposite side of the body. Since there was no standard skin surface temperature, the distribution of temperature differences between the affected side and the healthy side was obtained. Subsequently, the mean temperatures of both the affected area and the contralateral healthy area were calculated and the difference between the averages was found. However, various problems have been reported in this method. One of the problems was the identification of an abnormal area larger or smaller than the actual abnormal area. This could change the difference in average temperature between the two sides and thus prevented significant differences from being detected.

Zavisek [168], [169] claimed that the differences in vascular patterns and the hot and cold spot appearances in the left and right breasts were the most important thermopathological features. In these studies, various methods such as histogram analysis, temperature co-occurrence matrix (COM), Fourier spectrum analysis, moment and cluster analysis have been used for feature extraction. Statistics such as commonly used energy, entropy, contrast, and homogeneity could also be generated based on COM for the classification of vessels of breasts [168], [169]. Using the points in the contralateral images, COM could be modified to evaluate the symmetry and to evaluate the roughness and direction of the sought features to be cross-COM (X-COM). Thanks to some of the parameters used, they have achieved more than 80% sensitivity and specificity in the classification of thermograms.

Koay et al. [153] used first-order parameters derived from histograms for the determination of thermal properties in asymmetry analysis. Asymmetry-based features were obtained by evaluating the difference between statistical parameters including mean, variance, standard deviation, median, maximum, minimum, skewness, kurtosis,

entropy, area, and temperature content between contralateral breasts. In the analysis of asymmetry, the difference statistic was examined for the entire breast image and each quadrant of the breast.

Herry and Frize [150] compared symmetric density distributions using low, high, and Kolmogorov-Smirnov statistics. Using a statistical analysis and comparisons made, they used a decision support scheme to summarize the results for each thermal image. In asymmetry analyzes of Tarnawski et al. [170], a number of statistical calculations such as absolute temperature difference averages, absolute difference of standard deviation, median temperature and 90 percentile temperature, image moments, histogram properties, COM-based properties (homogeneity, energy, contrast and symmetry) were used as features. Each breast thermogram was then categorized using a combination of all asymmetry-based features (a total of 38 features per breast thermogram, defining the asymmetry between the two sides). Each property was normalized to a range of 0 to 1 so that it could be compared within the descriptors.

Qi et al. [146] performed asymmetry analysis using the ratio of extracted properties. As the ratio approaches 1, more correlation features and less asymmetry between the segments were observed. Asymmetry based features were obtained by evaluating the low and high order statistics (mean, variance, skewness and kurtosis), the peak pixel density, entropy and joint entropy.

Merla and Romani [143] performed a quantitative evaluation of symmetric / asymmetric temperature distributions using a first-order statistical algorithm based on two parameters: symmetric asymmetry factor and spatial correlation factor. First, they identified the asymmetry factor between temperature distributions on the left and right sides of contralateral regions. Then, the homologous contralateral regions were compared with homologous contralateral regions. This approach allowed the quantitative evaluation of regional variations of temperature distributions, thus allowing the identification of functional asymmetries related to the human posture. It has been reported that advanced quantitative diagnostic applications are now routinely used in clinical settings.

Most of the asymmetry based properties are used in quantitative asymmetry analysis. Tang and Ding [147] also performed qualitative analysis on the asymmetry of breast thermograms. Quantitatively, the authors performed asymmetry analysis of breast thermograms based on extraction properties (such as skewness, variation, kurtosis, temperature difference, and maximum rate between temperature difference and area). They then calculated the two-sided ratio of these properties. If the ratio was more than 1, asymmetry increased. In a qualitative analysis, the left and right heat patterns were performed using the curve of the cumulative histogram describing the field temperature change. When the curve of the cumulative histogram was vertical, it was understood that the temperature distribution was more abnormal.

Herry and Frize [164] proposed a method based on distance measurements (Manhattan or absolute distance, Euclidean distance, maximum distance, chi-square distance, Jeffrey divergence distance, and Mallows distance) to assess the degree of asymmetry between contralateral ROIs. This approach has been used to derive from the limitations of the asymmetry analysis, which is based on the difference in statistics that ignores the importance of temperature distribution. Quantitative assessment using contralateral ROI thermograms of normal and painful patients has shown that the method based on the Euclidean distance has left behind other methods considered, including comparison of statistical parameters such as mean, variance, skewness, kurtosis, and maximum values.

2.3.3. Other Features

Other features used as indicators for abnormalities in thermograms include vascular pattern (hyperthermia, hypothermic or atypical complexity), abnormal physical contour, localized heat along the abnormal physical contour (edge signal), and response to the autonomic control procedure (dynamic imaging) [36], [160], [167]. Acharya et al. [171], [172] used texture features such as homogeneity, energy, entropy, moments of various mechanisms, angular second moment, contrast, mean, short time emphasis, long time emphasis, percentage of work, gray level uneven uniformity and length irregularity in their work with thermograms for breast cancer detection. However, only four features were identified that were clinically significant when

compared to other features. These were moments at first and third degrees, percentage of work, and irregularities at gray level.

Thermal properties such as the maximum temperature in the eye area and the maximum temperature in the forehead zone have been found to be promising for the diagnosis of SARS, headache, migraine, vascular disorders, sleep apnea and similar diseases [173]–[177]. Quek et al. [177] used the fuzzy neural network to extract the maximum temperature in the eye region. In migraine patients, hot spots were more frequent in the orbital intima [178], [179]. In arthritis and stress fracture analysis, thermal properties such as major axis length, side-axis length, and area were extracted from the hotspot regions for further analysis [163].

In the Carpal Tunnel Syndrome (CTS) analysis, the mean temperature and the ambient temperature of each section of a hand thermogram without cold stress testing were categorized as healthy and CTS by an artificial neural network [180]. For massive screening, Ng and Kee [181] extracted the temperature data from the front and side profiles of a hundred thermograms. The temperature data were then normalized and statistical analysis was performed to obtain the minimum, maximum, mean, median and standard deviation over the temperature data. Varga and Khanka [182] selected the mean temperature and variance of the different diseases as the most important features for the classification of diseases based on the Kittler and Young [183] attribute method.

Selvarasu et al. [163] used the major and minor axis length, area, and variance in the pixels of the extracted hot spots to characterize the severity and severity of the abnormality in arthritis and stress fracture thermograms. Nurhayati et al. [184] have reported that distinction could be made especially early and advanced cases in abnormal breast thermograms by using skewness curves, standard deviation, and entropy values. Moreover, they have found that normal breast thermograms had the smallest standard deviation and skewness values, unlike especially the abnormal ones from advances cases. Also, in contrast to these findings, normal breast thermograms had the highest mean value, which was different from the advanced and early breast cancer thermograms.

Wiecek et al. [28] obtained thermal properties using image histograms, COMs, and wavelet transforms for image classification. Using raw data analysis, three of the seven original features were selected based on the first two from COM (first squares and differential difference moments) and the third wavelet transform. Wavelet transform was performed with low pass and high pass filtering, followed by decimation at all scales until the size of the image was reduced to a single pixel. From the wavelet transformed image, the gradient of the temperature (obtained from high pass filtering), the global temperature distribution (obtained from low pass filtering) and the level of temperature (estimated from the energy of the signal) were obtained. The classification based on these properties was then performed using a neural network and compared with the nearest neighbors classification.

In a study of facial expressions, transitional facial features were used in classification [185], [186]. In this study, with CMView Plus software, each thermogram was divided into a grid of squares and the thermal intensity values (TIVs) of the faces were measured to obtain sample data. The highest temperature value in each grid was recorded as the TIV value of square. Later, variation in TIVs was measured by multivariate analysis and exploratory reordering. These methods were used to identify TIVs with significant thermal changes and to generate 75 squares (using a 128-frame grid) known as facial thermal points (FTFPs). FTFPs provided information about the hundred facial thermal variations. Prior to thermal property extraction, TIV datas were normalized using the average thermal value. Then, a thermal feature vector consisting of projection coefficients on eigenvalues for classification was found using PCA.

For thermogram analysis, Underwood [187] used active appearance models (APMs), including not only the shape but also the tissue data of the hands, independent of the palm position. In the model of APMs, a set of parameters defining shape and gray level changes, shape modification, affine transformation methods were used. The parameters of the image and gray level variations were then combined and then used in a PCA. In order to achieve this model, two parallel educational approaches have been used. These were total approach (using all images) and serial approach (only using corresponding points from various images).

2.3.4. Results

Thanks to IR thermal imaging technology, image processing techniques and advances in the pathophysiological understanding of thermograms, infrared imaging is very useful for health monitoring and clinical diagnosis as a primary aid complement. IR thermal imaging can be more effective in medical field since it has been found to be useful for early screening and detection of a wide range of diseases (neurology, vascular disorders, rheumatic diseases, tissue viability, oncology (breast cancer in particular), dermatological disorders, neonatal, ophthalmology and pain, stress, anxiety, sleep disorders, surgery and monitoring efficiency of drugs and therapies [18], [28], [42], [131], [134], [145], [153], [188]–[192]). Changes in blood perfusion caused by inflammation, infection, injuries, angiogenesis and tumor growth appear as hot or cold spots in the thermograms. Thus, examining the abnormalities observed in thermograms and examining the heat exchange processes of the human body can provide information about the pathology of the underlying diseases [17], [18], [138], [140].

In medical practice, thermograms are known to be substantially symmetrical in temperature patterns. Asymmetries formed by the formation of these hot and cold spots in the thermograms are often indicative of physiological abnormalities. For this reason, an asymmetry analysis approach based on image processing methods seems to be very popular for the diagnosis of hemilateral diseases such as breast cancer and hemilateral radiculopathy. The asymmetry approach removes both internal and external variables and allows small changes in the body surface in the affected regions to be detected and evaluated even for smaller and deeper tumors. In addition to asymmetry-based features, the average temperature of abnormal regions, variations, contours, and other properties obtained by wavelet transform can also help in thermogram analysis.

As a result, a rapid, effective, and robust system based on thermal imaging can be very useful in the analysis of medical thermograms and therefore allows mass scanning for a disease. It is supported by non-invasive, non-radiation based, fast and cost-effective compared to other imaging modalities. For this reason, image processing and analysis methods need to be developed to evaluate changes in body surface temperature distribution for disease diagnosis. However, it should be kept in mind that changes in

blood perfusion may occur for a variety of reasons other than previous inflammation and angiogenesis, such as trauma. For this reason, in some cases it may be useful to support thermography with different imaging modalities such as ultrasound, MRI, tomography. Thus, the information obtained from the thermal image can be evaluated with better accuracy.

2.4. THERMOGRAPHY STANDARD PROTOCOL

Since human skin is severely affected by environmental factors, it is very important to use a standard protocol while taking IRT images. The environment for imaging needs to be ideal, the patient should not be sweating or shivering because of too hot or cold [37]. In the literature, room temperatures have been set between 20 and 24 ° C [193]–[199]. Although the skin has high emissivity ($\varepsilon \approx 0.98$ [4], [27]), there should be no radiation source near the skin [200]. In addition, subjects should not be exposed to IR sources or airflow [37]. To remove effects from ambient temperature, the clothes must be removed for a sufficient period of time before the image is taken [201]. In various studies, this time was ranged from 5 minutes [55], [202], [203], 10 minutes [194], [204], [205], 15 minutes [104], [197], [206]–[211], 20 minutes [212]–[214]. Besides, topical cosmetic or ointment application [215], inhalation of cigarette smoke [216]–[219] or drinking alcohol should not be allowed prior to imaging [220]. Despite the fact that there is no definite information about skin temperature effect, heavy meals, coffee and tea consumption are not recommended [221]–[224]. Again, intensive exercise, massage, and other physiotherapy methods should be avoided prior to thermography as it can change skin temperature [225]. Finally, if there are diseases that affect the skin, such as sunburn [226], it should be taken into account when interpreting the results of IRT.

In this study, when the patients came to the hospital for the first time, they first had routine examinations and were subjected to appropriate tests if they have any preliminary diagnosis. After these tests, they were directed to the imaging room where the ideal conditions have been established. To limit external factors, the ideal room was formed where the temperature was set between 22-24 degrees Celsius with climate control, with a humidity of about 60 percent with a tolerance of 5 percent, no daylight, illuminated with fluorescent lamps, no ventilation directly affecting the patient, no

external heat source. To limit internal factors, within the last 2 hours, those who consume meals, coffee, tea, cigarettes, caffeinated beverages, alcohol, drugs that alter blood flow, use cosmetics and do physical activity were not included in the study.

After all these conditions were met, patients were allowed to rest for 15 minutes to balance the basal metabolism in such a way that their imaging body area were naked. After this process, the images were taken with the Testo 875i model thermal cameras by experienced physicians. When the image was taken, the patient was seated comfortably in a vertical or horizontal position, the camera was focused vertically on the area to be imaged, and only the body region and underlying cover were included. The numbers of the received images were saved in the patient file.

CHAPTER III

THERMAL IMAGE PROCESSING METHODOLOGY

This section discusses in detail the methods used to develop the image processing approach for the analysis of infrared thermal images to diagnose diseases. The proposed system consists of six stages: image preprocessing, image enhancement, ROI segmentation, statistical analysis, decision-making and performance evaluation.

3.1. Image Preprocessing

The images obtained by the thermal camera are actually 2D real temperature values in terms of centigrade. This data should be converted to 8-bit grayscale images with normalization [224], [227]. With the aid of the current temperature information and a linear mapping function, this matrix is transformed into an 8-bit grayscale image according to Eqn 3.1.

$$I_n = (I - Minimum) \, x \left(\frac{NewMaximum - NewMinimum}{Maximum - Minimum} \right) + NewMinimum \qquad (3.1)$$

Here, I represents the unprocessed thermal data where the minimum and maximum values are extracted. The NewMaximum and NewMinimum are defined as 255 and 0 to normalize the image to an 8-bit grayscale.

3.2. Image Enhancement

A three-part process is proposed for enhancing the images: noise reduction, contrast enhancement and background removal. Each step is discussed in detail in order to understand methods and the logic behind their use.

3.2.1. Noise Reduction Approaches

Noise is a natural feature of all electronic devices [228]. Even though noise is minimized by methods such as calibration, it is seen during image acquisition. Noise has the potential to create an unusual texture in the image, causing metrics to deteriorate [229]. For this reason noise reduction methods must be used.

The main purposes of noise reduction methods are to determine whether differences in pixel values within an image are real values and, to average these values to reduce the overall effect, if noise is detected. Since the amount of noise content can not be determined precisely, there is a balance between noise reduction and the preserving fine details such as edges. Different methods are discussed in the following.

In this study, spatial filters, which are defined as kernels, are used to represent neighborhood shape and size. It is common practice to use odd numbered spatial filters as a dimension to ensure that each pixel is located in the neighborhood center [230]. At the same time, the larger the neighborhood size, the more noise is reduced, but the degree of blur increases. Normally, 3x3, 5x5, and 7x7 dimensions are selected for analysis, because sizes larger than them can cause more blur and remove significant content. In addition, to preserve the brightness of the original image, the sum of all the items of the filter must equal one.

Mean (or average) filtering is one of the simplest ways to reduce noise and remove noise [228]. In this filtering, each pixel in the image is replaced by the average density value of its neighbors. In other words, the differences in values between neighbors are softened and the noises are removed by significantly smoothing. A 3x3 average kernel is as below.

1/9	1/9	1/9
1/9	1/9	1/9
1/9	1/9	1/9

Figure 3. 1 Example of a 3x3 kernel for mean filtering

The median filter is a known nonlinear filter that preserves the edges and fine details of the image in terms of noise reduction [228]. In this method, when an *MxN* neighborhood is given, the pixel values are sorted and the median value is assigned as output pixel [230]. The complexity of the method is increased when using even-size dimensions.

It is known that the Weiner filter is one of the best ways to remove the noise in the signal. This adaptive technique has achieved superior results over linear methods due to the high frequency content protection in the image. A Weiner filter is generated for each pixel in the image using the mean (μ, Eqn 3.2) and variance (σ^2, Eqn 3.3) values of a local area. Here, η is the neighborhood of *MxN* according to the pixel a. These calculations are used to create a pixel-based Weiner filter (Eqn 3.4). In this equation, v^2 is the noise variance determined by averaging all estimated variances. Edges are preserved with this method, because when the variance is low, smoothness is high and variance is high, smoothness is minimized. For this reason, this method is suitable for noise reduction in thermal images.

$$\mu = \frac{1}{MN} \sum_{n_1,n_2 \in \eta} a^2\left(n_1,n_2\right)$$ (3.2)

$$\sigma^2 = \frac{1}{MN} \sum_{n_1,n_2 \in \eta} a^2\left(n_1,n_2\right) - \mu$$ (3.3)

$$b\left(n_1,n_2\right) = \mu + \frac{\sigma^2 - v^2}{\sigma^2}\left(a\left(n_1,n_2\right) - \mu\right)$$ (3.4)

In this study, a simulation was performed to determine which noise reduction technique is most appropriate. As suggested in the literature, white Gaussian noise with a mean [231], [232] of 0 and a variance of 0.001 was added to the images. A comparison was made between the original image and the filtered image to evaluate the performance of an image restoration technique. The comparisons were based on the mean square error (MSE) defined in Eqn 3.5. Where *M* and *N* represent the dimensions of the image, while m and n represent the pixel coordinates.

$$MSE = \frac{1}{MN} \sum_{m=0}^{M-1} \sum_{n=0}^{N-1} \left[\hat{a}\left(m,n\right) - a\left(m,n\right)\right]^2$$ (3.5)

Among the three noise removal techniques, the selection criterion was based on the minimum MSE value. The average filter performance was the worst in all kernel values. The best Wiener filter (5 x 5) performed slightly better than the best median filter (5 x 5) MSE. When 7×7 kernel size was used, all three filters show visible blurring. As a result, a Wiener (5 x 5) filter was selected to perform the noise reduction process.

3.2.2. Contrast Enhancement

Contrast enhancement methods are designed to enhance certain features by improving image contrast without altering the structural information of the view [233]. An increase in the current contrast level of the image makes it easier to reveal hidden details. Histogram equalization is a way of adjusting the image intensities by increasing global contrast. This concept is based on the spread of frequencies stuck on a narrow histogram over a wider range. The transformation of these intensities is described in Eqn 3.6 [230]. However, this transformation method may cause noise amplification, depending on the fact that a number of pixels are in a certain intensity range [234].

$$I_k = T\left(r_k\right) = \sum_{j=0}^{k} p_r\left(r_j\right) = \sum_{j=0}^{k} \frac{n_j}{n} \;\;, 0 \le r_k \le 1 \; and \; k \in \left[0,...,L-1\right] \tag{3.6}$$

where I_k = intensity value of the enhanced image

r_k = intensity value of the original image

L = number of intensity levels

$p_r(r_j)$ = probability density function of a particular intensity

n_j = number of pixels at the intensity j

n = total number of pixels

Contrast-Limited Adaptive Histogram Equalization (CLAHE) is a commonly used contrast enhancement method that has proven to be effective for medical imaging [233], [234]. Unlike other histogram equalization methods, this technique performs contrast enhancement on divided small regions of the image. The pixel intensity is converted to a value within the display range that is proportional to the order of the pixel density for the local region. The difference between CLAHE and adaptive

histogram equalization (AHE) is that the local histogram height is a user-determined maximum (clip level or clip limit). In other words, the histogram values are cropped to a certain extent and the remainder is redistributed to other bins. This results in a low contrast enhancement in the homogeneous areas of the image, thereby reducing the extreme increase in noise due to the increase in pixel variations and reducing the loss of edges to a minimum [233]. The size of the neighborhood and the clip level are the user-defined input parameters required for CLAHE.

The CLAHE method is used to increase contrast in this study. Similar to noise reduction, a simulation was performed to determine the appropriate clip limits of the CLAHE method [235] used in a previous study for contrast enhancement. Increasing the clip limits has been seen to increase the MSE value. So, clip-limit values of 0.005 and 0.01 were selected as appropriate for asymmetry analysis [235]. This clip limit increased the contrast to a level that would not disturb the accuracy of the image, and only slight changes were recorded.

3.2.3. Background Removal and Contralateral Body Segmentation

The purpose of removing the background in the image is to eliminate the unwanted parts of the image while preserving essential information. In this study, objects such as clothes, cables, rooms, etc., which are located outside the area of interest of the body, are defined as the background. Particularly when thermal imaging is considered, the background separation is relatively easy, as the intensity values of the infrared radiation emitted by the skin are greater than those of the background. For this reason, it is preferable to use intensity based segmentation algorithms that can distinguish the body area and the background by identifying the gray level threshold automatically.

After background removal, the foreground image of the corresponding body region is divided into two region for the detection of the contralateral body segments by using Roberts edge detection method [236]. The image is divided by vertically controlling the vertical edge to start from the center of the picture. Then, using the following algorithms, the two images are evaluated independently of each other and the region of interest is made without any interaction.

Otsu Algorithm

In this study, the Otsu algorithm as one of the background removal algorithm was chosen to automatically remove the background from the thermal image [237]. This method has been chosen because of its simple, stable and widespread use in medical image processing. Segmentation is based on calculating the optimal gray level threshold. The use of the algorithm is as follows.

In the Otsu thresholding algorithm, the goal is to find the threshold that minimizes the within cluster variances, or maximizes the variance between classes to allow the data to be divided into two groups. So, grayscale images can be converted into binary images and separated into a foreground and a background.

The weighted sum of within cluster variance is defined as:

$$\sigma_w^2(t) = \omega_1(t)\sigma_1^2 + \omega_2(t)\sigma_2^2 \tag{3.7}$$

where, ω_i is the probability of occurrence for class i that is separated by threshold t.

$$\omega_1(t) = \sum_{i=1}^{t} P(i), \quad \omega_2(t) = \sum_{i=t+1}^{l} P(i) \tag{3.8}$$

Therefore, mean of each cluster is calculated by

$$\mu_1(t) = \sum_{i=1}^{t} \frac{iP(i)}{\omega_1(t)}, \quad \mu_2(t) = \sum_{i=t+1}^{l} \frac{iP(i)}{\omega_2(t)} \tag{3.9}$$

Moreover, individual class variances are defined as

$$\sigma_1(t) = \sum_{i=1}^{t} \left[i - \mu_1(t)\right]^2 \frac{P(i)}{\omega_1(t)} \tag{3.10}$$

$$\sigma_2(t) = \sum_{i=t+1}^{l} \left[i - \mu_2(t)\right]^2 \frac{P(i)}{\omega_2(t)} \tag{3.11}$$

When all possible threshold values *(t)* are attempted, the threshold value that minimizes σ_w^2 *(t)* could be found.

To reduce the cost of calculation, a faster method can be created using recursive operations. This calculation uses the definition of the total variance for any threshold to be the weighted sum of within the cluster variances and between the cluster variance (the sum of the weighted squared distances between the class averages and the overall average). The total variance can be written as,

$$\sigma^2 = \sigma_w^2(2) + \omega_1(t)\left[1 - \omega_1(t)\right]\left[\mu_1(t) - \mu_2(t)\right]^2 \tag{3.12}$$

Since the total variance is constant, it can be used to maximize the cluster variances rather than to minimize within the cluster variances. This provides recursive computation between cluster variances. The algorithm is as follows: calculate the normalized histogram of the input image, calculate the global average, calculate the between cluster variances for each possible threshold value, and select the threshold value that maximizes the variance between the cluster variances.

The Watershed Algorithm

In this study, the Watershed algorithm as another background removal algorithm was chosen to automatically remove the background from the thermal image. Mathematical morphology provides theoretical background and techniques for processing and analysis of geometric structures in images based on set theory, lattice theory, topology and random processes [238]–[241]. The main method of image segmentation in mathematical morphology is the watershed algorithm [242]. In the Watershed algorithm, an image appears as a topographic surface: the higher the value of a pixel, the higher the height at the corresponding point in the topographic surface. The algorithm is like as follows.

Let *f* be the grayscale image under consideration, represented as a function $R^2 \rightarrow R$ defined on the domain D_f ; let $p = (x, y) \in D_f$ be a particular location in the image. Let

h_{max} and h_{min} be the largest and smallest values taken by f on its domain. Let $T_h(f)$ be the threshold at level h, defined as

$$T_h(f) = \{p \in D_f; f(p) \leq h\} \tag{3.13}$$

The catchment basins will be constructed step by step corresponding to stepwise flooding. Let $C_h(M_i)$ be the part of the catchment basin associated with the minimum M_i, which is flooded at level h. In other words,

$$C_h(M_i) = C(M_i) \cap T_h(f) \tag{3.14}$$

Let $M = \{M_1, M_2, \ldots, M_k\}$ be the set containing all of the minima at level h. The union of all catchment basins is denoted by $C(M)$, and its flooded part at the level or time h is denoted by $C_h(M)$. Let the geodesic influence zone $iz_h[C_h(M_i)]$ of a connected component $C_h(M_i)$ within T_h be defined as

$$iz_h\left[C_h(M_i)\right] = \left\{p \in T_h \mid \forall_j \in [1,k]/\{i\}: d_h\left[p, C_h(M_i)\right] < d_h\left[p, C_h(M_j)\right]\right\} \tag{3.15}$$

where $d_h[p, C_h(M_i)]$ is the geodesic distance between p and $C_h(M_i)$ in T_h, defined as the infimum of the lengths of all of the paths going from p to $C_h(M_i)$ in T_h. In the same way, we denote by $IZ_h(M)$ or the influence zone of M in T_h the union

$$IZ_h(M) = \bigcup_{i=1}^{K} iz_h(M_i) \tag{3.16}$$

with K being the number of regional minima in T_h.

According to the definitions given above, in the first stage of flooding, $T_{hmin}(f)$ is identified with the deepest minimum and $C_{hmin}(M_i) = T_{hmin}(f)$. Let the time h be increasing, so that the flood reaches the level $h - 1$. The threshold $T_h(f)$ is made of k connected particles, B_i for $i = 1, 2, \ldots, k$, so that $\cup_i B_i = T_h(f)$ and $\cap_i B_i = \emptyset$. Each connected particle $C_{h-1}(M_i)$ is contained in one and only one connected particle of $T_h(f)$. However, there can be connected particles of $T_h(f)$ with zero, one, or several connected particles of $C_{h-1}(M)$. If a connected particle B_i of $T_h(f)$ contains only one

connected particle $C_{h-1}(M_j)$, then B_i belongs completely to the catchment basin associated with the minimum M_j. In other words, B_i is the geodesic influence zone of $C_{h-1}(M_j)$ within $T_h(f)$, that is, $B_i = iz_h[C_{h-1}(M_j)]$. If a connected particle B_i does not contain any connected particle $C_{h-1}(M_j)$, then a new minimum has just been flooded. A minimum that appears at the level of flooding h is called Min_h. Finally, if a particle B_i contains several connected particles $C_{h-1}(M_j)$, a dam must be constructed within B_i to separate the converging floods; at the end of the procedure, all dams correspond to the complement of the set $C_{hmax}(M)$.

In summary, the following recursive algorithm may be defined:

1. $C_{hmin}(M_j) = T_{hmin}(f)$.
2.   For $h \in [h_{min} + 1, h_{max}] : C_h(M) = IZ_h \cup Min_h$.
3. $DL = D_f \setminus C_{hmax}(M)$, where DL is the dividing line or the position of the dam.

3.3. Finding Region of Interest (ROI)

3.3.1. ROI determination in the Deep Vein Thrombosis Application

After the background is removed and contralateral body regions are detected, heat maps are created using the contours of the two separate regions and classified using heat averages to have high and low temperatures. As a result of the classification, the body area with high temperature is considered suspicious and the ROI is determined by the threshold value shown in Eqn 3.17. In this examination, if the heat distribution is not homogeneous and there is an abnormality, the potential disease area (ROI) is determined by the threshold value, and a new heat map is created according to the ROI, otherwise a homogeneous distribution (non-complaining body area) will yield itself as ROI. Accordingly, there is also no need to find an ROI when the same threshold value is applied to the leg with low heat, as it usually gives shape of the leg itself.

$$Threshold\ Value = \frac{\max(Comp.\ Leg\ Heat\ Map) + \min(Comp.\ Leg\ Heat\ Map)}{2} \qquad (3.17)$$

So, individual heat maps are created for the complaining and non-complaining body areas by using ROI analysis. These maps contains thermal data corresponding to each pixels. For statistical analysis, these vectors are used to determine first order statistics of patient and normal subjects.

3.3.2. ROI determination in the Raynaud Phenomenon Application

In this study, the ROI areas are identified for patients with Raynaud phenomena using morphological operations in image processing.

One way of extracting image components to express the details, such as the shape, boundaries, area, and so on for a region in digital image processing is morphological processing [236]. To understand the methods used in this thesis, two primitive and commonly used morphological operations, dilation and erosion are discussed in the following sections.

Dilation

Dilation is the method used to smooth the boundaries of regions or to cover very small gaps between adjacent regions. According to Gonzalez and Woods [236], the formal definition of the dilation of cluster A and B is $A \oplus B$ and is defined by:

$$A \oplus B = \left\{ z \mid (\hat{B})_z \cap A \neq 0 \right\} \tag{3.18}$$

where $\hat{B}$ is the reflection of B.

This definition means that dilation of A by B is done by reflecting B and then shifting B over A by z. Then all the displacements of B are set such that B and A overlap by at least one element, which gives the dilation. Set B is also referred to as the dilation mask or structuring element (STREL). In Figure 3.2, an example of set A and a set B are shown to illustrate the effect of dilation. The center of the mask B is marked by a small black square. In this case, the reflection $\hat{B}$ is equivalent to B. Now, if B is moved within and outside A, then dilation is given by the set of all points traversed

by the center of *B*, until *A* and *B* are overlapped by at least one element. The resultant is shown as the shaded square that is bigger in size than *A* as indicated by dashed lines.
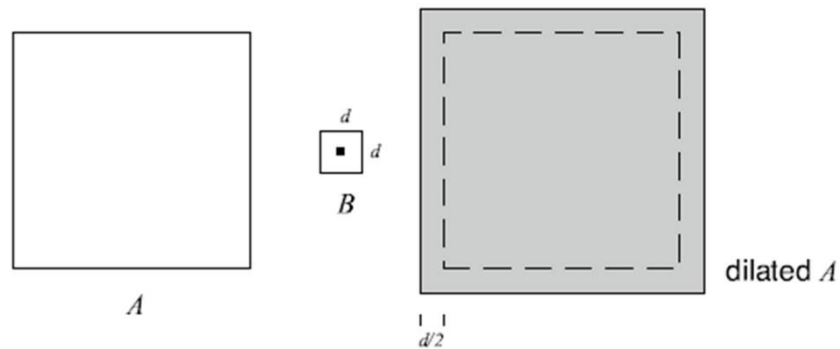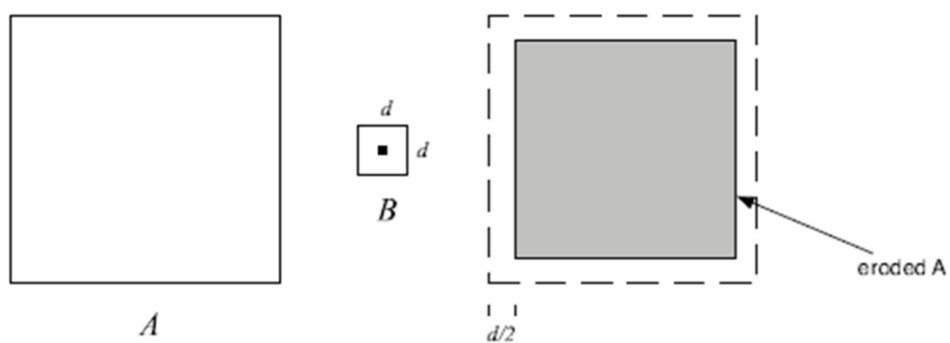

Figure 3. 2 An example of dilation of set *A* by set *B*

Erosion

Erosion produces an opposite effect of dilation. Following the same notation for dilation in Eqn. 3.18, a formal definition of erosion is given by [236]:

$$A \ominus B = \{z \mid (B)_z \subseteq A\} \tag{3.19}$$

In other words, erosion of *A* by *B* is set of all points traversed by center of *B* such that *B* is totally contained within *A* at all times. Figure 3.3 shows an example of set *A* and a set *B* to illustrate the effect of erosion. Erosion can be used for removing small unwanted components, such as thread like structures, from an image by using a structuring element (STREL) with an area that is bigger than the unwanted regions.

Figure 3. 3 An example of erosion of set *A* by set *B*

Morphological Opening and Closing

In digital image processing, morphological dilation and erosion processes can come together with different combinations to make interesting changes in the images. Morphological opening and closing also occurs with specific variations of dilation and erosion. While morphological opening is often used to smooth contours of the region and to remove fine specks in the images, the morphological closing combines the two large regions separated or add smoothness to the image contours [236].

In mathematical morphology, opening is the dilation of the erosion of a set A by a structuring element B:

$$A \circ B = (A \Theta B) \oplus B \qquad (3.20)$$

In mathematical morphology, the closing of a set (binary image) A by a structuring element B is the erosion of the dilation of that set,

$$A \bullet B = (A \oplus B) \Theta B \qquad (3.21)$$

where $\oplus$ and Θ denote the dilation and erosion, respectively.

3.4. Statistical Analysis

The Shapiro-Wilk test is based on the null hypothesis that the data is sampled from a Gaussian distribution. If the *p-value* in the test is less than the threshold α, the null hypothesis is rejected [243]. The *α-value* can be considered as a level of significance and is normally set to a value of 0.05, which in principle represents 95% confidence interval and thus the equivalent level of *2σ* values in the normal distribution.

Student t-test is used to determine whether two separate samples were normally distributed in the same population [244]. The null hypothesis assumes that the samples are from the same population, thus if the value of p is statistically significant at a certain level of significance, i.e., if the value of p is less than α, the null hypothesis is rejected. Two samples are dependent on a paired test while an unpaired test assumes independence between each measurement.

The analysis of the data obtained in this study is performed by using the Shapiro-Wilk test since the Shapiro-Wilk test gives more reliable results for data sets smaller than 2000. Independent-sample t test is used for paired comparisons of independent and normal distribution data. On the other hand, Mann-Whitney U test is used for paired comparisons of independent and non-normal distribution data. Since the *p* value indicates the amount of possible error and shows a statistically significant difference in a comparison, *p*<0.05 is considered statistically significant in all comparisons.

3.5. Decision-Making for Disease Diagnosis

In the empirical sciences, the three sigma rule means a heuristic method in which "almost all" values are taken to lie in the three standard deviations of the mean, i.e., 99.7% probability that "close to certainty" is useful [245]. A sample normal distribution plot is shown in Fig. 3.4 with a 3 sigma rule. The benefit of this intuition is largely dependent on the problem that is being considered. For example, in social sciences two sigma effects (95%) can be considered "important" for a result whereas in particle physics five sigma effects (99.99994%) are described as a "discovery". In this study, infrared imaging is considered to be only a preliminary test and the best possible sigma value is determined according to objective evaluations and explained in the following sections. First, sigma values (σ) were calculated separately (Eqns. 3.22-3.23) for each subject by using heat maps.
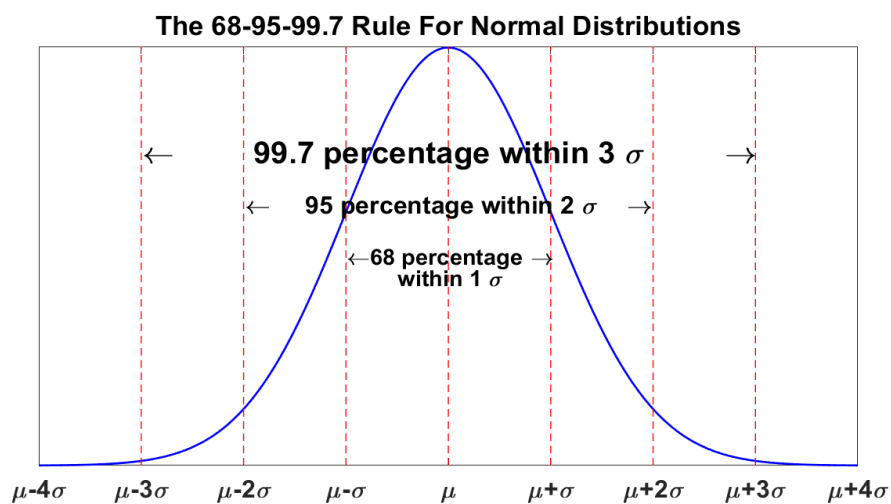
Figure 3. 4 3-Sigma Rule for Normal Distributions

$$\sigma = \frac{\mu}{\xi} \qquad (3.22)$$

$$\mu = \mu_P - \mu_N \text{ and } \xi = \sqrt{\xi_P^2 + \xi_N^2} \qquad (3.23)$$

where $\sigma = Sigma\ Value$, $\mu = Mean\ Difference$

$\mu_P = Mean\ of\ Complaining\ Leg\ Heat\ Map$,

$\mu_N = Mean\ of\ Non - Complaining\ Leg\ Heat\ Map$

$\xi = Total\ Standard\ Deviation$

$\xi_P = Standard\ Deviation\ of\ Complaining\ Leg\ Heat\ Map$

$\xi_N = Standard\ Deviation\ of\ Non - Complaining\ Leg\ Heat\ Map$

3.6. Performance Evaluation

In clinical trials, the performance of a diagnostic test is commonly assessed by some statistical measurements such as sensitivity, specificity, positive predictive value, negative predictive value, accuracy and Youden's Index [246]. Sensitivity is defined as the probability of obtaining a positive test result because the individual being tested actually has the disease. On the contrary, specificity is defined as the probability that the test result is negative for an individual who does not have the disease [247].

The confusion matrix shows the relationship between different performance indices for binary classification in Table 3.1. The four performance indicators (TP, TN, FP and FN) in Table 3.2 for the computerized classification of the patient and the normal person are calculated by comparing the expected output from the developed system with the actual labels determined by a gold standard.

By using these four performance measures, some statistical measurements for binary classification can be calculated (Eqns. 3.24-29).

Table 3. 1 Confusion Matrix

		PREDICTED CONDITION	
		Prediction Positive	**Prediction Negative**
TRUE CONDITION	**Condition Positive**	True Positive (TP)	False Negative (FN)
	Condition Negative	False Positive (FP)	True Negative (TN)

$$Sensitivity \ = \frac{TP}{TP + FN} \tag{3.24}$$

$$Specifity \ \ = \frac{TN}{TN + FP} \tag{3.25}$$

$$Positive \ Predictive \ Value \ \ = \frac{TP}{TP + FP} \tag{3.26}$$

$$Negative \ Predictive \ Value = \frac{TN}{TN + FN} \tag{3.27}$$

$$Accuracy = \frac{TP + TN}{TP + FN + FP + TN} \tag{3.28}$$

$$Youden's \ Index, J \ = \ Sensitivity + Specifity - 1 \tag{3.29}$$

where *TP*, *FN*, *TN*, and *FP* represent true positive, false negative, true negative, and false positive values, respectively.

In a Receiver Operator Characteristics (ROC) curve, the sensitivity representing patients correctly classified in the study is plotted against 1-specificity corresponding to misclassified normal persons for different cut-offs values as shown in Fig. 3.5. ROC analysis is usually used to determine an optimal cut-off value in medical diagnostic tests. Thus, it is possible to obtain an optimal balance between sensitivity and specificity for a particular purpose. This can be achieved by changing the system's cutoff value. Furthermore, if the cost of detecting a particular disease is high, the cut-off value can be changed to achieve a very high sensitivity but only to a lower specificity [248].

Table 3. 2 Binary Classification Performance Measures

Performance Measure	Definition
True Positive (TP)	Patient is also classified as Patient by the diagnostic method.
False Positive (FP)	Patient is classified as Normal by the diagnostic method.
True Negative (TN)	Normal is also classified as Normal by the diagnostic method.
False Negative (FN)	Normal is also classified as Patient by the diagnostic method.
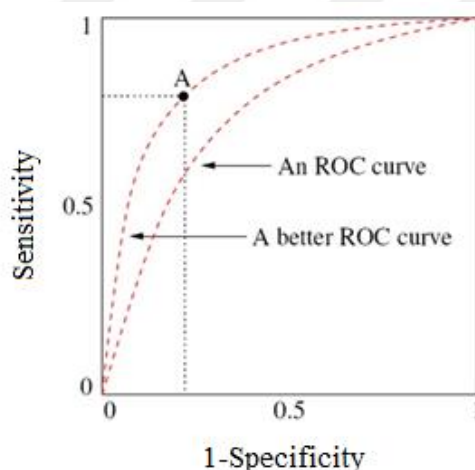
Figure 3. 5 A Receiver Operating Characteristic curve (a ROC curve)

The total area under the curve (AUC) of the ROC curve is a quantitative measure of the binary classification performance, as it reflects the test performance of the diagnostic method at all possible cutoff levels. The larger the AUC is in the 0.5-1 range of the vertical axis, the better the classification performance [248]. In most medical diagnostic trials, there is usually a limited number of points in the ROC curve. If there are more points, the prediction of the curve and the correctness of the binary classifier will be better.

CHAPTER IV

THE USE OF INFRARED THERMAL IMAGING IN THE DIAGNOSIS OF DEEP VEIN THROMBOSIS

4.1. INTRODUCTION

Venous thrombosis is the name given to the formation of blood clots (thrombosis) in the veins. This clot prevents blood flow in the vein, leading to regional swelling and pain. Venous thrombosis is often referred to as deep vein thrombosis because it most commonly occurs in veins found in the legs, calves and hips.

Deep venous thrombosis (DVT) is often painless, but the most important aspect is that it dislodges from the site of the clot, causing death by clogging the lung vessels through blood circulation. It is an emergency situation and can lead to death if not treated immediately. In DVT, the clot is often not completely dissolved, or even if dissolved over time, it causes obstruction, narrowing, and deterioration of the lids inside the vein. In this case, after years of clotting, the flow of venous blood, which should return from the legs gradually, is blocked and the blood starts to accumulate in the veins and the pressure starts to increase. Then, high blood pressure in the veins can damage the tissues, resulting in swelling of the legs, pain, color change, and venous insufficiency with wrist wounds (venous ulcer). Also, as a result of blood pooling in the leg due to blocked veins, the leg swells gradually and eventually the circulation of the artery is disturbed and gangrene develops in the leg and may cause loss of the leg. DVT is a pathology with high complications of mortality and morbidity in both acute and chronic stages. Immediate initiation of treatment with deep vein thrombosis diagnosis will significantly prevent these possible complications.

Venography is accepted as the most reliable test. Although venography is a reliable imaging method for DVT, it can only be performed by the related branch physician, which restricts the accessibility of this examination. However, due to concerns such as an invasive procedure, exposure to radiation and developments in alternative methods, it is much less frequent nowadays.

The method used for the laboratory test is the D-dimer measurement. If the D-dimer is normal, it most likely indicates that there is no DVT. On the other hand, the steady increase of D-dimer does not always point to DVT. The most widely used and reliable method currently available for DVT is Color Doppler Ultrasonography (CDUSG). With CDUSG, DVT diagnosis can be painless, easy, cheap and accurate. Although there are not many of these risks in this method, reaching a radiologist at any time in emergency situations and waiting for the reporting process can lead to a clinical concern such as delayed treatment and the patient to wait for a long time in the emergency service. In the study carried out by Caronia et al., 19 medical assistants performed CDUSG in 75 patients and patients were then directed to radiology for confirmation. The radiologist reported an average of 14.7 hours of CDUSG [249]. In a similar study, the required CDUSG reporting from radiology caused an average delay of 13.8 hours [250].

The use of a thermography to diagnose a DVT disease has been suggested to alleviate these problems. Previously, many equipment that had already been worked on but had not gained practical use due to the disadvantages such as the high cost of the devices, the size and the cumbersome, has come back again with the reduction in cost and the development of more compact designs. Especially with the development of computer software and the progress of artificial intelligence work, the devices become suitable for use.

In patients with DVT, it is seen in the literature that the complaining leg was found to be warmer than the normal leg [251]–[254]. Harding et al. in 1997 found that that thermal imaging has many advantages when compared with Ultrasonography (USG) and Venography. According to study, when thermography is used as the first test, the USG and Venography requirements are reduced by a factor of 33 percent. In this study, it is seen that none of the patients who excluded DVT by thermal imaging developed pulmonary emboli later. As a result of this, both unnecessary diagnostic tests and unnecessary anticoagulation therapy are not performed. This study is the pioneering work of thermography in this field [251].

In a study conducted by Deng et al. on New Zealand rabbits in 2012, it was found that subjects with experimental thrombosis generated in femoral vein had significant asymmetric heat distribution when comparing the heat differences between the legs before and after the study, and significant temperature increase on the side where thrombus was formed [252]. Another study by Kalodiki and colleagues has been performed with liquid crystal thermography, duplex USG and venography on 100 patients with clinical suspicion of DVT. A negative predictive value of 97% was found for the thermography performed within one week from the onset of symptoms. Based on these results, unnecessary USG and venography in 39 of 100 patients were prevented. USG alone was sufficient in 56 of the remaining 61 patients, but USG was not performed due to strained and sensitive legs in 6 patients and venography was required. When this method is used, 1 thrombus is bypassed and 3 patients are given unnecessary treatment. The algorithm in this study alone reduced costs even though it was not fully effective [253]. In a study conducted by Holmgren et al. in 1990 with 102 patients; thermography, thermal profile and impedance plethysmography, venography are compared, the sensitivity of the thermal imager measurements was 83% and the specificity was 55% [254]. In recent years, according to the study by Deng et al. sensitivity was found to be 88.33%, specificity was 65.00%, false-positive diagnosis 11.67, and false-negative diagnosis 35.00% [255]. However, the region of interest is determined by the user and personal experience can affect the result.

In this study; a computer-aided pre-diagnostic system has been developed using infrared thermal imaging for the diagnosis of DVT disease and the integration of the currently available tests has been proposed.

4.2. MATERIAL AND METHOD

4.2.1. Experimental Conditions in Medical Thermography

Infrared radiation emitted from a surface is correlated with the experimental conditions since it is dependent on the humidity, air flow and ambient temperature. For this reason, in medical applications where only a few degrees of difference are observed, controlled environmental environments for thermography experiments are an absolute necessity. Therefore, a standard protocol should be followed for comparison of thermographic images.

To minimize the effects of external factors, an ideal imaging room was created, with temperatures between 20 and 22 degrees Celsius, humidity levels of around 60 percent with a tolerance of 5 percent, no daylight and fluorescent lamps illuminated, no ventilation directly affecting patients and no external heat source. Under these conditions, patients were allowed to rest for 15 minutes to balance the basal metabolism in such a way that their legs were exposed. The data was taken from the front or back of the leg (Fig. 4.1), from the wrist alignment to the knee joint with the Testo 875i model thermal cameras, followed by a standard protocol by experienced physicians.

Figure 4. 1 Image acquisition with thermal camera

4.2.2. Material

In this study, the use of the information and materials of the volunteers and the patients was carried out with the approval of Gaziantep University Ethics Committee no. 2015/33 (09.02.2015).

Seventy patients who were suspected of DVT by complaints such as leg pain, swelling, color change to their emergency clinic were selected for the study. Two patients who had previously undergone subtotal limb amputation due to trauma and circulatory disturbance in the lower extremity were excluded from the study. Two patients who were not able to position because of orthopedic problems were not included in the study. A patient also was not included in the study because he was opposed to taking images from his leg. In addition, 26 people who were not complainants and who were healthy due to the evaluation were determined as the control group. Firstly infrared

thermal images were taken from the subjects under ideal conditions. The CDUSG reviews made both in the Emergency Medicine and the Radiology departments were then reported for comparison.

4.3. THEORY AND CALCULATIONS

4.3.1. Developed System

Non-invasive imaging is an application that is easy to apply without any harm to the patient but requires interpretive knowledge and experience. With subjective interpretations of limited trained operators, full reliability of diagnosis is sometimes not possible. A software system developed for clinical use will increase reliability by contributing to objective evaluation. When thermal imaging methods used in the literature are examined; it has been seen that clinicians focus on only certain points of the images in the direction of their experience, and a result is obtained with the statistical calculations of the data obtained from them. Because the software that comes with the thermal camera does not allow detailed examination and causes the problems mentioned. As a matter of fact, the first images taken from the patients before the study were evaluated in this way and it was concluded that these patients should be evaluated independently of the person who receives or interprets leg images. Thus, a completely software-based computer-aided diagnostic system has been developed for this purpose. The flow diagram of the proposed system is shown in Figure 4.2.
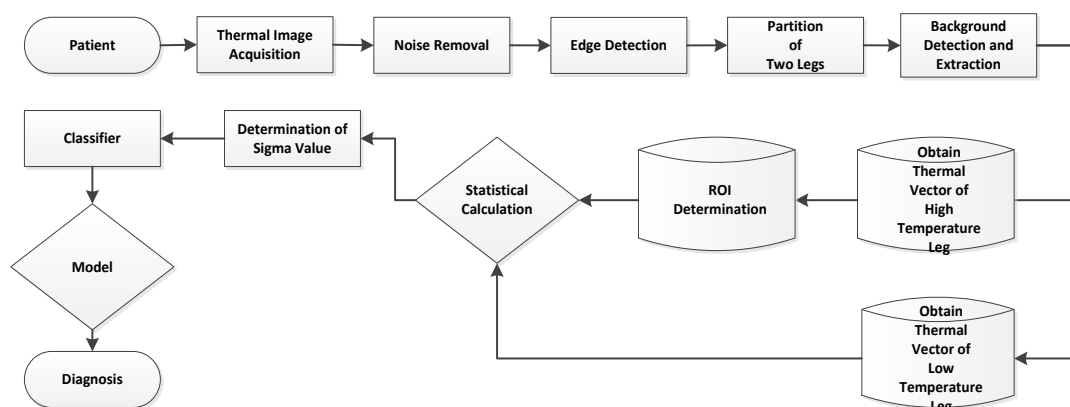
Figure 4. 2 Flow diagram of the developed system

i. Converting Data to Image

Since the camera software does not allow detailed examination, the received data are recorded as real temperature values in ℃ of 160x120 matrix size. This data patient-specific minimum and maximum temperature values are referenced and scaled into 8-bit grayscale images.

ii. Noise Reduction and Sharpening

The obtained images are passed through 5 x 5 Wiener filter for noise reduction and in order to make the segmentation more comfortable, the contrast of low and high valued pixels has been increased by CLAHE method.

iii. Background Extraction and Object Segmentation

By using Roberts edge detection method [236], all the edges are found in the image. The picture is divided into two by vertically controlling the vertical edge to start from the center of the picture. Then, using the following algorithms, the two leg images were evaluated independently of each other and the segmentation was made without any interaction. Three separate algorithms have been used to operate the partition in each condition, but the final algorithm has been left to the operator according to the results.

Otsu Thresholding Algorithm

In the developed system, Otsu method [237], which is widely used in the literature, was used as a first method. In this method, it is assumed that the image consists of two color classes, the background and the foreground. After the grey level histogram is computed, the in-class variance value (Eqn. 4.1) of these two color classes for all threshold values is calculated. The threshold value that allows this value to be the smallest is the optimum threshold value.

The weighted in-class variance is:

$$\sigma_w^2(t) = q_1(t)\sigma_1^2(t) + q_2(t)\sigma_2^2(t) \qquad (4.1)$$

where

$$q_1(t) = \sum_{i=1}^{t} P(i) \, , q_2(t) = \sum_{i=t+1}^{I} P(i)$$

$$\sigma_1^2(t) = \sum_{i=1}^{t} [i - \mu_1(t)]^2 \frac{P(i)}{q_1(t)} \, , \sigma_2^2(t) = \sum_{i=t+1}^{I} [i - \mu_2(t)]^2 \frac{P(i)}{q_2(t)}$$

Using the threshold, the image is converted to a dual color system in black and white. Subsequently, the fields formed by the connected pixels are found independently of each other and the largest object with the maximum number of pixels is determined. The leg is removed from the background owing to the obtained position.

Correcting Non-uniform Illumination Algorithm

When the images taken from the patients are examined, it is seen that the central region where the legs are located generally has a brighter illumination compared to the edge regions because it is aligned to the center of the picture. In some patients, it has been seen that the Otsu algorithm caused the error.

In the correcting non-uniform illumination algorithm, an artificial image estimation is performed in which the center is bright and the edge regions are dark for the background. For this reason, a disk-shaped structuring element is used. The artificial image is removed from the original image to ensure that the illumination is correct (Eqn. 4.2). Thereafter, the sharpening process was again performed like the pre-processing section. After this process, Otsu algorithm is repeated and the leg is separated from the background.

$$\text{Corrected Image} = \text{Image} - \text{Artificial Image} \tag{4.2}$$

Marker controlled Watershed Segmentation Algorithm

In the Watershed Transform algorithm, image segmentation is performed using image topology [242]. The image is considered to be a geographical shape as a low valued pixels like pit and a high valued pixel like peak. Segmentation is done by drawing junction points. Over-segmentation is the biggest disadvantage of watershed transformation. Pointer controlled segmentation is done to remove the problem of over-segmentation.

In this algorithm, a segmentation function is firstly established for the detection of objects in dark areas. Subsequently, each object associated pixels in the foreground of the picture and its non-object pixels in the background are determined. The segmentation function is changed by using the mark pixels obtained from the foreground and background. Finally, the leg is separated from the background by finding the watershed transformation of the segmentation function. The block diagram of the algorithm is given in Figure 4.3.
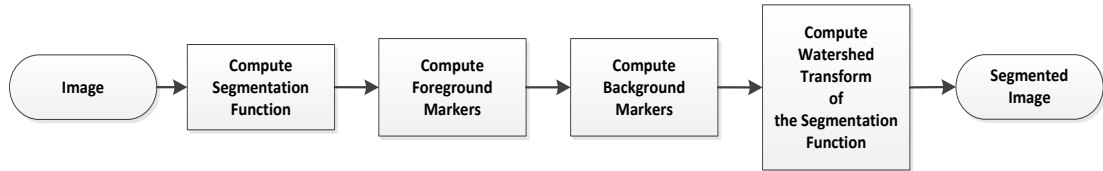
Figure 4. 3 Flow diagram of the Marker Controlled Watershed Segmentation

### 4.3.2. Determination of Region of Interest

After background removal, heat maps of two legs are generated. Legs with high and low heat are classified using heat averages of individual legs. As a result of classification, the leg with high temperature is considered as suspicious and the region of interest (ROI) is determined according to the threshold value (Eqn. 4.3). In this examination, if the heat distribution is not homogeneous and there is an abnormality, the potential disease area (ROI) is determined by the threshold value, and a new heat map is created according to the ROI, otherwise a homogeneous distribution (non-complaining leg) will yield itself as ROI. Accordingly, there is also no need to find an ROI when the same threshold value is applied to the leg with low heat, as it usually gives shape of the leg itself.

$$Threshold\ Value = \frac{\max(Comp.Leg\ Heat\ Map) + \min(Comp.Leg\ Heat\ Map)}{2} \qquad (4.3)$$

So, individual heat maps are created for the complaining and non-complaining legs by using ROI analysis. These maps contain thermal data corresponding to each pixels obtained from the leg. For statistical analysis, these vectors are used to determine the mean and standard deviation of patient and normal subjects. The use of the developed software on images taken from patients and normal person is shown in Fig. 4.4, 4.5 and 4.6 (See Appendix for more images).
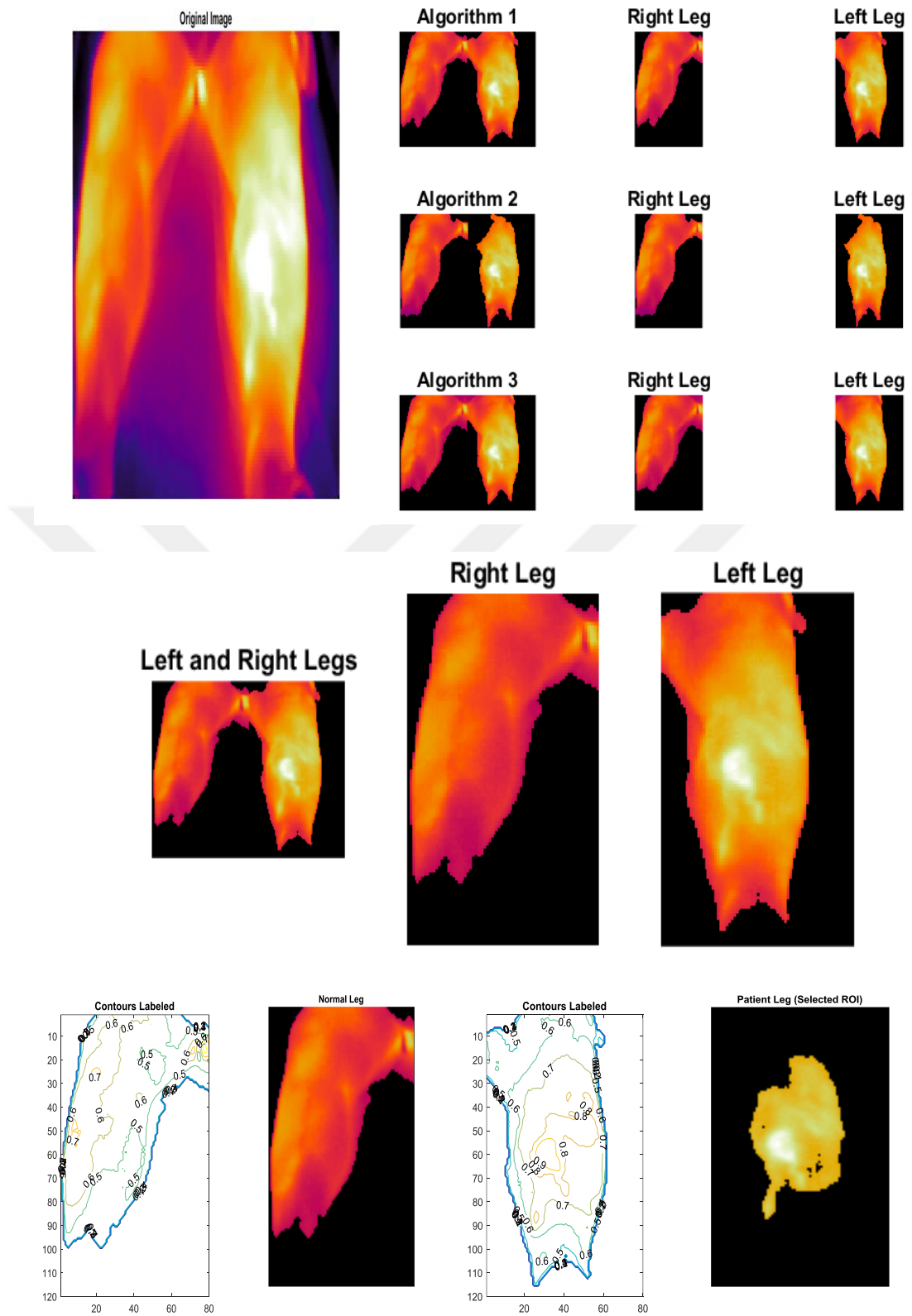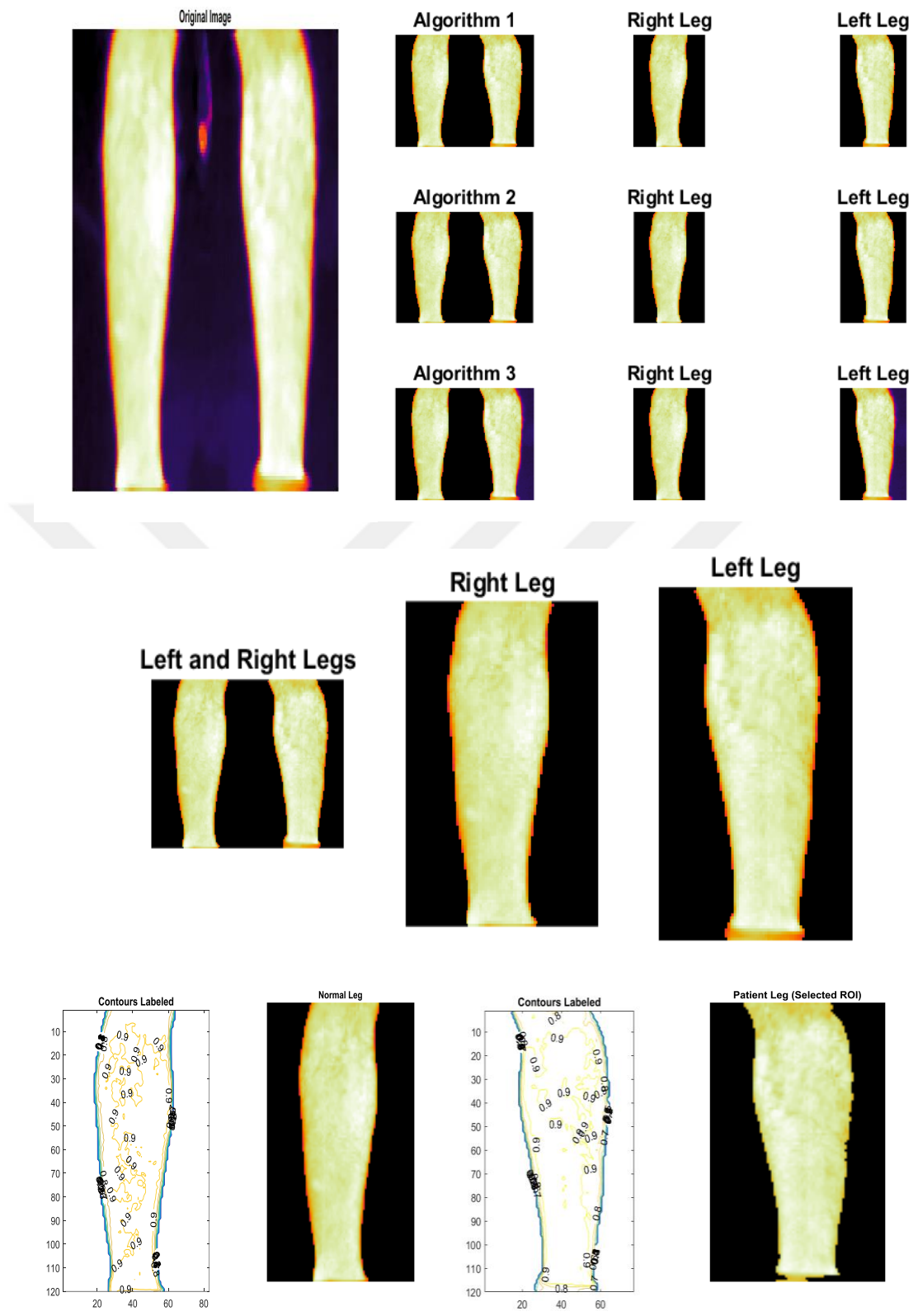
Figure 4. 4 Resultant Images of the Developed Software (PATIENT 1)
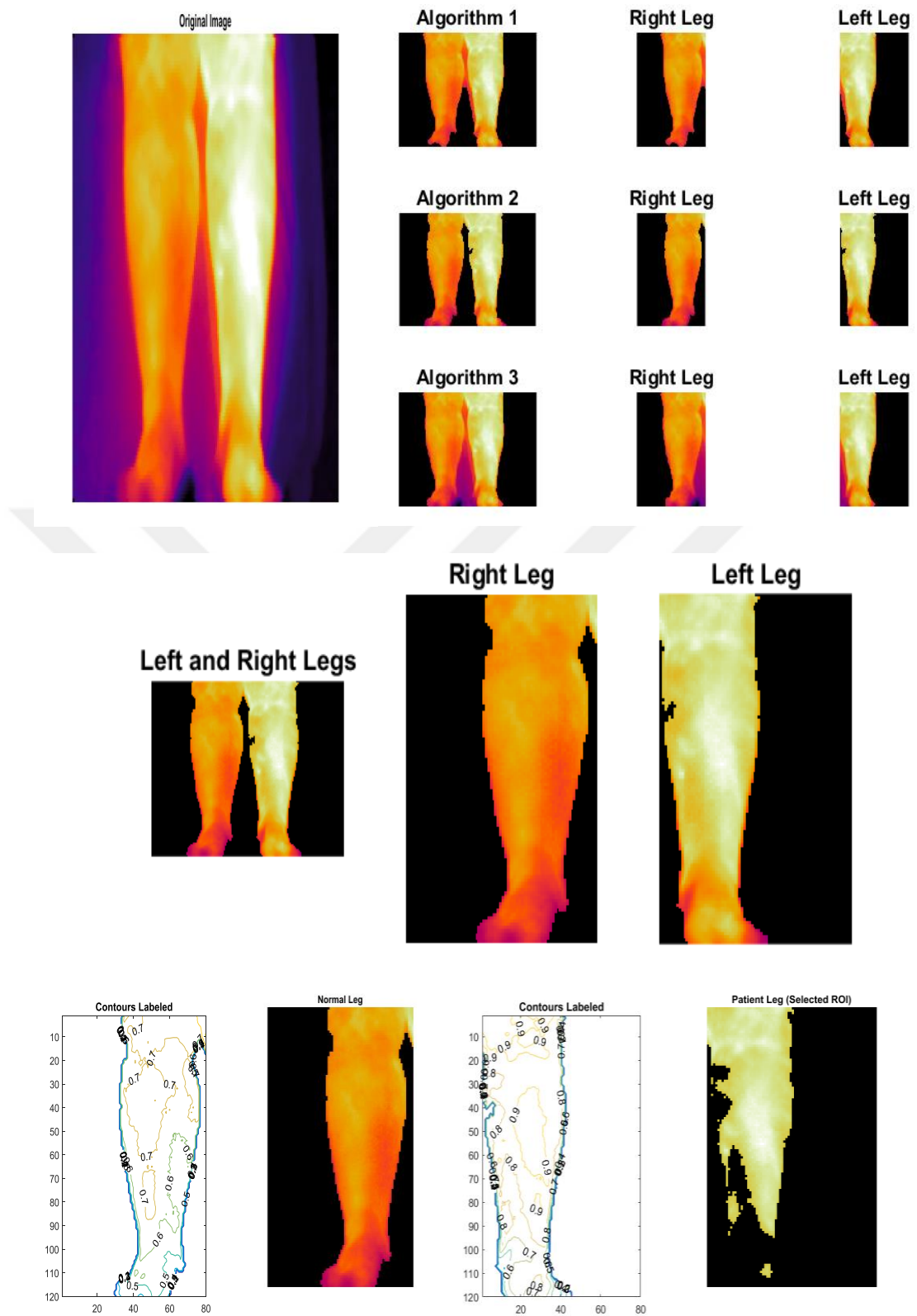
Figure 4. 5 Resultant Images of the Developed Software (PATIENT 2)

Figure 4. 6 Resultant Images of the Developed Software (NORMAL)

4.3.3. Statistical Analysis

The analysis of the data obtained in this study was performed by using the Shapiro-Wilk test since the Shapiro-Wilk test gives more reliable results for data sets smaller than 2000. As it is in Table 4.1, the significant values are above 0.05 for Acute, Subacute and Chronic DVT, we can reject the alternative hypothesis and say that the data come from a normal distribution. Independent-sample t test was used for paired comparisons of independent and normal distribution data. On the other hand, Mann-Whitney U test was used for paired comparisons of independent and non-normal distribution data. The results of the nominal value groups were analyzed by Chi-Square test. The results were expressed as mean ± standard deviation. Since the p value indicates the amount of possible error and shows a statistically significant difference in a comparison, $p<0.05$ was considered statistically significant in all comparisons.

Table 4. 1 Tests of normality for all subjects

|	DIAGNOSIS	Kolmogorov-Smirnov			Shapiro-Wilk		
		Statistic	df	Sig.	Statistic	df	Sig.
TEMPERATURE MEAN DIFFERENCE	**ACUTE DVT**	0.125	15	0.2	0.942	15	**0.412**
	SUBACUTE DVT	0.209	7	0.2	0.919	7	**0.465**
	CELLULITE	0.19	13	0.2	0.93	13	**0.337**
	OTHER	0.182	30	0.012	0.878	30	**0.003**
	CHRONIC DVT	0.164	4	.	0.994	4	**0.975**
	NORMAL	0.185	27	0.019	0.908	27	**0.02**

In all study groups, regardless of diagnosis, the mean temperature of the complaining and non-complaining legs was 33.62 ± 1.22 and 31.93 ± 1.44 ℃, respectively, and a mean difference of 1.69 ℃ between the two legs was determined and this was statistically significant ($p<0.0001$). The statistical analysis of the average leg temperature values between control and study groups is summarized in Table 4.2. In the control group formed with twenty-seven participants, the aim was to find the natural temperature difference between the two legs of healthy individuals. In this group, the average temperatures of the legs of the individuals were 32.74 ± 0.86 ℃ and 32.61 ± 0.87 ℃. The mean temperature difference for both legs was measured as 0.13 ℃ and statistically insignificant ($p=0.5903$).

Table 4. 2 Comparison of the average leg temperature values between control and study groups

Group	Leg temperature with high temperature (℃)	Leg temperature with low temperature (℃)	P*
Control Group	32.74±0.86	32.61±0.87	0.5903
Study Group	33.62±1.22	31.93±1.44	<0.0001

*Independent sample test

The participants were classified according to the diagnosis and the comparison of temperatures of the complaining and non-complaining legs according to the diagnosis of them is shown in Table 4.3 and in Figure 4.7. As can be seen from the Fig. 4.7, while normal patients are located near y = x axis, patients in the study group are getting away from the axis.
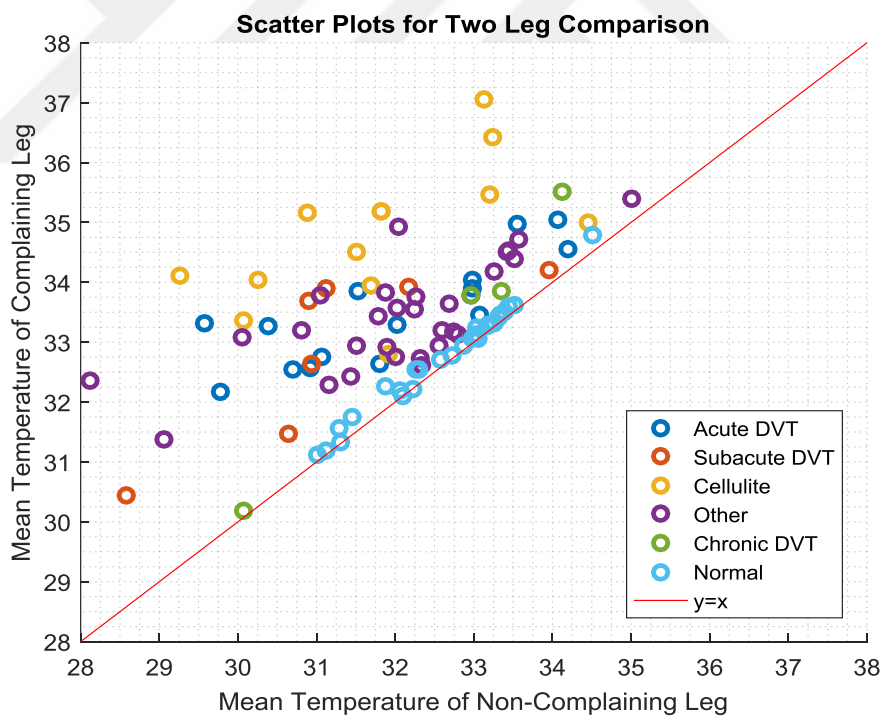
Figure 4. 7 Scatter plots of leg temperatures according to the all groups

Table 4. 3 Comparisons of leg temperatures according to the study groups

Diagnosis	# of Cases	Mean Temperature of Complaining Leg (°C)	Mean Temperature of Non-Complaining Leg (°C)	P*
Acute DVT	15	33.49±0.90	31.91±1.51	0.0017
Subacute DVT	7	32.89±1.45	31.18±1.62	0.0595
Chronic DVT	4	33.33±2.24	32.63±1.76	0.6406
Cellulite	13	34.79±1.17	31.79±1.46	<0.0001
Other	30	33.43±0.88	32.08±1.36	<0.0001

*Mann-Whitney U test

4.3.4. Decision-Making for Disease Diagnosis

In the empirical sciences, the three sigma rule means a heuristic method in which "almost all" values are taken to lie in the three standard deviations of the mean, i.e., 99.7% probability that "close to certainty" is useful [245]. A sample normal distribution plot is shown in Fig. 4.8 with a 3 sigma rule. The benefit of this intuition is largely dependent on the problem that is being considered. For example, in social sciences two sigma effects (95%) can be considered "important" for a result whereas in particle physics five sigma effects (99.99994%) are described as a "discovery". In this study, infrared imaging is considered to be only a preliminary test and the best possible sigma value is determined according to objective evaluations and explained in the following sections. First, sigma values (σ) are calculated separately (Eqns. 4.4-4.5) for each subject by using heat maps.

$$\sigma = \frac{\mu}{\xi} \tag{4.4}$$

$$\mu = \mu_P - \mu_N \text{ and } \xi = \sqrt{\xi_P{}^2 + \xi_N{}^2} \tag{4.5}$$
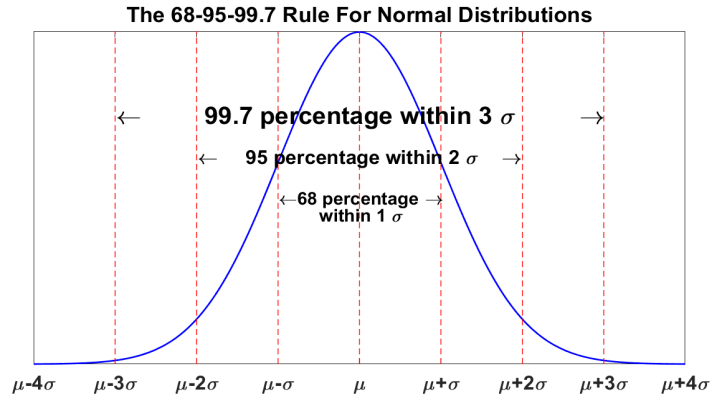
where $\sigma = Sigma\ Value,\ \mu = Mean\ Difference$

$\mu_P = Mean\ of\ Complaining\ Leg\ Heat\ Map$

$\mu_N = Mean\ of\ Non-Complaining\ Leg\ Heat\ Map$

$\xi = Total\ Standard\ Deviation$

$\xi_P = Standard\ Deviation\ of\ Complaining\ Leg\ Heat\ Map$

$\xi_N = Standard\ Deviation\ of\ Non-Complaining\ Leg\ Heat\ Map$

Figure 4. 8 3-Sigma Rule for Normal Distributions

Some statistical measurements such as sensitivity, specificity, positive predictive value, negative predictive value, accuracy and Youden's Index [246] are important test instruments used to evaluate the performance of the diagnostic test. The confusion matrix (Table 4.4) is used to calculate these statistical values (Eqns. 4.6-4.11).

Table 4. 4 Confusion Matrix

		PREDICTED CONDITION	
		Prediction Positive	**Prediction Negative**
TRUE CONDITION	**Condition Positive**	True Positive (TP)	False Negative (FN)
	Condition Negative	False Positive (FP)	True Negative (TN)

$$Sensitivity \ = \frac{TP}{TP + FN} \tag{4.6}$$

$$Specifity \ \ = \frac{TN}{TN + FP} \tag{4.7}$$

$$Positive\ Predictive\ Value \ = \frac{TP}{TP + FP} \tag{4.8}$$

$$Negative\ Predictive\ Value = \frac{TN}{TN + FN} \tag{4.9}$$

$$Accuracy = \frac{TP + TN}{TP + FN + FP + TN} \tag{4.10}$$

$$Youden's\ Index, J \ = \ Sensitivity + Specifity - 1 \tag{4.11}$$

where *TP*, *FN*, *TN*, and *FP* represent true positive, false negative, true negative, and false positive values, respectively.

Using the calculated sigma values from Eqn. 4.4 for all subjects, a general sigma value is set to provide the maximum diagnostic accuracy and the Youden's index for diagnosis as seen from Fig. 4.9 and 4.10. That is; a specific sigma value, which is 0.33, is chosen as the corresponding peak value of accuracy and Youden's index. As a result of objective evaluations, subjects are classified as 'PATIENT' when the sigma is above 0.33 and classified as 'NORMAL' when it is below. The same sigma value is also consistent with 'DVT or NOT' discrimination. Graphical representations of the performance of the diagnostic test based on different sigma values are shown in Fig. 4.9 and 4.10.
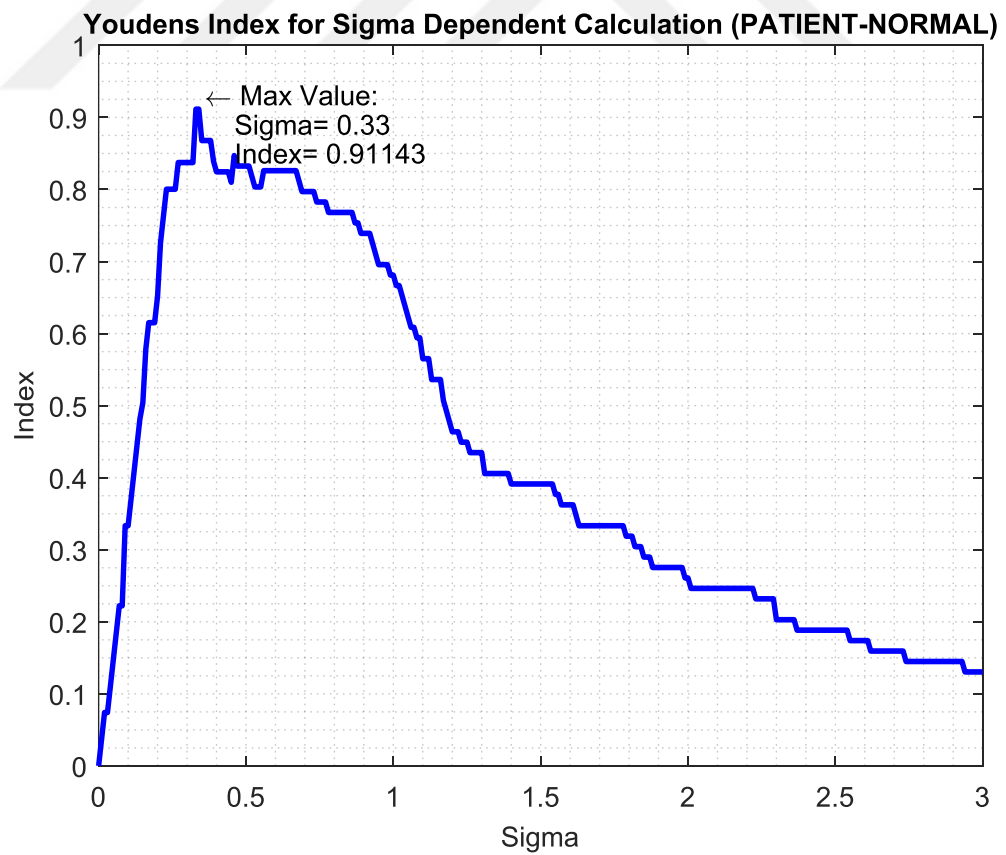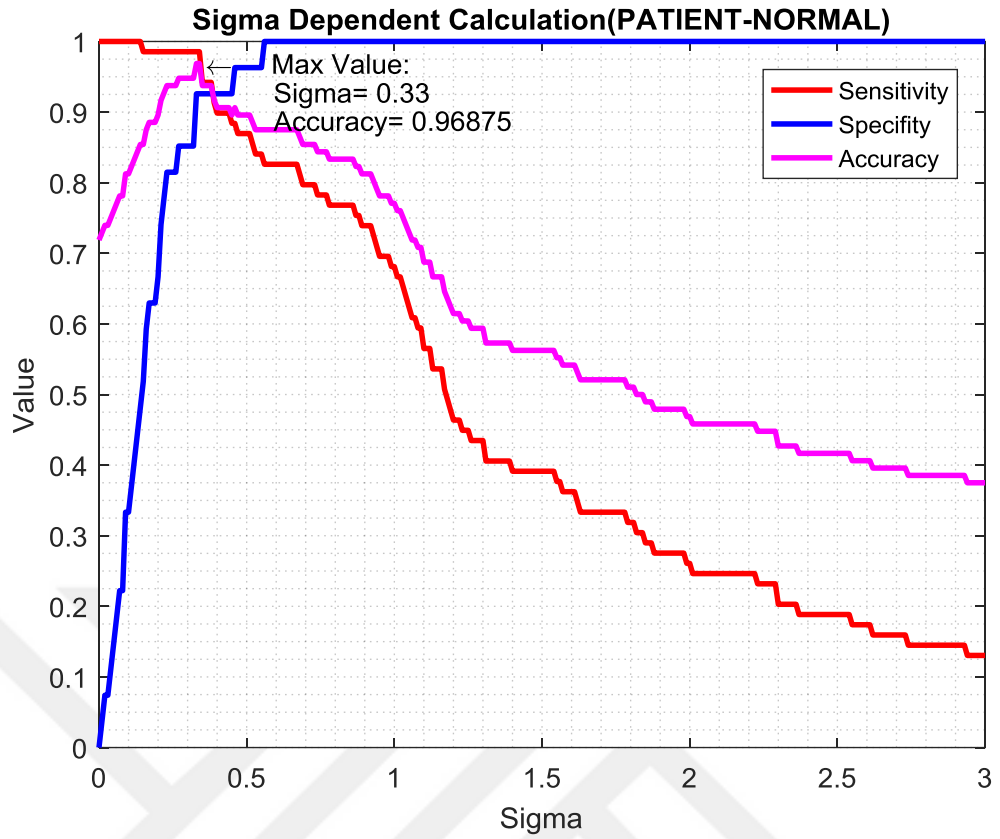
Figure 4. 9 Graphical Representation of Maximum Accuracy and Maximum Youden's Index Value (PATIENT - NORMAL)
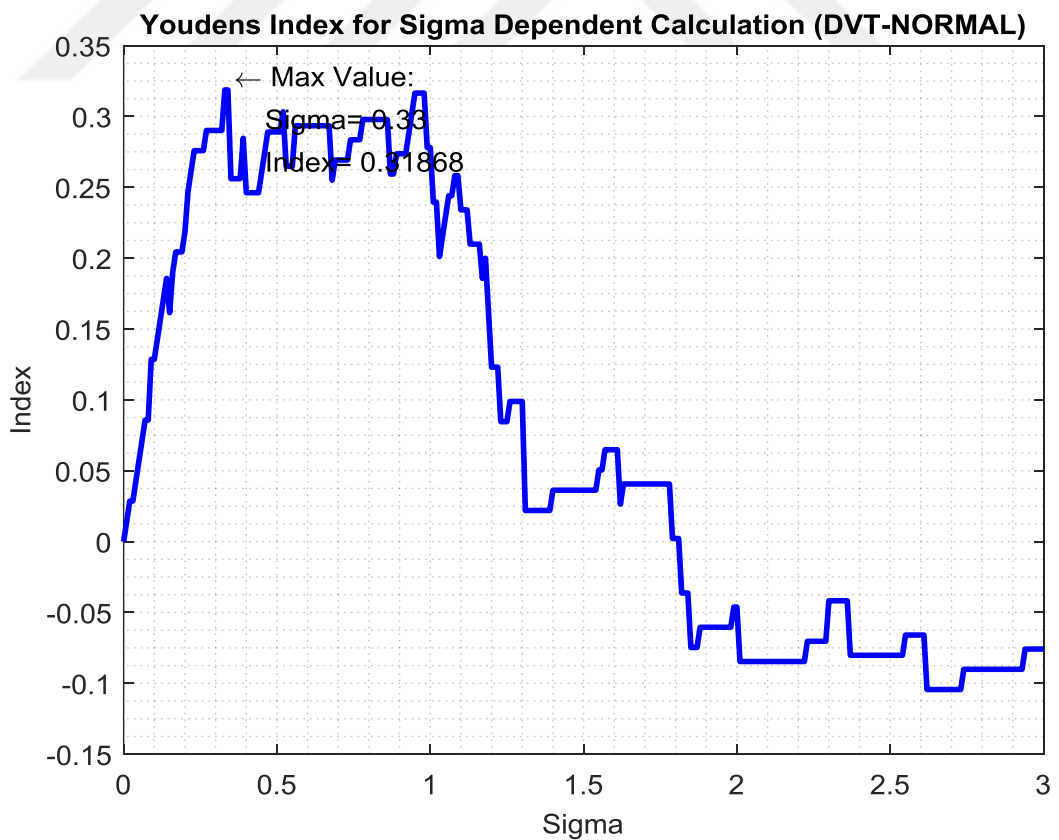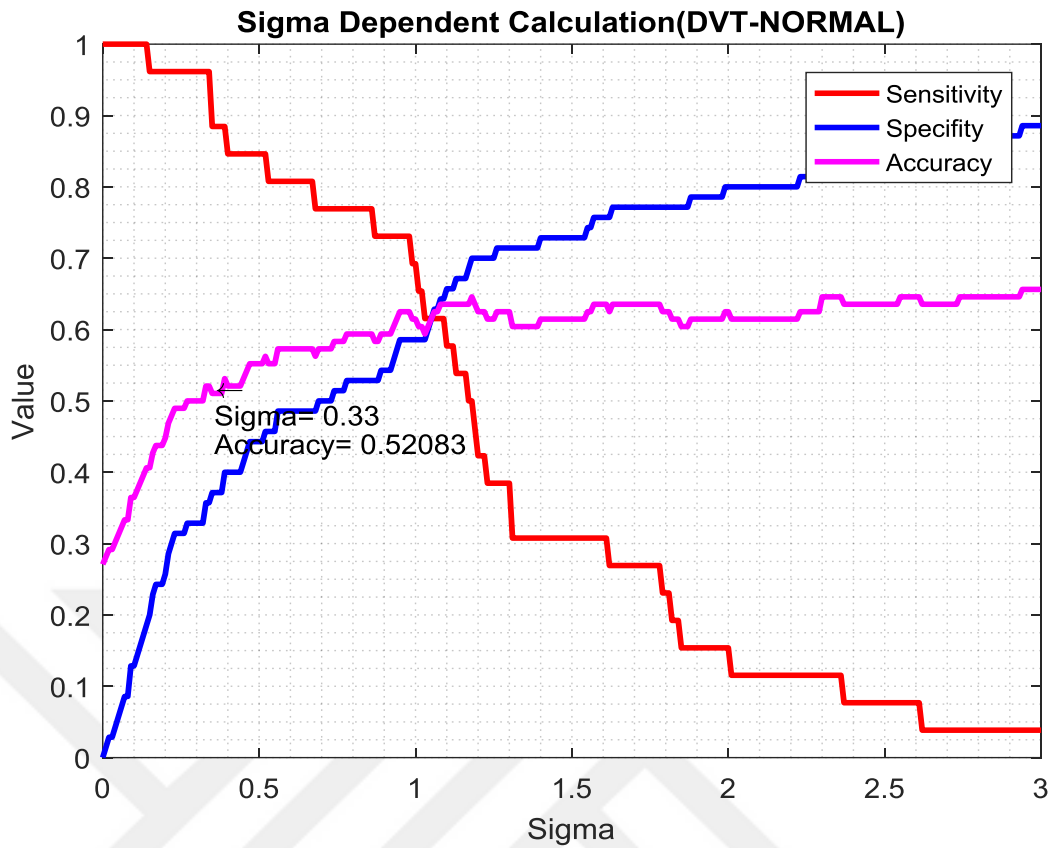
Figure 4. 10 Graphical Representation of Accuracy and Maximum Youden's Index Value (DVT or NOT)

4.4. RESULTS AND DISCUSSION

In this study; acute DVT was diagnosed in 21.74% of patients ($n = 15$), subacute DVT in 10.14% ($n = 7$), chronic DVT in 5.79% ($n = 4$) and cellulitis in 18.84% of patients ($n = 13$). Significant sigma differences were detected in all 15 patients with acute DVT and in all 7 patients with subacute DVT by using infrared camera. No significant difference in sigma was found in 1 of 4 patients with chronic DVT. Sigma significance in patients with DVT diagnosis is presented in Table 4.5. For different subjects, overall scatter and box plots according to sigma values are also shown in Figure 4.11. As can be seen from Fig. 4.11, any disease increases sigma value.

Table 4. 5 Results obtained with Thermal camera in patients with DVT.

Diagnosis	Significant Sigma Difference	Meaningless Sigma Difference	Total
Acute DVT	15	0	15
Subacute DVT	7	0	7
Chronic DVT	3	1	4

With the infrared imaging, 98.55% ($n = 68$) of the patients had significant sigma differences and 36.76% ($n = 25$) of the patients had DVT diagnosis. DVT was determined by radiological evaluation in only 1 patient with no significant temperature difference with the developed system. Comparisons of CDUSG according to infrared thermal imaging with 'PATIENT or NORMAL' and 'DVT or NOT' at a given sigma value is reported in Table 4.6.

Table 4. 6 Comparisons of IR Camera-CDUSG

PATIENT - NORMAL (Sigma>0.33)					DVT or NOT (Sigma>0.33)				
		IR Camera					IR Camera		
		PATIENT	NORMAL	Total			DVT+	DVT-	Total
CDUSG	PATIENT	68 (TP)	1 (FN)	69	CDUSG	DVT+	25 (TP)	1 (FN)	26
	NORMAL	2 (FP)	25 (TN)	27		DVT-	45 (FP)	25 (TN)	70
	Total=	70	26	96		Total=	70	26	96

Sensitivity = 0,985507246
Specifity = 0,925925925
Accuracy = 0,96875

Sensitivity = 0,961538462
Specifity = 0,357142857
Accuracy = 0,520833333
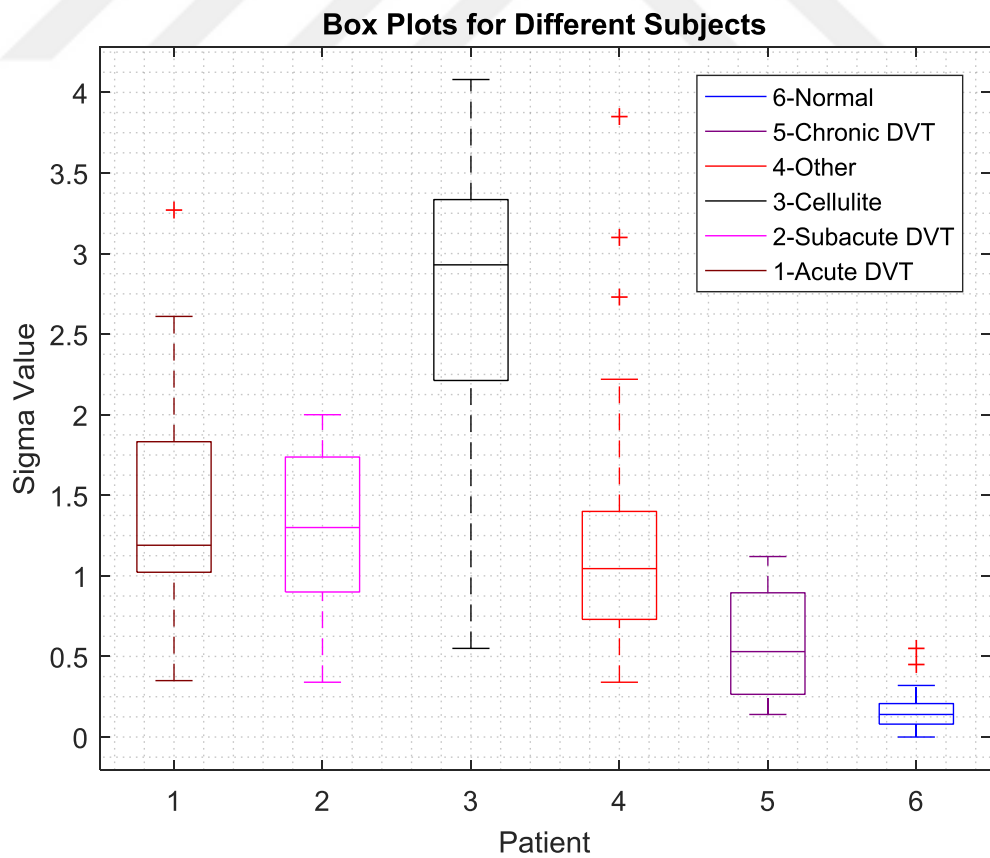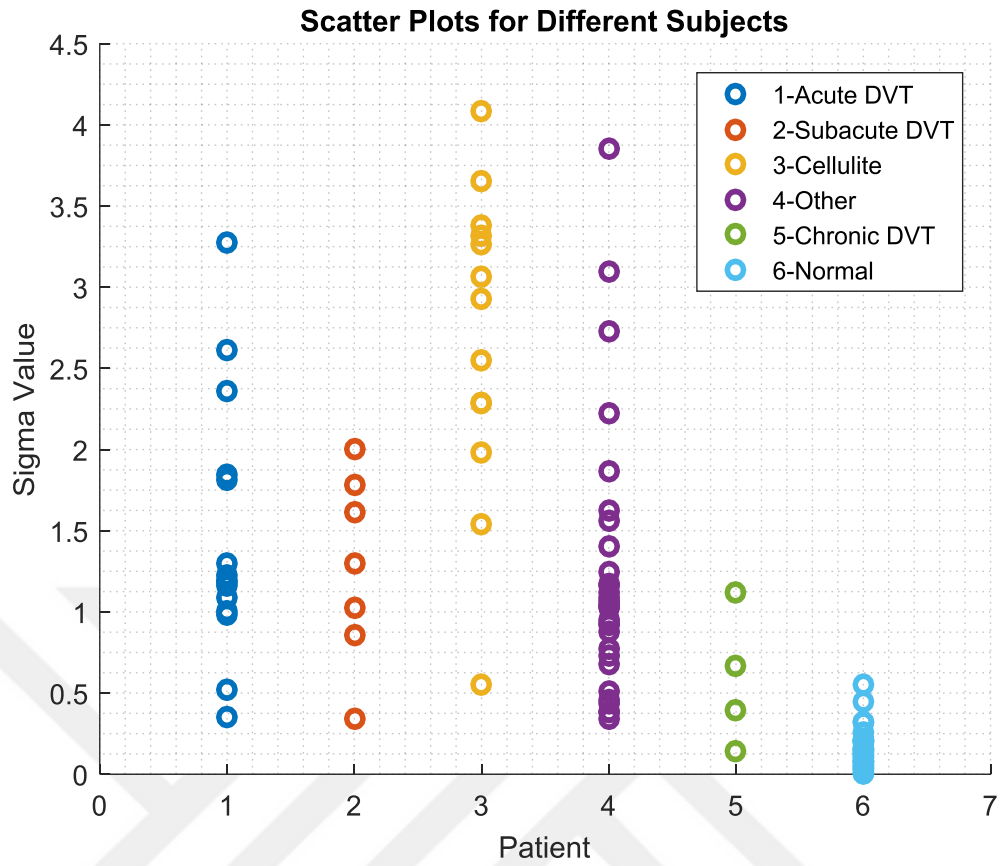
Figure 4. 11 Scatter and Box Plots according to sigma values for different subjects

Using the data in Table 4.6, the performance of the diagnostic test according to Eqns. 4.6 – 4.10 can be calculated separately as 'Patient-Normal' and 'DVT or Not'. The sensitivity of the diagnostic test in performing 'Patient-Normal' discrimination is 98.55%, specifity is 92.59%, positive predictive value is 97.14% and negative predictive value is 96.15%, while the sensitivity of the diagnostic test in making 'DVT or Not' discrimination is 96.15%, specifity is 35.71%, positive predictive value is 35.71% and negative predictive value is 96.15%. According to these results, thermal imaging has such good results in 'Patient-Normal' division, but it is not successful enough to distinguish 'DVT or Not' with the addition of other diseases. However, due to the fact that almost all DVT patients and Healthy people were diagnosed accurately in this study, infrared thermal imaging can be safely used as a preliminary test.

The data obtained from the clinical evaluation, laboratory results and imaging methods used in this study are compared with the CDUSG performed by radiology and are summarized in Table 4.7. The quantitative measure of the binary classification performance (ROC curve) of the system is also shown in Figure 4.12 and 4.13. Figure 4.14 shows combination of usage of IR camera, emergency bedside CDUSG (EB-USG) and D-dimer and control with radiology CDUSG (R-USG).

Table 4. 7 Performances of different diagnostic tests of DVT in this study according to the gold standard
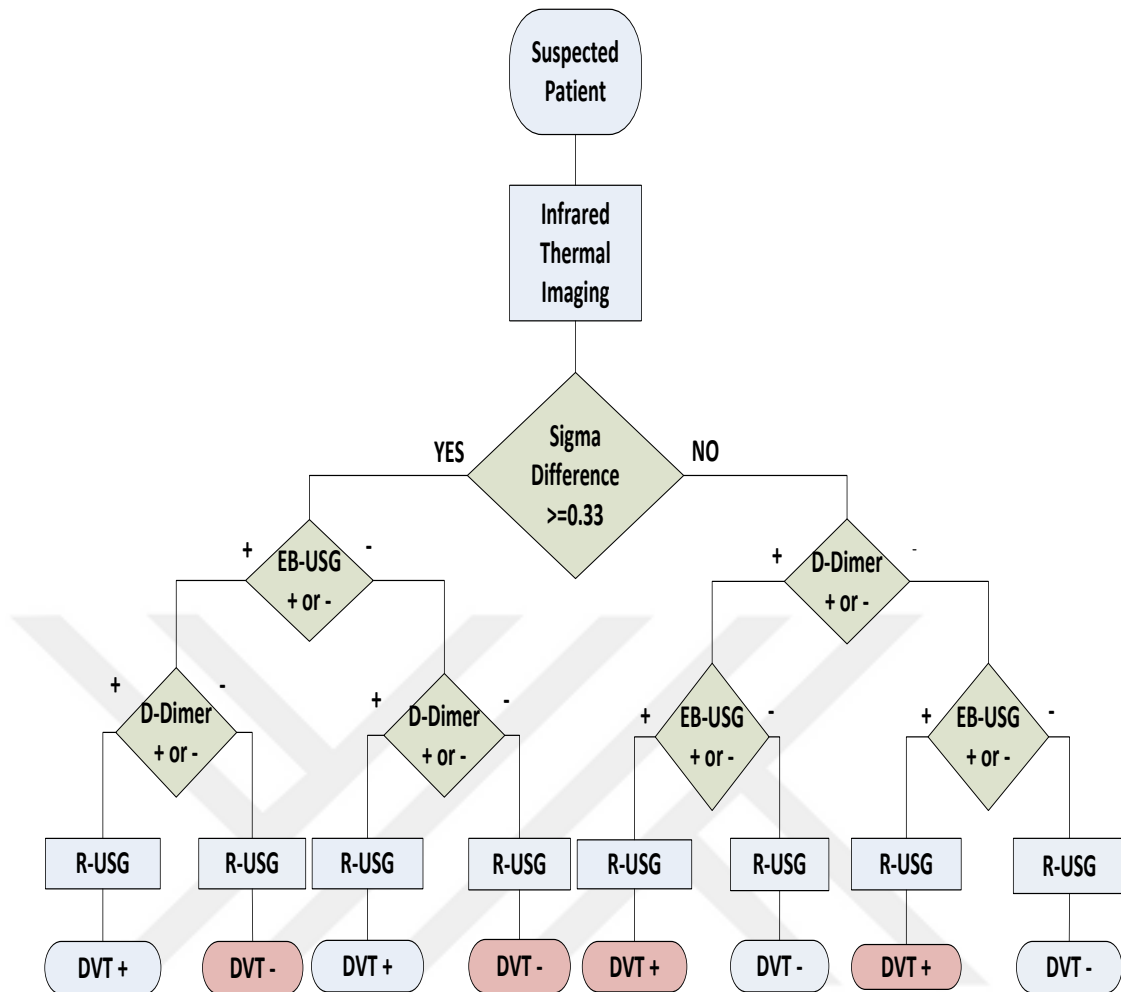
	Emergency Physician Bedside CDUSG	Infrared Camera	Wells Score	D-dimer
Sensitivity	%100	%96.15	%96.15	%96.15
Specificity	%95.55	%35.71	%6.66	%24.44
Positive Predictive Value	%92.85	%35.71	%37.31	%42.37
Negative Predictive Value	%100	%96.15	%75	%91.66
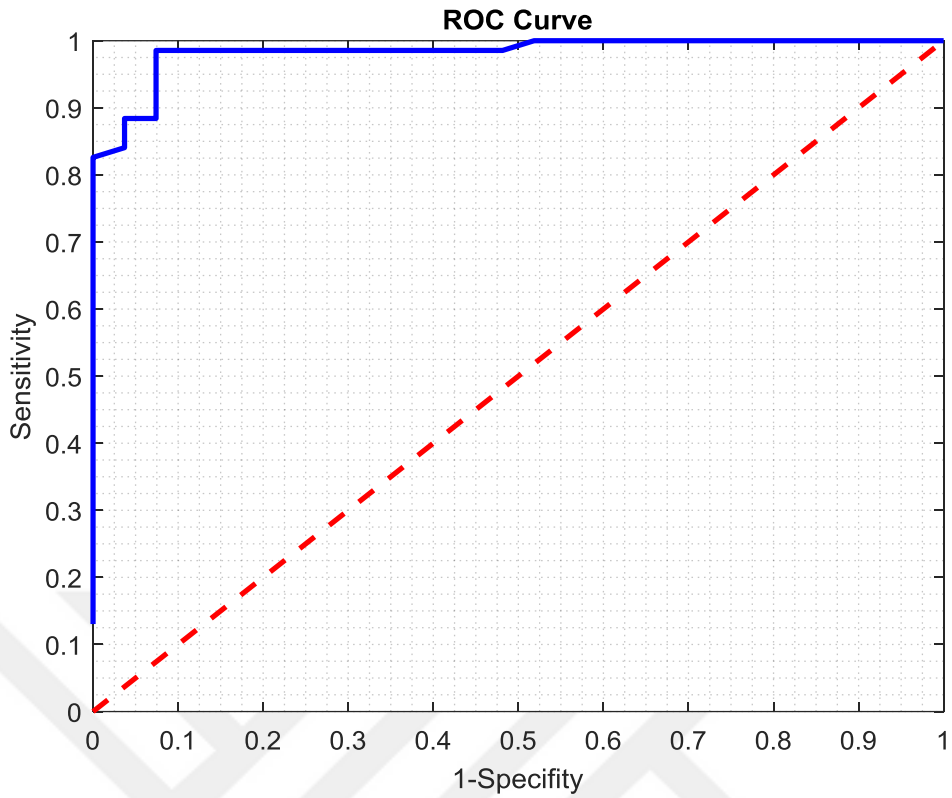
Figure 4. 12 ROC Curve for PATIENT-NORMAL Classification
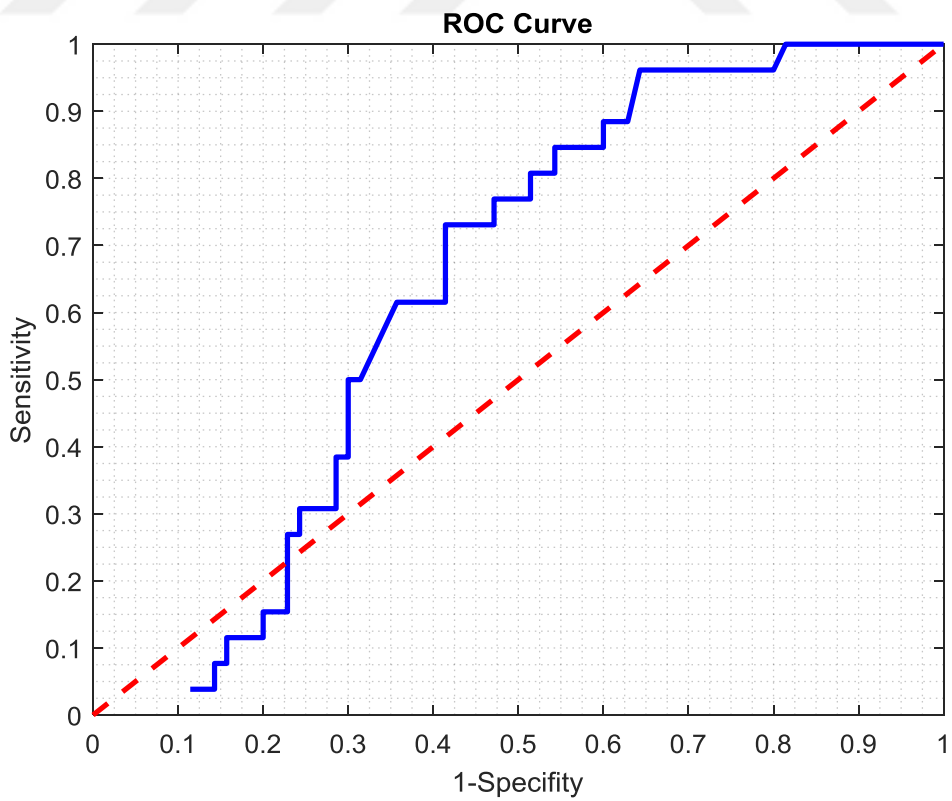
Figure 4. 13 ROC Curve for DVT-NOT Classification

Figure 4. 14 Combination of IR camera, Emergency bedside CDUSG (EB-USG) and D-dimer and control with Radiology CDUSG (R-USG)

4.5. CONCLUSIONS

Complaints such as pain, swelling, and redness in the legs are one of the common reasons among emergency patients, and there are many different diagnostic tools and algorithms that are accepted in determining the cause of these complaints like other diseases. However; these tools, algorithms and combinations should be continuously improved and upgraded for a better diagnosis. Therefore, patients can be treated quickly and correctly because the time lost is minimized and unnecessary treatments are avoided. As the cost of thermal imaging devices continues to fall and become mobile, the use of these devices will reduce both costs and delays due to physician shortages. Accordingly, the developed system can help such problems and be used as a pre-screening test for DVT.

In this study, except for healthy individuals, it is determined that the given sigma difference between two legs is significant in each of the subjects with any discomfort in the leg. Also, the temperature measurement with infrared camera is a successful first test for DVT in the acute phase while the diagnostic value is decreased due to the deterioration of arterial circulation of the leg in the subacute and chronic period of the disease. So, thermography can safely be used in patients with symptoms lasting from the onset of symptoms to 1 week.

As a diagnostic method, infrared thermography has high potential in scientific and medical research. Although thermal imaging is not yet considered as a reliable method, many diseases can be diagnosed by advanced research and development. If enough patient data are collected, the success rate will be further increased by applying machine learning algorithms for the possibility of person-specific diagnosis.

CHAPTER V

THE THERMAL IMAGING SYSTEM DESIGN IN THE DIAGNOSIS AND FOLLOW-UP OF PRIMARY AND SECONDARY RAYNAUD'S PHENOMENON

5.1. INTRODUCTION

Raynaud phenomenology is a triphasic color change that typically results in episodic ischemia at the fingertips caused by cold exposure and emotional stress. In this disease, pallor caused by vasospasm occurs first, followed by cyanosis and then hyperemia. In addition to these changes, pain, numbness, and burning sensation may be accompanied. Diagnosis of the disease without any connective tissue disease is called primary Raynaud phenomena or Raynaud disease.

If there is an underlying disease or pathology, it is called the Secondary Raynaud Phenomena and the result is the vasospasm of structurally abnormal vessels. The prevalence of Secondary Raynaud Phenomenon depends on the underlying disease. Approximately 5% of Raynaud phenomenon cases, a connective tissue disease occurs on the progressive stages, especially Systemic Sclerosis (Scleroderma, SSc). It is thought that the Raynaud Phenomenon may be a secondary to collagen tissue disorder if there is loss and enlargement in the nail bed capillaries. Raynaud's phenomenon is usually one of the first findings of patients with Scleroderma and is found in 95% of cases.

Scleroderma means skin hardening as a word. Although the most specific characteristic of the clinic is skin fibrosis (scleroderma), the disease is termed as "systemic sclerosis" because it can also be seen in internal organs such as the gastrointestinal tract, kidney, lung and heart. It is crucial to detect this disease at an early stage, where more aggressive treatment can be achieved in the early stages [256], [257]. Although the etiology of the disease cannot be fully elucidated, genetic susceptibility, environmental factors and infections are shown as possible agents triggering the pathogenic process.

Especially in those patients who have not been diagnosed or diagnosed correctly in the early period, finger and foot injuries caused by vascular disease can turn into gangrene over time and lead to finger, hand or foot loss. A similar disorder develops in our internal organs, and the vessel in the pulmonary artery, which carries the dirty blood from the heart to the lung, also begins to deteriorate. Especially in late-diagnosed patients, deterioration starts in the thin veins that go to the kidney. All these vascular disorders increase blood pressure in the described areas and can lead to severe heart and kidney diseases. Scleroderma does not only affect veins and skin. The basic logic of the disease is the deterioration of normal connective tissues. Because the connective tissue is all around the body, the amount of unaffected regions is very small.

In these patients, pulmonary disease may develop due to impaired normal development in the lungs. Breathlessness and dry cough are the first complaints of the lung. An important problem that develops in patients due to the same cause is the destruction of the entire food intake, stomach and intestines starting from the mouth. In addition, reflux-related chest burns, bloating in the abdomen and stomach areas, rapid satiety, diarrhea and constipation episodes, and serious weight loss are seen in these patients. Common features of all inflammatory rheumatic diseases are joint pain and swelling. At the same time, arthritis occurs in the hands and wrists and in the fingers. However, although joint damage does not appear as it is in rheumatoid arthritis, the hand is gradually becoming neither fully opened nor fully closed in order for the skin and subcutaneous connective tissue to be affected and the skin to adhere well to the underlying bone tissue.

Unlike all diseases in which the immune system is impaired, additional diseases are also seen in scleroderma. Thyroid diseases, other immune system disorders (systemic lupus, Sjögren, myosit, etc.) are the most typical examples. Pregnancy problems, early and stillbirths are common problems.

The most important point of treatment in such a complicated, difficult and long-lasting disease process is that all these changes can be diagnosed before they begin. With the developing technology in recent years, there has been considerable improvement in non-invasive imaging methods. Nowadays, portable optical imaging systems performing microvascular measurements have become faster and easier to acquire

images. These developments help to reveal premature pathology by allowing them to monitor extreme formations and changes (such as microvascular structure, blood volume, oxygenation and blood flow in the tissue) in the body.

The relationship between skin temperature and microvascular dermal perfusion is highly complex and depends on the body region. Unlike heat from environmental agents, skin temperature can be easily affected by many factors, such as subcutaneous and intramuscular blood flow, skin thickness and sweating. When such thermal changes occur, it is first necessary to investigate the environmental and later changes in the body. A number of thermographic studies have been conducted in the literature on what diseases are indicative of temperature changes in the body surface [9], [258], [259].

Human fingertips are very sensitive to external stimulation due to the presence of numerous blood vessels and neural structures in the finger. Investigation of thermoregulation and blood flow patterns in human hands is of great importance in the diagnosis of peripheral diseases. In various studies, the thermal and hemodynamic responses of the human extremities to different stimuli have been investigated.

In a study conducted, it was shown that infrared imaging can be used to distinguish between healthy persons who have cold hands and those with impaired perfusion on the hand [260]. In another study, thermography was used as a common method to determine the rewarming rate of fingers during vasospastic diseases such as Raynaud's phenomenon (RF) after cold stress applied to the hands [261].

Shitzer et al. [262] measured the temperature and blood perfusion of the fingers in cold air exposed environments. Bornmyr and Svensson [263] observed changes in skin blood flow and temperature in the finger after smoking. Zontak et al. [264] investigated the response to skin temperature using dynamic thermography and wanted to detect hemodynamic changes due to variations in thermal images. Ducharme et al. [265] observed blood flow and temperature in the fingers to identify the critical factor for sustaining finger motility during cold air exposure. Sakashita [266] also measured blood temperature and blood pressure in the hands to investigate the relationship between autonomic nervous system (ANS) regulation and human physiological

parameters after mental activity and exercise or before and after eating. Hara and Nagaya [267] measured the temperature changes of a hand and a glove filled with gelatin using an electric heater. They observed that the temperature of the human hand increased and gradually approached a constant temperature, but the temperature of the gelatin-containing glove was constantly increasing.

Blank and Kargel [268] developed digital image processing techniques for dynamic thermal images and analyzed the temperature changes in the palm of different people who chew nicotine gum or smoke over time. It was observed that the temperature of the palms and fingers decreased significantly when smokers smoked, while that of the nicotine chewing gums increased and decreased in half. In the non-smoking group, temperature increases were seen during both smoking and chewing nicotine gum. Although the effects of nicotine on vasomotor control and temperature were difficult to assess, they had the conclusion that nicotine was a powerful and immediate effect on the human body. Image processing techniques developed by them are useful for most dynamic image processing applications.

A number of IR imaging studies have been performed using the finger response to the controlled cold challenge to differentiate the primary RF from the secondary RF. In fact, SSc, healthy controls (HCS) and PRP show different thermal recovery as a result of functional stimulation to the same standard [219], [269]–[274]. Examples of temperature vs. time curves obtained from experimental recovery data in HCS, SSc, and PRP are reported in Fig. 5.1 [261].
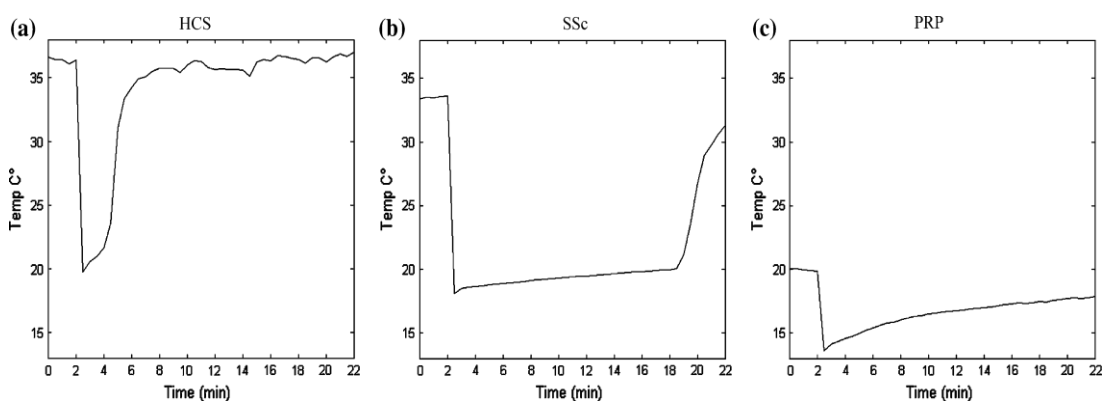
Figure 5. 1 Temperature vs. time curves obtained from thermal imaging data during cold stress test in (a) HCS, (b) SSc, and (c) PRP **[261]**

When the applications of the various imaging modalities discussed in the literature are examined, the precision of most studies depends on the experience of the clinicians. In such studies, statistical calculations are made with the information obtained by the observations of the clinicians. Such studies have only established the link to disease, but have not made an objective contribution to the assessment of the severity of the disease. For a more accurate assessment of the results, it is seen that there is a need for studies in which the clinician's intervention had little or no intervention. In this study, image processing method is proposed to help objective assessment of the diagnosis of the primary and secondary Raynaud phenomenon.

5.2. MATERIAL AND METHOD

This study includes both primary (PR) and secondary Raynaud patients (Scleroderma, SSc) and healthy volunteers (HCS). These groups are routinely examined in their first application and take appropriate tests if they have any diagnosis. Raynaud's condition score, Modified Rodnan Criteria, Finger Palmar Flexion Distance, Valentini Disease Cycle Index, Visual Analogue Scale, Scleroderma Disease Severity Index, UK Functional Scoring Questionnaire are used to evaluate disease activity and functional capacity for Raynaud patients. In addition, ESR, CRP, whole blood count, routine biochemical tests and urinalysis are evaluated in all patients. In patients with scleroderma, ANA, Anti Scl-70, ACA. EKG, EKO, PAB and SVSF, PFT with DLCO, FEV1, FVC and HRCT are also evaluated.

After initial examination and routine testing, patients are sent to the imaging room where the ideal conditions for taking images are established. After all conditions are met described before, the first images are taken with thermal cameras from hands to the wrist. The cold stress test is then applied to observe the response of the body to the cold and to increase the accuracy of the evaluation. Cold stress application is defined as drying the paper towel after being immersed for 1 minute in a container filled with water held at 15 degrees. After cold stress test, on the 5th, 10th, and 20th minutes, the thermal images of the hands that do not touch any place are taken again. Primary Raynaud patients are screened when they first arrive, secondary Raynaud patients diagnosed with scleroderma are screened at 0, 6, and 12 months to follow up the disease. All images must be taken by the same person between the hours of 13:00 and 15:00 in the middle of the day.

5.3. DEVELOPED SYSTEM

The developed software is designed to obtain statistical data from palm and fingertips automatically in the thermal hand images. These images are completely evaluated with image processing algorithms without any human intervention. Procedures are summarized for image processing is as follows: preprocessing of thermal images, segmentation of hands from images, extraction of fingertips and palm and computation of temperature variations in palm and fingertips.

After that, pure left and right palm and all fingertip heat vectors are generated independently by using some morphological operations. The generated heat vectors is used to calculate average values. This provides a completely objective assessment, allowing the diagnosis of the disease according to the rewarming state. The block diagram of the designed system is shown in Fig 5.2.
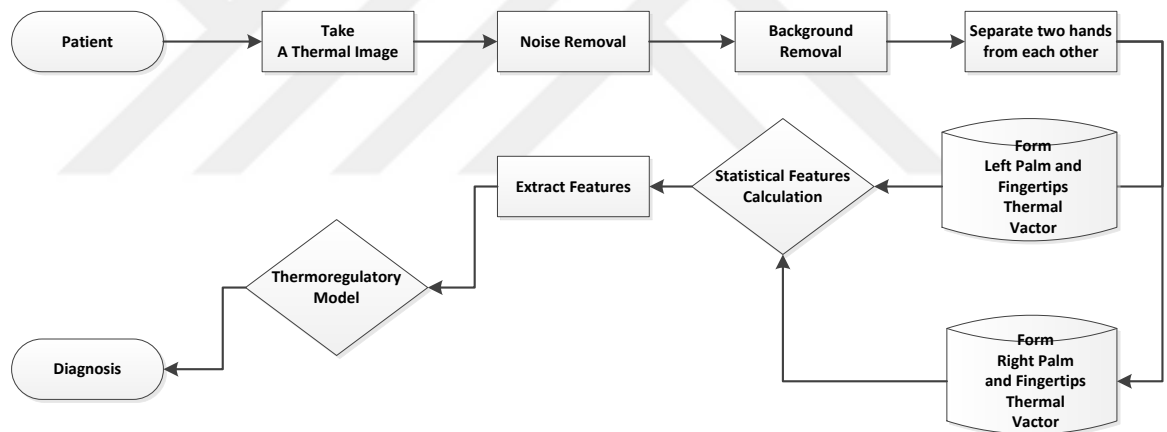
Figure 5. 2 Block diagram of the designed system

Preprocessing of thermal images

In the first stage, since the received data are recorded as real temperature values in ℃ of 160x120 matrix size, it is normalized to 8-bit grayscale images explained in Section 2. After that, as similar to DVT application, the image are passed through 5 x 5 Wiener filter for noise reduction and the image contrast is increased by CLAHE method to make the segmentation more comfortable. In Fig 5.3, original image and preprocessed image are shown.
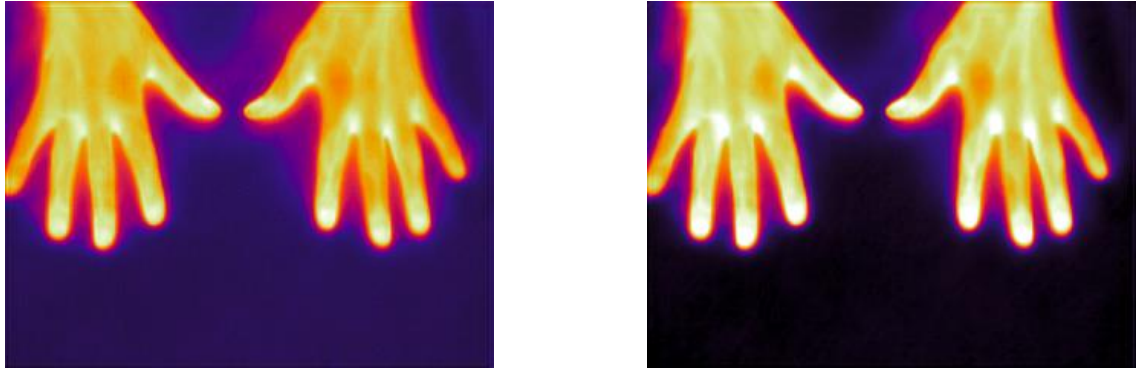
Figure 5. 3 (a) Original image and (b) Preprocessed image, respectively

Segmentation of hands from thermal images

First two hands are separated from each other by Roberts edge detection method. The image is divided into two by vertically controlling the vertical edge to start from the center. The Otsu algorithm expressed in detail in the section 3.2 is chosen to automatically eliminate the unwanted parts of the image from the thermal image as the segmentation method. After background removal, thermal images of two hands are generated independently.

Extraction of fingertips and palm

In this step, we perform mathematical morphological image processing assuming three characteristic values that we find in our experiments.

Noise Length, L_n = 1 - 3 pixels

Finger Width, W_f = 15 - 20 pixels

Palm Width, W_p = 50 - 150 pixels

By using a disk-shaped structural element larger than diameter L_n and less than W_f, morphological opening is performed on the binary image. Thus, background noises and many points on the edges can be deleted. Thereafter, a morphological closing is carried out using the same construction element to remove the noises in the concave points and palms at the edges again. Before and after noise removal, the binary images are shown in Fig. 5.4.
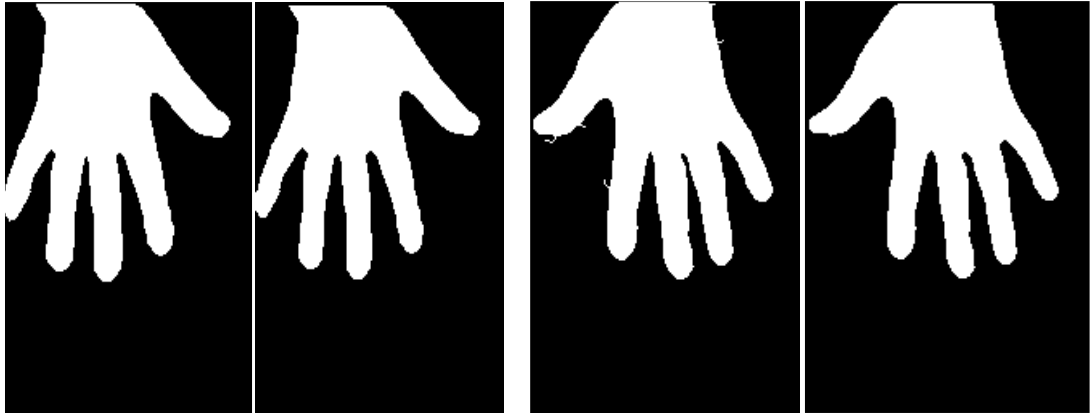
Figure 5. 4 (a) Left side (LS) noisy image (b) LS Cleaned Image (c) Right side (RS) noisy image (d) RS Cleaned image, respectively

The palm image is obtained by a morphological opening operation using a disk-like construction element whose diameter is smaller than W_p and larger than W_f. Figure 5.5 shows the extracted palm images.
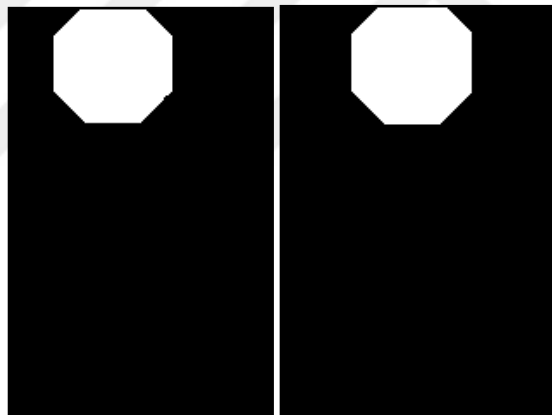

Figure 5. 5 (a) Left side palm image (b) Right side palm image, respectively

The fingertips are extracted by a thinning process formed by morphological erosion operation and with additional conditions. After a few iterations of thinning process, an image with thin lines and end points of the pixels are obtained. The end points at the end of the line are seen as the positions of the fingertips (Fig. 5.6 a, c) and thus the fingertips are obtained by a dilation operation (Fig. 5.6 b, d) after the palm is removed. Finally, all of palms and fingertips are obtained from thermal image as shown in Fig. 5.7.
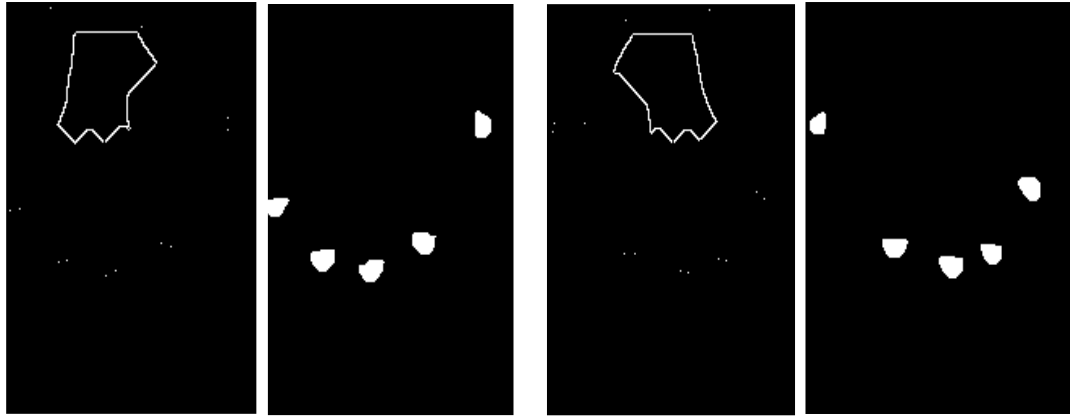
Figure 5. 6 (a) Left side (LS) endpoints (b) LS fingertips (c) Right side (RS) endpoints (d) RS fingertips, respectively
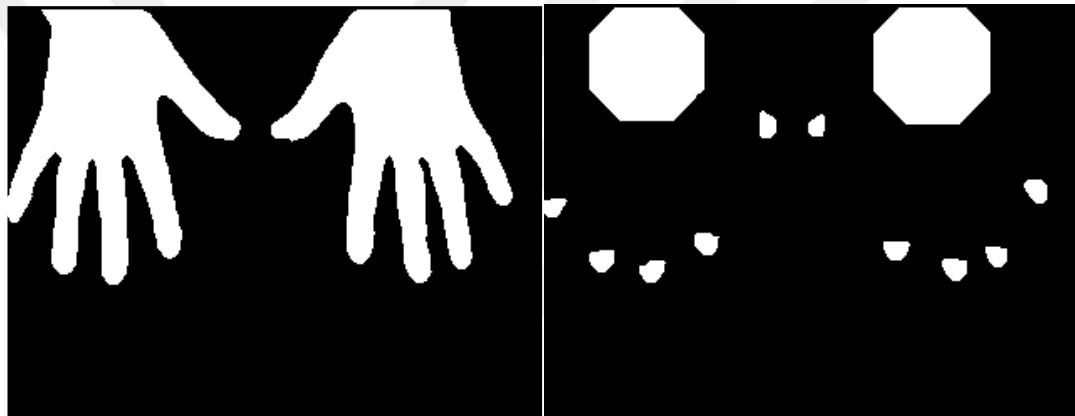
Fig. 5.7. (a) Segmented binary image of thermal image (b) Obtained binary image of palms and fingertips, respectively

Computation of temperature variations in palm and fingertips

Using the processed images, the correlation between gray level and temperature is established and the average temperature value in the palms and fingers is determined.

5.4. CONCLUSION

Many patients who have encountered a variable list of complaints, such as color change and cold in hands since young ages, skin thickening and sometimes dryness, small wounds on the fingertips, dry cough and shortness of breath, chest pain, palpitation, gastrointestinal problems, red rash on the body and especially in palms and palms, can not open mouth, lips infertility. And they can not be diagnosed for many years. Primer and Secondary Raynaud's phenomenology are also important among the

diseases that can not be diagnosed. Fully automated, objective, rapid, and non-invasive thermal imaging will provide useful information as a pre-screening test to diagnose this disease.

Infrared imaging is a biomedical imaging technique based on the modeling of heat exchange and control processes in the skin layer. This technique aims to provide quantitative diagnostic parameters by functional examination of thermoregulatory processes. It also provides more information to doctors about the disease being treated, such as explaining the possible physical causes of certain thermal behaviors and their relationship to the physiology of the processes involved. The greatest advantages of thermal imaging are rapid and noninvasive imaging techniques. Thus, if sufficient research is done, it will be easily used as a pre-test for many diseases.

In this study, a method based on image processing is proposed to examine the temperature change in a certain part of the hands in the diagnosis and follow-up of the primary and secondary Raynaud's disease. In literature, when the applications of the thermal imaging modalities studied are examined, it has been seen that clinicians focus on only certain points of the images in the direction of their experience and obtained a result with the statistical calculations of them. In this study, unlike the studies done, the entire image is evaluated by image processing algorithms and the temperature changes related to the disease are automatically determined without human intervention.

CHAPTER VI

CONCLUSION AND FUTURE WORKS

As technology develops, various alternative diagnostic methods are emerging. Along with the development of currently available methods, alternative methods are increasing day by day. Among the potential methods, infrared thermal imaging has recently been supported by more clinical studies around the world due to its cheap, rapid and non-invasive nature. At this point, the potential of infrared thermal imaging is being investigated in every medical field.

In this thesis study, two independent diseases were investigated specifically. These are deep vein thrombosis and primary and secondary Raynaud phenominic diseases. Automatic diagnostic methods have been developed to analyze and evaluate the infrared thermal images obtained from these patients. In developed systems, various image processing techniques have been used to extract the relevant properties of infrared thermal images. In addition, statistical analysis was performed on related features to facilitate objective evaluations of these images and to find clinical results.

According to the results obtained, it has been shown that the developed system is an effective alternative method for the diagnosis of deep vein thrombosis and can be used as a pre-screening test. This system does not make a complete diagnosis, but it reduces the need for other imaging methods to a certain extent and speeds up the detection of vital situations. The method developed in this study is not only specific to deep vein thrombosis, it can be applied to all organs and limbs that are symmetrical in the body and can help to diagnose these diseases.

In the other part of the study, a system was developed for the diagnosis of primary and secondary Raynaud patients. In this system, relevant areas in the hands are automatically detected and prepared for statistical analysis. Although the method works well in a hand image, it has not been evaluated as a performance because it is not tested in the patient image.

It is well known that early diagnosis leads to increased survival and a significant reduction in health care costs. As a result, the developed techniques will contribute to the current multi-imaging clinical environment and will help to identify these diseases more quickly. In addition to its usefulness, the second critical benefit may be used in the follow-up of patients by monitoring the effectiveness of treatments.

Although thermal imaging is not yet considered to be a completely reliable method, many diseases will only become identifiable by infrared thermal imaging through advanced research and development. This requires continuous improvement in the areas of IR camera systems designed for medical diagnosis, advanced image processing and analysis techniques, physiological investigation of thermal signatures, quantitative evaluation of clinical data. It is also necessary to create a larger image database to increase the success of automated infrared thermal imaging systems. If enough patient data are collected, machine learning and deep learning algorithms can be applied for personalized diagnosis to increase the success rate.

Infrared thermal imaging system to be developed as a whole body scan can be used as a screening tool and can help to reduce the number of patients referred to private healthcare. Such inexpensive and portable screening tools may be particularly useful in developing countries where specialized healthcare facilities and advanced equipment are not available.

REFERENCES

[1]   Houdas Y. and Ring E. F. J. 2013. Human Body Temperature: Its Measurement and Regulation. Springer Science & Business Media.

[2]   Ring E. F. J. (2007). The historical development of temperature measurement in medicine, *Infrared Physics & Technology*. **49**, 3, 297–301.

[3]   Tan J. H., Ng E. Y. K., Acharya U. R., and Chee C. (2009). Infrared thermography on ocular surface temperature: a review, *Infrared physics & technology*. **52**, 4, 97–108.

[4]   Jones B. F. (1998). A reappraisal of the use of infrared thermal image analysis in medicine, *IEEE Transactions on Medical Imaging*. **17**, 6, 1019–1027.

[5]   Bouzida N., Bendada A., and Maldague X. P. (2009). Visualization of body thermoregulation by infrared imaging, *Journal of Thermal Biology*. **34**, 3, 120–126.

[6]   Blume S. S. (1993). Social Process and the Assessment of a New Imaging Technique, *International Journal of Technology Assessment in Health Care*. **9**, 3, 335–345.

[7]   Lahiri B. B., Bagavathiappan S., Jayakumar T., and Philip J. (2012). Medical applications of infrared thermography: A review, *Infrared Physics & Technology*. **55**, 4, 221–235.

[8]   Anbar M. 1994. Quantitative dynamic telethermometry in medical diagnosis and management. CRC press.

[9]   Uematsu S. (1985). Symmetry of skin temperature comparing one side of the body to the other, *Thermology*. **1**, 1, 4–7.

[10] Collins A. J., Ring E. F., Cosh J. A., and Bacon P. A. (1974). Quantitation of thermography in arthritis using multi-isothermal analysis. I. The thermographic index., *Annals of the Rheumatic Diseases*. **33**, 2, 113–115.

[11] Aubry-Frize M., Quartey G. R. C., Evans H., and LaPalme D. (1981). The thermographic detection of pain, in *Proceedings of the 3rd Canadian Clinical Engineering Conference. Saskatoon, Canada*, 82–83.

[12] Gautherie M., Kotewicz A., and Gueblez P. (1983). Accurate and objective evaluation of breast thermograms: basic principles and new advances with special reference to an improved computer-assisted scoring system, *Thermal assessment of breast health*. 72–97.

[13] Feig S. A., Shaber G. S., Schwartz G. F., *et al.* (1977). Thermography, mammography, and clinical examination in breast cancer screening: review of 16,000 studies, *Radiology*. **122**, 1, 123–127.

[14] So, Y. T., Aminoff M. J., and Olney R. K. (1989). The role of thermography in the evaluation of lumbosacral radiculopathy. Neurology. **39**, 9, 1154-1154.

[15] Anbar M. (1991). Objective assessment of clinical computerized thermal images, in *Medical Imaging V: Image Processing*. **1445**, 479–485.

[16] Fujimasa I. (1986). Development of an on-line real-time computed thermography system (CTS), *Medinfo86*. 709–711.

[17] Fujimasa I. (1998). Pathophysiological expression and analysis of far infrared thermal images, *IEEE engineering in medicine and biology magazine*. **17**, 4, 34–42.

[18] Ng E. K. (2009). A review of thermography as promising non-invasive detection modality for breast tumor, *International Journal of Thermal Sciences*. **48**, 5, 849–859.

[19] FLIR A. (2010). The Ultimate Infrared Handbook for R&D Professionals, *Boston: FLIR Systems*.

[20] Pidwirny M. and Jones S. (2006). The nature of radiation, *Fundamentals of Physical Geography*.

[21] Hymes I., Boydell W., and Prescott B. 1996. Thermal radiation: physiological and pathological effects. Institution of Chemical Engineers.

[22] English M. J. M. (2001). Physical principles of heat transfer, *Current Anaesthesia and Critical Care*. **12**, 2, 66–71.

[23] Davis A. P. and Lettington A. H. (1988). Principles of thermal imaging, *Applications of thermal imaging*. 1–34.

[24] Grenn M. W., Perconti P., Vizgaitis J., and Pellegrino J. G. 2006. Infrared camera and optics for medical applications. CRC Press.

[25] Pryputniewicz R. J. (2002). Lecture 29 (2): radiation-heat transfer, properties, shape factor and relations between shape factors, *Based on Textbook by JP Holman*.

[26] Principle of thermal imaging retrieved from http://www.inmes.hr/pdf/thermography.pdf (Accessed in August 2018).

[27] Steketee J. (1973). Spectral emissivity of skin and pericardium, *Physics in Medicine & Biology*. **18**, 5, 686.

[28] Bronzino J. D. and Diakides N. A. 2007. Advances in Medical Infrared Imaging, in *Medical Infrared Imaging*. CRC Press, 19–32.

[29] Gulyaev Y. V., Markov A. G., Koreneva L. G., and Zakharov P. V. (1995). Dynamical infrared thermography in humans, *IEEE Engineering in Medicine and Biology Magazine*. **14**, 6, 766–771.

[30] Boris G Vainer. (2005). FPA-based infrared thermography as applied to the study of cutaneous perspiration and stimulated vascular response in humans, *Physics in Medicine & Biology*. **50**, 23, R63.

[31] Kargel C. (2005). Infrared thermal imaging to measure local temperature rises caused by handheld mobile phones, *IEEE Transactions on Instrumentation and Measurement*. **54**, 4, 1513–1519.

[32] Taurisano M. D. and Vorst A. V. (2000). Experimental thermographic analysis of thermal effects induced on a human head exposed to 900-MHz fields of mobile phones, *IEEE Transactions on Microwave Theory and Techniques*. **48**, 11, 2022–2032.

[33] Tarver T. (2012). American Cancer Society. Cancer facts and figures 2014, *J Consumer Health Internet*. **16**, 366–367.

[34] Sheets S. S. F. 2016. Female Breast Cancer.

[35] Ng E. Y. K. and Sudharsan N. M. (2001). Numerical computation as a tool to aid thermographic interpretation, *Journal of Medical Engineering & Technology*. **25**, 2, 53–60.

[36] Kennedy D. A., Lee T., and Seely D. (2009). A Comparative Review of Thermography as a Breast Cancer Screening Technique, *Integr Cancer Ther*. **8**, 1, 9–16.

[37] Amalu W. C., Hobbins W. B., Head J. F., and Elliot R. L. (2006). Infrared imaging of the breast—an overview, *Medical Devices and Systems: The Biomedical Engineering Handbook. CRC Press, Connecticut, USA*, 25–1.

[38] Deng Z. S. and Liu J. (2005). Enhancement of Thermal Diagnostics on Tumors Underneath the Skin by Induced Evaporation, in *2005 IEEE Engineering in Medicine and Biology 27th Annual Conference*. 7525–7528.

[39] Amalric R. (1983). Does infrared thermography truely have a role in present day breast cancer management?, *Biomed Thermology*.

[40] Gautherie M., Haehnel P., Walter J. P., and Keith L. (1982). Long-term assessment of breast cancer risk by liquid-crystal thermal imaging., *Progress in clinical and biological research*. **107**, 279–301.

[41] Gamigami P. Atlas of Mammography: New Early Signs in Breast Cancer. 1996. Blackwell Science, Cambridge, MA, USA.

[42] Head J. F., Wang F., and Elliott R. L. (1993). Breast thermography is a noninvasive prognostic procedure that predicts tumor growth rate in breast cancer patients, *Annals of the New York Academy of Sciences*. **698**, 1, 153–158.

[43] Aweda M. A., Ketiku K. K., Ajekigbe A. T., and Edi A. A. (2010). Potential role of thermography in cancer management, *Archives of Applied Science Research*. **2**, 6, 300–312.

[44] Arora N., Martins, D., Ruggerio, D., Tousimis, E. *et al.* (2008). Effectiveness of a noninvasive digital infrared thermal imaging system in the detection of breast cancer, *The American Journal of Surgery*. **196**, 4, 523–526.

[45] Amalu W. C. and DIACT F. (2003). A review of breast thermography, *International Academy of. Clinical Thermology, http://www. iact-org. org/articles/articles-review-btherm. html* (Accessed in August 2018)

[46] Sims D. S., Cavanagh P. R., and Ulbrecht J. S. (1988). Risk Factors in the Diabetic FootRecognition and Management, *Phys Ther*. **68**, 12, 1887–1902.

[47] Bharara M., Schoess J., and Armstrong D. G. Coming events cast their shadows before: detecting inflammation in the acute diabetic foot and the foot in remission, *Diabetes/Metabolism Research and Reviews*. **28**, S1, 15–20.

[48] Jiang G., Shang Z., and Zhang M. (2002). Metabolism parameter analysis of diabetics based on the thermography, in *Proceedings of the Second Joint 24th Annual Conference and the Annual Fall Meeting of the Biomedical Engineering Society, Engineering in Medicine and Biology*. **3**, 2226–2227 vol.3.

[49] Brånemark P. I., Fagerberg S. E., Langer L., and Säve-Söderbergh J. (1967). Infrared thermography in diabetes mellitus a preliminary study, *Diabetologia*. **3**, 6, 529–532.

[50] Sun P. C., Lin H. D., Jao S. H. E., Ku Y. C., Chan R. C., and Cheng C. K. (2006). Relationship of skin temperature to sympathetic dysfunction in diabetic at-risk feet, *Diabetes Research and Clinical Practice*. **73**, 1, 41–46.

[51] Bagavathiappan S., Philip J., Jayakumar T., Raj B. *et al.* (2010). Correlation between plantar foot temperature and diabetic neuropathy: a case study by using an infrared thermal imaging technique, *Journal of diabetes science and technology*. **4**, 6, 1386–1392.

[52] Armstrong D. G., Lavery L. A., Liswood P. J., Todd W. F., and Tredwell J. A. (1997). Infrared dermal thermometry for the high-risk diabetic foot, *Physical Therapy*. **77**, 2, 169–175.

[53] Hosaki Y., Mitsunobu F., Ashida K., Tsugeno H. *et al.* (2002). Non-invasive study for peripheral circulation in patients with diabetes mellitus, *Annual reports of Misasa Medical Branch*. **72**, 31–37.

[54] Bagavathiappan S., Saravanan T., Philip J. *et al.* (2008). Investigation of peripheral vascular disorders using thermal imaging, *Diabetes & Vascular Disease*. **8**, 2, 102–104.

[55] Bagavathiappan S., Saravanan, T., Philip, J., Jayakumar, T. *et al.* (2009). Infrared thermal imaging for detection of peripheral vascular disorders, *Journal of medical physics/Association of Medical Physicists of India*. **34**, 1, 43.

[56] Nguyen A. V., Cohen N. J., Lipman H., Brown C. M. *et al.* (2010). Comparison of 3 Infrared Thermal Detection Systems and Self-Report for Mass Fever Screening, *Emerging Infectious Diseases*. **16**, 11, 1710–1717.

[57] Chamberlain J. M., Terndrup T. E., Alexander D. T., Silverstone F. A. *et al.* (1995). Determination of Normal Ear Temperature with an Infrared Emission Detection Thermometer, *Annals of Emergency Medicine*. **25**, 1, 15–20.

[58] Ring F. and Mercer J. (2007). Thermal imaging for fever screening, *The Magazine of the International Organization for Standardization*. **4**, 33–35.

[59] Ring F. (2007). Pandemic: thermography for fever screening of airport passengers, *Thermology International*. **17**, 2, 67.

[60] Ng E. Y., Kawb G. J., and Chang W. (2004). Analysis of IR thermal imager for mass blind fever screening, *Microvascular Research*. **68**, 2, 104–109.

[61] Ohta J. (2010). Case study: influenza pandemic countermeasures utilizing infrared thermography, *NEC Technical Journal*. **5**, 65–69.

[62] Ohta J. and Hamada E. (2009). Detection of body surface temperature by infrared thermography for prevention of influenza pandemic, *NEC Technical Journal*. **62**, 88–92.

[63] Chiu W., Lin P. W. *et al.* (2005). Infrared Thermography to Mass-Screen Suspected Sars Patients with Fever, *Asia Pac J Public Health*. **17**, 1, 26–28.

[64] Chiang M. F., Lin P. W. *et al.* (2008). Mass Screening of Suspected Febrile Patients with Remote-sensing Infrared Thermography: Alarm Temperature and Optimal Distance, *Journal of the Formosan Medical Association*. **107**, 12, 937–944.

[65] Ng E. Y. K. (2005). Is thermal scanner losing its bite in mass screening of fever due to SARS?, *Medical Physics*. **32**, 1, 93–97.

[66] Nishiura H. and Kamiya K. (2011). Fever screening during the influenza (H1N1-2009) pandemic at Narita International Airport, Japan, *BMC Infectious Diseases*. **11**, 1, 111.

[67] Bitar D., Goubar A., and Desenclos J. C. (2009). International travels and fever screening during epidemics: a literature review on the effectiveness and potential use of non-contact infrared thermometers, *Eurosurveillance*. **14**, 6, 19115.

[68] Ring E. F. J., Jung A., Zuber J., Rutowski P., Kalicki B., and Bajwa U. (2008). Detecting fever in Polish children by infrared thermography, in *Proceedings of the 9th International Conference on Quantitative Infrared Thermography*. **2**.

[69] Pascoe D. D., Ring E. F., Mercer J. B., Snell J., Osborn D., and Hedley-Whyte J. (2010). International standards for pandemic screening using infrared thermography, in *Medical Imaging 2010: Biomedical Applications in Molecular, Structural, and Functional Imaging*. **7626**, 76261Z.

[70] Mercer J. B. and Ring E. F. J. (2009). Fever screening and infrared thermal imaging: concerns and guidelines, *Thermology International*. **19**, 3, 67–69.

[71] Ring E. F. J., Mcevoy H., Jung A., Zuber J., and Machin G. (2010). New standards for devices used for the measurement of human body temperature, *Journal of Medical Engineering & Technology*. **34**, 4, 249–253.

[72] Thermal imagers for human temperature screening Part1: Requirements and test methods (TR 15: Part 1: 2003 ISBN 9971-67-963-9).

[73] Thermal imagers for human temperature screening Part 2: Implementation guidelines (TR 15: part 2: 2004 ISBN 9971-67-977-9).

[74] ISO/TR 13154:2009. < https: //www.iso.org/standard/51236.html>. (Accessed in August 2018)

[75] Weinstein S. A. (1986). Standards for neuromuscular thermographic examination, *Special Supplement: Modern Medicine*. **1**, 5–7.

[76] Gratt B. M., Graff-Radford S. B., Shetty V., Solberg W. K., and Sickles E. A. (1996). A 6-year clinical assessment of electronic facial thermography., *Dentomaxillofacial Radiology*. **25**, 5, 247–255.

[77] Gratt B. M. and Sickles E. A. (1995). Electronic facial thermography: an analysis of asymptomatic adult subjects., *Journal of orofacial pain*. **9**, 3.

[78] Graft B. M., Sickles E. A., Ross J. B., Wexler C. E., and Gornbein J. A. (1994). Thermographic assessment of craniomandibular disorders: diagnostic interpretation versus temperature measurement analysis., *Journal of orofacial pain*. **8**, 3.

[79] Canavan D. and Gratt B. M. (1995). Electronic thermography for the assessment of mild and moderate temporomandibular joint dysfunction, *Oral Surgery, Oral Medicine, Oral Pathology, Oral Radiology, and Endodontology*. **79**, 6, 778–786.

[80] Gratt B. M., Shetty V., Dent M., Saiar M., and Sickles E. A. (1995). Electronic thermography for the assessment of inferior alveolar nerve deficit, *Oral Surgery, Oral Medicine, Oral Pathology, Oral Radiology and Endodontics*. **80**, 2, 153–160.

[81] Hastings R. C., Brand P. W., Mansfield R. E., and Ebner J. D. (1968). Bacterial density in the skin in lepromatous leprosy as related to temperature., *Leprosy review*. **39**, 2, 71–4.

[82] Sabin T. D. and Ebner J. D. (1969). Patterns of sensory loss in lepromatous leprosy, *International Journal of Leprosy*. **37**, 239–248.

[83] Vargas J. V. C., Brioschi M. L. *et al.* (2009). Normalized methodology for medical infrared imaging, *Infrared Physics & Technology*. **52**, 1, 42–47.

[84] Benko I., Koteles G. J., and Nemeth G. (1996). Thermal imaging of the effects of beta-irradiation on human body surface, in *Proceeding of the Conference on Quantitative Infrared Thermography (QIRT'96), Eurotherm Series*. **50**, 354–359.

[85] Thomas R. A., Donne K. E., Clement M., and Kiernan M. N. (2002). Optimized laser application in dermatology using infrared thermography, in *Thermosense XXIV*. **4710**, 424–435.

[86] Mason B. R., Graff A. J., and Pegg S. P. (1981). Colour thermography in the diagnosis of the depth of burn injury, *Burns*. **7**, 3, 197–202.

[87] Cole R. P., Jones S. G., and Shakespeare P. G. (1990). Thermographic assessment of hand burns, *Burns.* **16**, 1, 60–63.

[88] Schnell H. M. and Zaspel J. G. (2008). Cooling extensive burns: Sprayed coolants can improve initial cooling management: A thermography-based study, *Burns.* **34**, 4, 505–508.

[89] Mercer J. B., Nielsen S. P., and Hoffmann G. (2008). Improvement of wound healing by water-filtered infrared-A (wIRA) in patients with chronic venous stasis ulcers of the lower legs including evaluation using infrared thermography, *GMS German Medical Science.* **6**, Doc11.

[90] de Weerd L., Mercer J. B., and Weum S. (2011). Dynamic infrared thermography, *Clinics in plastic surgery.* **38**, 2, 277–292.

[91] Flores-Sahagun J. H., Vargas J. V. C., and Mulinari-Brenner F. A. (2011). Analysis and diagnosis of basal cell carcinoma (BCC) via infrared imaging, *Infrared Physics & Technology.* **54**, 5, 367–378.

[92] Costello J. T., McInerney C. D., Bleakley C. M., Selfe J., and Donnelly A. E. (2012). The use of thermal imaging in assessing skin temperature following cryotherapy: a review, *Journal of Thermal Biology.* **37**, 2, 103–110.

[93] De R. C., Grimaldi A., Balestrazzi M., Ranieri G., Chiarappa R., and Avantaggiato F. (1985). Changes in blood pressure and thermographic values resulting from use of a beta-blocker plus diuretic and of an alpha-beta-blocker plus diuretic., *Drugs under experimental and clinical research*. **11**, 10, 725–729.

[94] Cherkas L. F., Carter L., Spector T. D., Howell K. J., Black C. M., and MacGregor A. J. (2003). Use of thermographic criteria to identify Raynaud's phenomenon in a population setting., *The Journal of Rheumatology*. **30**, 4, 720–722.

[95] Ring E. F. J., Aarts N. J. M., Black C. M., and Boesiger P. (1988). Raynaud's phenomenon: assessment by thermography, *Thermology*. **3**, 69–73.

[96] Hirschl M., Katzenschlager R., Francesconi C., and Kundi M. (2004). Low level laser therapy in primary Raynaud's phenomenon--results of a placebo controlled, double blind intervention study., *The Journal of Rheumatology*. **31**, 12, 2408–2412.

[97] Chikura B., Moore T., Manning J., Vail A., and Herrick A. L. (2010). Thumb Involvement in Raynaud's Phenomenon as an Indicator of Underlying Connective Tissue Disease, *The Journal of Rheumatology*. jrheum.091117.

[98] Schiavenato M. and Thiele R. G. (2012). Thermography Detects Subclinical Inflammation in Chronic Tophaceous Gout, *The Journal of Rheumatology*. **39**, 1, 182–183.

[99] McHugh N. J., Elvins D. M., and Ring E. F. J. (1993). Elevated anticardiolipin antibodies in a patient with vibration-white-finger, valvular heart disease and psoriatic arthritis, *Clinical rheumatology*. **12**, 1, 70–73.

[100] Arnold M. H., Preston S. J. L., Beller E. M., and Buchanan W. W. (1989). Infrared surface thermography. Evaluation of a new radiometry instrument for measuring skin temperature over joints, *Clinical Rheumatology*. **8**, 2, 225–230.

[101] Ring E. F. (1975). Thermography and rheumatic diseases., *Bibliotheca radiologica*. 6, 97–106.

[102] Frize M., Adéa C., Payeur P., Di Primio G., Karsh J., and Ogungbemile A. (2011). Detection of rheumatoid arthritis using infrared imaging, in *Medical Imaging 2011: Image Processing*. **7962**, 79620M.

[103] Wu C. L., Yu K. L., Chuang H. Y., Huang M. H., Chen T. W., and Chen C. H. (2009). The Application of Infrared Thermography in the Assessment of Patients With Coccygodynia Before and After Manual Therapy Combined With Diathermy, *Journal of Manipulative and Physiological Therapeutics*. **32**, 4, 287–293.

[104] Park J. Y., Hyun J. K., and Seo J. B. (2007). The effectiveness of digital infrared thermographic imaging in patients with shoulder impingement syndrome, *Journal of Shoulder and Elbow Surgery*. **16**, 5, 548–554.

[105] Fujino H., Kohzuki H., Takeda I., Kiyooka T. *et al.* (2005). Regression of capillary network in atrophied soleus muscle induced by hindlimb unweighting, *Journal of Applied Physiology*. **98**, 4, 1407–1413.

[106] Vecchio P. C., Adebajo A. O., Chard M. D., Thomas P. P., and Hazleman B. L. (1992). Thermography of frozen shoulder and rotator cuff tendinitis, *Clinical Rheumatology*. **11**, 3, 382–384.

[107] Jeracitano D., Cooper R. G., Lyon L. J., and Jayson M. I. V. (1992). Abnormal temperature control suggesting sympathetic dysfunction in the shoulder skin of patients with frozen shoulder, *Rheumatology*. **31**, 8, 539–542.

[108] Thomas D., Siahamis G., Marion M., and Boyle C. (1992). Computerised infrared thermography and isotopic bone scanning in tennis elbow., *Annals of the Rheumatic Diseases*. **51**, 1, 103–107.

[109] Morgan P. B., Tullo A. B., and Efron N. (1995). Infrared thermography of the tear film in dry eye, *Eye*. **9**, 615.

[110] Tan J. H., Ng E. Y. K., Rajendra Acharya U., and Chee C. (2010). Study of normal ocular thermogram using textural parameters, *Infrared Physics & Technology*. **53**, 2, 120–126.

[111] Chang T. C., Hsiao Y. L., and Liao S. L. (2008). Application of digital infrared thermal imaging in determining inflammatory state and follow-up effect of methylprednisolone pulse therapy in patients with Graves' ophthalmopathy, *Graefe's Archive for Clinical and Experimental Ophthalmology*. **246**, 1, 45–49.

[112] Brunsmann U., Sauer U., Arba-Mosquera S., Magnago T., and Triefenbach N. (2010). Evaluation of thermal load during laser corneal refractive surgery using infrared thermography, *Infrared Physics & Technology*. **53**, 5, 342–347.

[113] Ng D. K., Chan C. H., Lee R. S., and Leung L. C. (2005). Non-contact infrared thermometry temperature measurement for screening fever in children, *Annals of Tropical Paediatrics*. **25**, 4, 267–275.

[114] Mansfield C. M., Farrell C., and Asbell S. O. (1970). The Use of Thermography in the Detection of Metastatic Liver Disease, *Radiology*. **95**, 3, 696–698.

[115] Knobel R. B., Guenther B. D., and Rice H. E. (2011). Thermoregulation and Thermography in Neonatal Physiology and Disease, *Biological Research For Nursing*. **13**, 3, 274–282.

[116] Milonov O. B., Lebedeva O. D., and Pomelova L. A. (1979). Use of echography and thermography in parasitic liver diseases, *Sovetskaia meditsina*. 4, 62–67.

[117] Bhatia M., Poley J. R., Haberman J. D., and Boon D. J. (1976). Abdominal thermography in infantile and childhood liver disease., *Southern medical journal*. **69**, 8, 1045–1048.

[118] Unger J. K., Lemke A. J., and Grosse-Siestrup C. (2006). Thermography as potential real-time technique to assess changes in flow distribution in hemofiltration, *Kidney International*. **69**, 3, 520–525.

[119] Kopsa H., Czech W., Schmidt P., Zazgornik J., Pils P., and Balcke P. (1978). Use of thermography in kidney transplantation: two year follow up study in 75 cases., *Proceedings of the European Dialysis and Transplant Association. European Dialysis and Transplant Association*. **16**, 383–387.

[120] Oosterlinck W. and De Sy W. A. (1981). Avascular nephrotomy by means of thermography, *European urology*. **7**, 25–26.

[121] Manginas A., Andreanides E., Leontiadis E. *et al.* (2010). Right ventricular endocardial thermography in transplanted and coronary artery disease patients: first human application., *The Journal of invasive cardiology*. **22**, 9, 400–404.

[122] Montana Thermography Centre: The Heart's Thermoscape. < https://www.thermographyofmontana.com/screening-heart-disease/ >. (Accessed in August 2018).

[123] De Grand A. M. and Frangioni J. V. (2003). An Operational Near-Infrared Fluorescence Imaging System Prototype for Large Animal Surgery, *Technology in Cancer Research & Treatment*. **2**, 6, 553–562.

[124] Madjid M., Willerson J. T., and Casscells S. W. (2006). Intracoronary thermography for detection of high-risk vulnerable plaques, *Journal of the American College of Cardiology*. **47**, 8 Supplement, C80–C85.

[125] Gershon-Cohen J., Haberman-Brueschke J. D., and Brueschke E. E. (1965). Obstetric and gynecologic thermography., *Obstetrics & Gynecology*. **26**, 6, 842–847.

[126] Loriaux C. (1975). Role of thermography in gynecology, *Journal de radiologie, d'electrologie, et de medecine nucleaire*. **56**, 57.

[127] Birnbaum S. J. and Kliot D. (1964). Thermography—obstetrical applications, *Annals of the New York Academy of Sciences*. **121**, 1, 209–222.

[128] Menczer J. and Eskin B. A. (1969). Evaluation of postpartum breast engorgement by thermography, *Obstetrics & Gynecology*. **33**, 2, 260–263.

[129] Shevelev I. A. (1998). Functional imaging of the brain by infrared radiation (thermoencephaloscopy), *Progress in Neurobiology*. **56**, 3, 269–305.

[130] Gorbach A. M., Heiss J. D., Kopylev L., and Oldfield E. H. (2004). Intraoperative infrared imaging of brain tumors, *Journal of neurosurgery*. **101**, 6, 960–969.

[131] Agnelli J. P., Barrea A. A., and Turner C. V. (2011). Tumor location and parameter estimation by thermography, *Mathematical and Computer Modelling*. **53**, 7, 1527–1534.

[132] Çetingül M. P. and Herman C. (2010). A heat transfer model of skin tissue for the detection of lesions: sensitivity analysis, *Physics in Medicine & Biology*. **55**, 19, 5933.

[133] Deng Z. S. and Liu J. (2004). Mathematical modeling of temperature mapping over skin surface and its implementation in thermal disease diagnostics, *Computers in biology and medicine*. **34**, 6, 495–521.

[134] Mital M. and Scott E. P. (2007). Thermal detection of embedded tumors using infrared imaging, *Journal of Biomechanical Engineering*. **129**, 1, 33–39.

[135] Pavlidis I., Levine J., and Baukol P. (2001). Thermal image analysis for anxiety detection, in *Image Processing, 2001. Proceedings. 2001 International Conference on*. **2**, 315–318.

[136] Pavlidis I. and Levine J. (2002). Thermal image analysis for polygraph testing, *IEEE Engineering in Medicine and Biology Magazine*. **21**, 6, 56–64.

[137] Pavlidis I. (2003). Continuous physiological monitoring, in *Engineering in Medicine and Biology Society, 2003. Proceedings of the 25th Annual International Conference of the IEEE*. **2**, 1084–1087.

[138] Pavlidis I., Dowdall J., Sun N., Puri C., Fei J., and Garbey M. (2007). Interacting with human physiology, *Computer Vision and Image Understanding*. **108**, 1–2, 150–170.

[139] Wren J., Loyd D., and Karlsson M. (2004). Investigation of medical thermal treatment using a hybrid bio-heat model, in *Engineering in Medicine and Biology Society, 2004. IEMBS'04. 26th Annual International Conference of the IEEE*. **1**, 2507–2509.

[140] Wilson S. B. and Spence V. A. (1988). A tissue heat transfer model for relating dynamic skin temperature changes to physiological parameters, *Physics in Medicine & Biology*. **33**, 8, 895.

[141] Xie Z., Liu G., Wu S., Fang Z., and Gan Y. (2010). Pennes equation based blood perfusion model and its application in face recognition, in *Information and Automation (ICIA), 2010 IEEE International Conference on*. 2443–2446.

[142] Mabuchi K., Chinzei T., Fujimasa I., Haeno S. *et al.* (1998). Evaluating asymmetrical thermal distributions through image processing, *IEEE Engineering in Medicine and Biology Magazine.* **17**, 2, 47–55.

[143] Merla A. and Romani G. L. (2006). Functional infrared imaging in medicine: a quantitative diagnostic approach, in *Engineering in Medicine and Biology Society, 2006. EMBS'06. 28th Annual International Conference of the IEEE*. 224–227.

[144] Qi H. and Nicholas A. D. (1998). "Infrared Imaging in Medicine", retrieved from http://www.iamtonline.org. (Accessed in August 2018).

[145] Qi H. and Head J. F. (2001). Asymmetry analysis using automatic segmentation and classification for breast cancer detection in thermograms, in *Engineering in Medicine and Biology Society, 2001. Proceedings of the 23rd Annual International Conference of the IEEE*. **3**, 2866–2869.

[146] Qi H., Kuruganti P. T., and Snyder W. E. (2012). Detecting breast cancer from thermal infrared images by asymmetry analysis, *Medicine and Medical Research*. **38**.

[147] Tang X. and Ding H. (2006). Asymmetry analysis of breast thermograms with morphological image segmentation, in *Engineering in Medicine and Biology Society, 2005. IEEE-EMBS 2005. 27th Annual International Conference*. 1680–1683.

[148] Ahmad Fadzil M. H., Izhar L. I., Venkatachalam P. A., and Karunakar T. V. N. (2007). Extraction and reconstruction of retinal vasculature, *Journal of medical engineering & technology*. **31**, 6, 435–442.

[149] Fadzil M. A. and Iznita I. L. (2009). A Non-Invasive Method for Analysing the Retina for Ocular Manifested Diseases, *Malaysia Patent patent filing no. PCT/MY2009/000025*.

[150] Herry C. L. and Frize M. (2002). Digital processing techniques for the assessment of pain with infrared thermal imaging, in *Engineering in Medicine and Biology, 2002. 24th Annual Conference and the Annual Fall Meeting of the Biomedical Engineering Society EMBS/BMES Conference, 2002. Proceedings of the Second Joint*. **2**, 1157–1158.

[151] Zhu Z., Tsiamyrtzis P., and Pavlidis I. (2008). The segmentation of the supraorbital vessels in thermal imagery, in *Advanced Video and Signal Based Surveillance, 2008. AVSS'08. IEEE Fifth International Conference on*. 237–244.

[152] Petrou M. and Petrou C. 2010. Image processing: the fundamentals. John Wiley & Sons.

[153] Koay J., Herry C., and Frize M. (2004). Analysis of breast thermography with an artificial neural network, in *Engineering in Medicine and Biology Society, 2004. IEMBS'04. 26th Annual International Conference of the IEEE*. **1**, 1159–1162.

[154] Motta L., Conci A., Lima R., Diniz E., and Luís S. (2010). Automatic segmentation on thermograms in order to aid diagnosis and 2D modeling, in *Proc. of 10th Workshop em Informática Médica*. 1610–1619.

[155] Akhloufi M. A. and Bendada A. (2008). Infrared face recognition using distance transforms, in *Proceedings of the 5th International Conference on Image and Vision Computing (ICIVC 2008)*. **30**, 160–163.

[156] Palfy M. and Papez B. J. (2007). Diagnosis of carpal tunnel syndrome from thermal images using artificial neural networks, in *Computer-Based Medical Systems, 2007. CBMS'07. Twentieth IEEE International Symposium on*. 59–64.

[157] Herry C. L., Frize M., and Goubran R. A. (2006). Segmentation and landmark identification in infrared images of the human body, in *Engineering in Medicine and Biology Society, 2006. EMBS'06. 28th Annual International Conference of the IEEE*. 957–960.

[158] Petrou M. and Sevilla P. G. 2006. Image processing: dealing with texture. **1**. Wiley Chichester.

[159] Jin-Yu Z., Yan C., and Xian-Xiang H. (2009). IR thermal image segmentation based on enhanced genetic algorithms and two-dimensional classes square error, in *Information and Computing Science, 2009. ICIC'09. Second International Conference on.* **2**, 309–312.

[160] Chang J. S., Liao H. Y. M., Hor M. K., Hsieh J. W., and Chern M. Y. (1997). New automatic multi-level thresholding technique for segmentation of thermal images, *Image and vision computing.* **15**, 1, 23–34.

[161] Boukharouba S., Rebordão J. M., and Wendel P. L. (1985). An amplitude segmentation method based on the distribution function of an image, *Computer Vision, Graphics, and Image Processing.* **29**, 1, 47–59.

[162] Selvarasu N., Vivek S., and Nandhitha N. M. (2007). Performance evaluation of image processing algorithms for automatic detection and quantification of abnormality in medical thermograms, in *Conference on Computational Intelligence and Multimedia Applications, 2007. International Conference on.* **3**, 388–393.

[163] Selvarasu N., Nachiappan A., and Nandhitha N. M. (2009). Feature extraction algorithms for abnormality quantification from medical thermograms, *International Journal of Recent Trends in Engineering.* **1**, 3, 350.

[164] Herry C. L. and Frize M. (2004). Quantitative assessment of pain-related thermal dysfunction through clinical digital infrared thermal imaging, *Biomedical engineering online.* **3**, 1, 19.

[165] Tsai D. M. (1995). A fast thresholding selection procedure for multimodal and unimodal histograms, *Pattern Recognition Letters.* **16**, 6, 653–666.

[166] Herry C. L., Frize M., and Goubran R. A. (2008). Search for abnormal thermal patterns in clinical thermal infrared imaging, in *Medical Measurements and Applications, 2008. MeMeA 2008. IEEE International Workshop on.* 61–65.

[167] Fujimasa I., Chinzei T., and Saito I. (2000). Converting far infrared image information to other physiological data, *IEEE Engineering in Medicine and Biology Magazine.* **19**, 3, 71–76.

[168] Zavisek M. 2011. Breast cancer diagnostics using infrared camera. .

[169] Zavisek M. (2012). Quantitative thermography in breast cancer detection—a survey of current research, *Retrieved in January 2011b from http://www. feec. vutbr. cz/EEICT/2004/sbornik/03-Doktorskeprojekty/01-Elektronika/40-michal. pdf (2011b). Accessed*, **12**.

[170] Tarnawski W., Schaefer G., Nakashima T., and Miroslaw L. (2010). Applications of fuzzy rule-based systems in medical image understanding, *SK Pal & JF Peters. 6.1–6.31.*

[171] Acharya U. R., Ng E. Y. K., Tan J. H., and Sree S. V. (2012). Thermography Based Breast Cancer Detection Using Texture Features and Support Vector Machine, *Journal of Medical Systems* **36**, 3, 1503–1510.

[172] Acharya U. R., Ng E. Y. K., Tan J. H., Sree S. V., and Ng K. H. (2012). An integrated index for the identification of diabetic retinopathy stages using texture parameters, *Journal of medical systems*. **36**, 3, 2011–2020.

[173] Drummond P. D. and Lance J. W. (1983). Extracranial vascular changes and the source of pain in migraine headache, *Annals of Neurology: Official Journal of the American Neurological Association and the Child Neurology Society*. **13**, 1, 32–37.

[174] Lance J. W., Anthony M., and Somerville B. (1970). Thermographic, hormonal and clinical studies in migraine, *Headache: The Journal of Head and Face Pain*. **10**, 3, 93–104.

[175] Marzec M., Koprowski R., and Wrobel Z. (2009). Automatic temperature measurement on thermograms for headache diagnosis, *Pomiary Automatyka Kontrola*. **55**, 11, 923–6.

[176] Ng E. Y. and Sudharsan N. M. (2004). Computer simulation in conjunction with medical thermography as an adjunct tool for early detection of breast cancer, *BMC cancer*. **4**, 1, 17.

[177] Quek C., Irawan W., and Ng E. Y. K. (2010). A novel brain-inspired neural cognitive approach to SARS thermal image analysis, *Expert Systems with Applications*. **37**, 4, 3040–3054.

[178] Ammer K. (2006). Does thermal imaging provide extra information in patients suffering from headache?, *Thermology International-Editorial (Austrian Society of Thermology, Vienna, Austria).* 45–48.

[179] Perrone P., Porazzi D., Carnaghi P. L., and Landi G. (1980). Thermographic patterns in migraine, *Acta Thermographica.* **5**, 129–132.

[180] Papež B. J., Palfy M., Mertik M., and Turk Z. (2009). Infrared thermography based on artificial intelligence as a screening method for carpal tunnel syndrome diagnosis, *Journal of International Medical Research*. **37**, 3, 779–790.

[181] Ng E. Y. K. and Kee E. C. (2007). Fever mass screening tool for infectious diseases outbreak: integrated artificial intelligence with bio-statistical approach in thermogram analysis, *Medical Infrared Imaging*. **1**, 16–1.

[182] Varga M. J. and Hanka R. (1992). Automatic thermal image analysis for medical diagnosis, in *Image Processing and its Applications, 1992., International Conference on.* 526–529.

[183] Kittler J. and Young P. C. (1973). A new approach to feature selection based on the Karhunen-Loeve expansion, *Pattern recognition*. **5**, 4, 335–352.

[184] Nurhayati O. D., Widodo T. S., Susanto A., and Tjokronagoro M. (2010). First order statistical feature for breast cancer detection using thermal images, *World Academy of Science, Engineering and Technology*. **70**, 1040–1042.

[185] Khan M. M., Ingleby M., and Ward R. D. (2006). Automated facial expression classification and affect interpretation using infrared measurement of facial skin temperature variations, *ACM Transactions on Autonomous and Adaptive Systems (TAAS)*. **1**, 1, 91–113.

[186] Khan M. M., Ward R. D., and Ingleby M. (2009). Classifying pretended and evoked facial expressions of positive and negative affective states using infrared measurement of skin temperature, *ACM Transactions on Applied Perception (TAP)*. **6**, 1, 6.

[187] Underwood P. Analysis of Thermal Images in the Diagnosis of Vascular Disease, PhD Thesis, University of Manchester, 2002.

[188] Frize M., Herry C., and Roberge R. (2002). Processing of thermal images to detect breast cancer: comparison with previous work, in *Engineering in Medicine and Biology, 2002. 24th Annual Conference and the Annual Fall Meeting of the Biomedical Engineering Society EMBS/BMES Conference, 2002. Proceedings of the Second Joint*. **2**, 1159–1160.

[189] Harding J. R. (1998). Investigating deep venous thrombosis with infrared imaging, *IEEE engineering in medicine and biology magazine*. **17**, 4, 43–46.

[190] Ng E. Y. K., Chen Y., and Ung L. N. (2001). Computerized breast thermography: study of image segmentation and temperature cyclic variations, *Journal of medical engineering & technology*. **25**, 1, 12–16.

[191] Qi H., Kuruganti P. T., and Liu Z. (2002). Early detection of breast cancer using thermal texture maps, in *Biomedical Imaging, 2002. Proceedings. 2002 IEEE International Symposium on*. 309–312.

[192] Kim S. W., Lee S. M., and Jeong S. H. (2004). Validation of thermography in the diagnosis of acute cervical sprain, *Journal of Korean Neurosurgical Society*. **36**, 4, 297–301.

[193] Brenner M., Braun C., Oster M., and Gulko P. S. (2006). Thermal signature analysis as a novel method for evaluating inflammatory arthritis activity, *Annals of the Rheumatic Diseases*. **65**, 3, 306–311.

[194] Denoble A. E., Hall N., Pieper C. F., and Kraus V. B. (2010). Patellar Skin Surface Temperature by Thermography Reflects Knee Osteoarthritis Severity, *Clinical Medicine Insights: Arthritis and Musculoskeletal Disorders*. **3**, CMAMD.S5916.

[195] Sanchez B. M., Lesch M., Brammer D., Bove S. E., Thiel M., and Kilgore K. S. (2008). Use of a portable thermal imaging unit as a rapid, quantitative method of evaluating inflammation and experimental arthritis, *Journal of pharmacological and toxicological methods*. **57**, 3, 169–175.

[196] Spalding S. J., Kwoh C. K. *et al.* (2008). Three-dimensional and thermal surface imaging produces reliable measures of joint shape and temperature: a potential tool for quantifying arthritis, *Arthritis Research & Therapy*. **10**, 1, R10.

[197] Varju G., Pieper C. F., Renner J. B., and Kraus V. B. (2004). Assessment of hand osteoarthritis: correlation between thermographic and radiographic methods, *Rheumatology*. **43**, 7, 915–919.

[198] Glehr M., Stibor A., Sadoghi P. *et al.* (2011). Thermal imaging as a noninvasive diagnostic tool for anterior knee pain following implantation of artificial knee joints, *International Journal of Thermodynamics*. **14**, 2, 71–78.

[199] Martini G., Murray K. J., Howell K. J., Harper J. *et al.* (2002). Juvenile-onset localized scleroderma activity detection by infrared thermography, *Rheumatology (Oxford)*. **41**, 10, 1178–1182.

[200] Sanchez-Marin F. J., Calixto-Carrera S., and Villaseñor-Mora C. (2009). Novel approach to assess the emissivity of the human skin, *Journal of Biomedical Optics*. **14**, 2, 024006.

[201] Nardin R. A., Fogerson P. M., Nie R., and Rutkove S. B. (2010). Foot Temperature in Healthy Individuals, *Journal of the American Podiatric Medical Association*. **100**, 4, 258–264.

[202] Liu C., Netten J. J. van, Baal J. G. van, Bus S. A., and Heijden F. van der. (2015). Automatic detection of diabetic foot complications with infrared thermography by asymmetric analysis, *JBO, JBOPFO*. **20**, 2, 026003.

[203] van Netten J. J., Prijs M., van Baal J. G., Liu C., van Der Heijden F., and Bus S. A. (2014). Diagnostic values for skin temperature assessment to detect diabetes-related foot complications, *Diabetes technology & therapeutics*. **16**, 11, 714–721.

[204] Ferreira J. J. A., Mendonça L. C. S., Nunes L. A. O., Andrade Filho A. C. C., Rebelatto J. R., and Salvini T. F. (2008). Exercise-Associated Thermographic Changes in Young and Elderly Subjects, *Ann Biomed Eng*. **36**, 8, 1420–1427.

[205] de Weerd L., Mercer J. B., and Setså L. B. (2006). Intraoperative Dynamic Infrared Thermography and Free-Flap Surgery, *Annals of Plastic Surgery*. **57**, 3, 279.

[206] Kells B. E., Kennedy J. G., Biagioni P. A., and Lamey P. J. (2000). Computerized infrared thermographic imaging and pulpal blood flow: Part 1. A protocol for thermal imaging of human teeth, *International Endodontic Journal*. **33**, 5, 442–447.

[207] Hakgüder A., Birtane M., Gürcan S., Kokino S., and Turan F. N. (2003). Efficacy of low level laser therapy in myofascial pain syndrome: An algometric and thermographic evaluation, *Lasers in Surgery and Medicine*. **33**, 5, 339–343.

[208] Lee J. G., Kim S. G., Lim K. J., and Choi K. C. (2007). Thermographic Assessment of Inferior Alveolar Nerve Injury in Patients With Dentofacial Deformity, *Journal of Oral and Maxillofacial Surgery*. **65**, 1, 74–78.

[209] Holey L. A., Dixon J., and Selfe J. (2011). An Exploratory Thermographic Investigation of the Effects of Connective Tissue Massage on Autonomic Function, *Journal of Manipulative and Physiological Therapeutics*. **34**, 7, 457–462.

[210] Park J., Jang W. S., Park K. Y., Li K. *et al.* (2012). Thermography as a predictor of postherpetic neuralgia in acute herpes zoster patients: a preliminary study, *Skin Research and Technology*. **18**, 1, 88–93.

[211] Ra J. Y., An S., Lee G.-H., Kim T. U., Lee S. J., and Hyun J. K. (2013). Skin temperature changes in patients with unilateral lumbosacral radiculopathy, *Annals of rehabilitation medicine*. **37**, 3, 355–363.

[212] Gold J. E., Cherniack M., Hanlon A., Dennerlein J. T., and Dropkin J. (2009). Skin temperature in the dorsal hand of office workers and severity of upper extremity musculoskeletal disorders, *International Archives of Occupational and Environmental Health*. **82**, 10, 1281–1292.

[213]   Devereaux M., Parr G., Lachmann S., Thomas D., and Hazleman B. (1986). Thermographic diagnosis in athletes with patellofemoral arthralgia, *The Journal of Bone and Joint Surgery. British volume*. **68**-**B**, 1, 42–44.

[214]   Niu H. H., Lui P. W., Hu J. S., Ting C. K. *et al.* (2001). Thermal symmetry of skin temperature: normative data of normal subjects in Taiwan, *CHINESE MEDICAL JOURNAL-TAIPEI*. **64**, 8, 459–468.

[215]   Collins A. J., Notarianni L. J., Ring E. F., and Seed M. P. (1984). Some observations on the pharmacology of "deep-heat", a topical rubifacient., *Annals of the Rheumatic Diseases*. **43**, 3, 411–415.

[216]   Gershon-Cohen, J. and Habennan J. D. (1968). Thermography of Smoking, *Archives of Environmental Health: An International Journal*. **16**, 5, 637–641.

[217]   Ijzerman R. G., Serne E. H., Weissenbruch M. M. van, Jongh R. T. de, and Stehouwer C. D. A. (2003). Cigarette smoking is associated with an acute impairment of microvascular function in humans, *Clinical Science*. **104**, 3, 247–252.

[218]   Usuki K., Kanekura T., Aradono K., and Kanzaki T. (1998). Effects of nicotine on peripheral cutaneous blood flow and skin temperature, *Journal of Dermatological Science*. **16**, 3, 173–181.

[219]   Di A. C. and Ippolito F. (2003). Early effects of cigarette smoking in hypertensive and normotensive subjects. An ambulatory blood pressure and thermographic study, *Minerva Cardioangiol*. **51**, 4, 387–393.

[220]   Wolf R., Tüzün B., and Tüzün Y. (1999). Alcohol ingestion and the cutaneous vasculature 1, *Clinics in Dermatology*. **17**, 4, 395–403.

[221]   Quinlan P. T., Lane J., Moore K. L., Aspen J., Rycroft J. A., and O'Brien D. C. (2000). The Acute Physiological and Mood Effects of Tea and Coffee: The Role of Caffeine Level, *Pharmacology Biochemistry and Behavior*. **66**, 1, 19–28.

[222]   Koot P. and Deurenberg P. (1995). Comparison of Changes in Energy Expenditure and Body Temperatures after Caffeine Consumption, *ANM*. **39**, 3, 135–142.

[223] Daniels J. W., Molé P. A., Shaffrath J. D., and Stebbins C. L. (1998). Effects of caffeine on blood pressure, heart rate, and forearm blood flow during dynamic leg exercise, *Journal of applied physiology*. **85**, 1, 154–159.

[224] Ammer K. and Ring E. F. J. (2006). Standard procedures for infrared imaging in medicine, *Biomedical Engineering Handbook, CRC Press*. **1**.

[225] Ng E. Y. K. and Kee E. C. (2008). Advanced integrated technique in breast cancer thermography, *Journal of Medical Engineering & Technology*. **32**, 2, 103–114.

[226] Kienzler J. L., Magnette J., Queille-Roussel C., Sanchez-Ponton A., and Ortonne J. P. (2005). Diclofenac-Na Gel Is Effective in Reducing the Pain and Inflammation Associated with Exposure to Ultraviolet Light – Results of Two Clinical Studies, *Skin Pharmacology and Physiology*. **18**, 3, 144–152.

[227] Ring E. F. J. and Ammer K. (2000). The technique of infrared imaging in medicine, *Thermology international*. **10**, 1, 7–14.

[228] Weeks A. R. 1996. Fundamentals of electronic image processing. SPIE Optical Engineering Press Bellingham.

[229] Haidekker M. (2011). Fractal Approaches to Image Analysis, *,” in Advanced Biomedical Image Analysis, Hoboken, NJ: John Wiley & Sons, Inc.* 310–349.

[230] Young I. T., Gerbrands J. J., and Van Vliet L. J. 1998. Fundamentals of image processing. Delft University of Technology Delft.

[231] Snyder W. E., Qi H., Elliott R. L., Head J. F., and Wang C. X. (2000). Increasing the effective resolution of thermal infrared images, *IEEE engineering in Medicine and Biology Magazine*. **19**, 3, 63–70.

[232] Dravida S., Woods J., and Shen W. (1984). A comparison of image filtering algorithms, in *Acoustics, Speech, and Signal Processing, IEEE International Conference on ICASSP'84*. **9**, 259–262.

[233] Pisano E. D., Zong S., *et al.* (1998). Contrast limited adaptive histogram equalization image processing to improve the detection of simulated spiculations in dense mammograms, *Journal of Digital imaging*. **11**, 4, 193.

[234] Zhao Y., Georganas N. D., and Petriu E. M. (2010). Applying contrast-limited adaptive histogram equalization and integral projection for facial feature enhancement and detection, in *Instrumentation and Measurement Technology Conference (I2MTC), 2010 IEEE*. 861–866.

[235] Nur R. and Frize M. (2013). Image processing of infrared thermal images for the detection of necrotizing enterocolitis, in *Medical Imaging 2013: Image Processing*. **8669**, 86692M.

[236] Gonzalez R. C. and Richard E. (2002). Woods, digital image processing, *ed: Prentice Hall Press. ISBN 0-201-18075-8*.

[237] Otsu N. (1975). A threshold selection method from gray-level histograms, *Automatica*. **11**, 285–296, 23–27.

[238] Dougherty E. and Astola J. (1994). An Introduction to Nonlinear Image Processing. *SPIE Press, Bellingham, WA*.

[239] Serra J. (1982). Image Analysis and Mathematical Morphology. *Academic, London, UK*, **1**.

[240] Dougherty E. (1992). An Introduction to Morphological Image Processing. *SPIE Press, Bellingham, WA*.

[241] Goutsias J. and Batman S. 2000. Morphological methods for biomedical image analysis. **2**. Handbook of medical imaging.

[242] Meyer F. and Beucher S. (1990). Morphological segmentation, *Journal of Visual Communication and Image Representation*. **1**, 1, 21–46.

[243] Goos P. and Meintrup D. 2016. Statistics with JMP: Hypothesis Tests, ANOVA and Regression. John Wiley & Sons.

[244] Mould R. F. 1998. Introductory medical statistics. CRC Press.

[245] Grafarend E. W. and Awange J. L. 2012. Applications of linear and nonlinear models: fixed effects, random effects, and total least squares. Heidelberg ; New York: Springer-Verlag.

[246] Youden W. J. (1950). Index for rating diagnostic tests, *Cancer*. **3**, 1, 32–35.

[247] Pagano M. and Gauvreau K. 2018. Principles of biostatistics. Chapman and Hall/CRC.

[248] Veropoulos K. Machine learning approaches to medical decision making, PhD Thesis, University of Bristol, 2001.

[249] Caronia J., Sarzynski A., Tofighi B. *et al.* (2014). Resident performed two-point compression ultrasound is inadequate for diagnosis of deep vein thrombosis in the critically Ill, *J Thromb Thrombolysis*. **37**, 3, 298–302.

[250] Kory P. D., Pellecchia C. M., Shiloh A. L., Mayo P. H., DiBello C., and Koenig S. (2011). Accuracy of ultrasonography performed by critical care physicians for the diagnosis of dvt, *Chest*. **139**, 3, 538–542.

[251] Harding J. R. and Barnes K. M. (1997). Is DVT excluded by normal thermal imaging?-an outcome study of 700 cases, in *Engineering in Medicine and Biology Society, 1997. Proceedings of the 19th Annual International Conference of the IEEE*. **2**, 649–651.

[252] Deng F., Tang Q., Zheng Y., Zeng G., and Zhong N. (2012). Infrared thermal imaging as a novel evaluation method for deep vein thrombosis in lower limbs, *Medical physics*. **39**, 12, 7224–7231.

[253] Kalodiki E., Marston R., Volteas N., Leon M. *et al.* (1992). The combination of liquid crystal thermography and duplex scanning in the diagnosis of deep vein thrombosis, *European journal of vascular surgery*. **6**, 3, 311–316.

[254] Holmgren K., Jacobsson H., Johnsson H., and LÖFSJÖG\AARD-NILSSON E. (1990). Thermography and plethysmography, a non-invasive alternative to venography in the diagnosis of deep vein thrombosis, *Journal of internal medicine*. **228**, 1, 29–33.

[255] Deng F., Tang Q., Jiang M., Zhong N., and Liu G. (2017). Infrared thermal imaging and Doppler vessel pressurization ultrasonography to detect lower extremity deep vein thrombosis: Diagnostic accuracy study: DENG et al., *The Clinical Respiratory Journal*.

[256] Sulli A., Secchi M. E., Pizzorni C., and Cutolo M. (2008). Scoring the nailfold microvascular changes during the capillaroscopic analysis in systemic sclerosis patients, *Annals of the Rheumatic Diseases*. **67**, 6, 885–887.

[257] Cutolo M., Sulli A., and Smith V. (2010). Assessing microvascular changes in systemic sclerosis diagnosis and management, *Nature Reviews Rheumatology*. **6**, 10, 578–587.

[258] Zaproudina N., Varmavuo V., Airaksinen O., and Närhi M. (2008). Reproducibility of infrared thermography measurements in healthy individuals, *Physiological Measurement*. **29**, 4, 515–524.

[259] Normal Temperature Asymmetry of the Back and Extremities by Computer-Assisted Infrared Imaging, *ResearchGate*. [Online]. Available: https://www.researchgate.net/publication/235432966_Normal_Temperature_A symmetry_of_the_Back_and_Extremities_by_Computer-Assisted_Infrared_Imaging. [Accessed: 06-Jun-2018].

[260] Pauling J. D., Shipley J. A., Harris N. D., and McHugh N. J. (2012). Use of infrared thermography as an endpoint in therapeutic trials of Raynaud's phenomenon and systemic sclerosis, *Clinical and Experimental Rheumatology*. **30**, 2 Suppl 71, S103-115.

[261] Mariotti A., Grossi G., Amerio P., Orlando G. *et al.* (2009). Finger thermoregulatory model assessing functional impairment in Raynaud's phenomenon, *Ann Biomed Eng*. **37**, 12, 2631–2639.

[262] Shitzer A., Stroschein L. A., Sharp M. W., and Gonzalez R. R. (1997). Simultaneous measurements of finger-tip temperatures and blood per fusion rates in a lid environment, *J. therm. Biol*. **22**, 3, 159–167.

[263] Bornmyr S. and Svensson H. (1991). Thermography and laser-Doppler flowmetry for monitoring changes in finger skin blood flow upon cigarette smoking, *Clinical physiology*. **11**, 2, 135–141.

[264] Zontak A., Sideman S., Verbitsky O., and Beyar R. (1998). Dynamic thermography: analysis of hand temperature during exercise, *Annals of Biomedical Engineering*. **26**, 6, 988–993.

[265] Ducharme M. B., Brajkovic D., and Frim J. (1999). The effect of direct and indirect hand heating on finger blood flow and dexterity during cold exposure, *Journal of Thermal Biology*. **24**, 5–6, 391–396.

[266] Sakashita S. (2002). A study on the relationship between life behavior and temperature variation in human face and palm, *Master's Thesis, Department of Mechanical Engineering, The University of Tokyo, Tokyo, Japan*.

[267] Hara T. and Nagaya J. (2003). Temperature Change and Heat Transport of Heated Human Palm, in *National Heat Transfer Symposium Of Japan*. **2**, 549–550.

[268] Blank M. and Kargel C. (2006). Infrared imaging to measure temperature changes of the extremities caused by cigarette smoke and nicotine gums, in *Instrumentation and Measurement Technology Conference, 2006. IMTC 2006. Proceedings of the IEEE*. 794–799.

[269] Di Carlo A. (1995). Thermography and the possibilities for its applications in clinical and experimental dermatology, *Clinics in dermatology*. **13**, 4, 329–336.

[270] Hahn M., Hahn C., Jünger M. *et al.* (1999). Local cold exposure test with a new arterial photoplethysmographic sensor in healthy controls and patients with secondary Raynaud's phenomenon, *Microvascular research*. **57**, 2, 187–198.

[271] Herrick A. L. and Clark S. (1998). Quantifying digital vascular disease in patients with primary Raynaud's phenomenon and systemic sclerosis, *Annals of the rheumatic diseases*. **57**, 2, 70–78.

[272] Merla A., Di Donato L., Di Luzio S., Farina G. *et al.* (2002). Infrared functional imaging applied to Raynaud's phenomenon, *IEEE Engineering in Medicine and Biology Magazine*. **21**, 6, 73–79.

[273] Merla A., Romani G. L., Di Luzio S. *et al.* (2002). Raynaud's Phenomenon: infrared functional imaging applied to diagnosis and drugs effects, *International journal of immunopathology and pharmacology*. **15**, 1, 41–52.

[274] O'Reilly D., Taylor L., El-Hadidy K., and Jayson M. I. (1992). Measurement of cold challenge responses in primary Raynaud's phenomenon and Raynaud's phenomenon associated with systemic sclerosis, *Annals of the rheumatic diseases*. **51**, 11, 1193.

APPENDIX

RESULTANT IMAGES OF DEEP VEIN THROMBOSIS APPLICATION
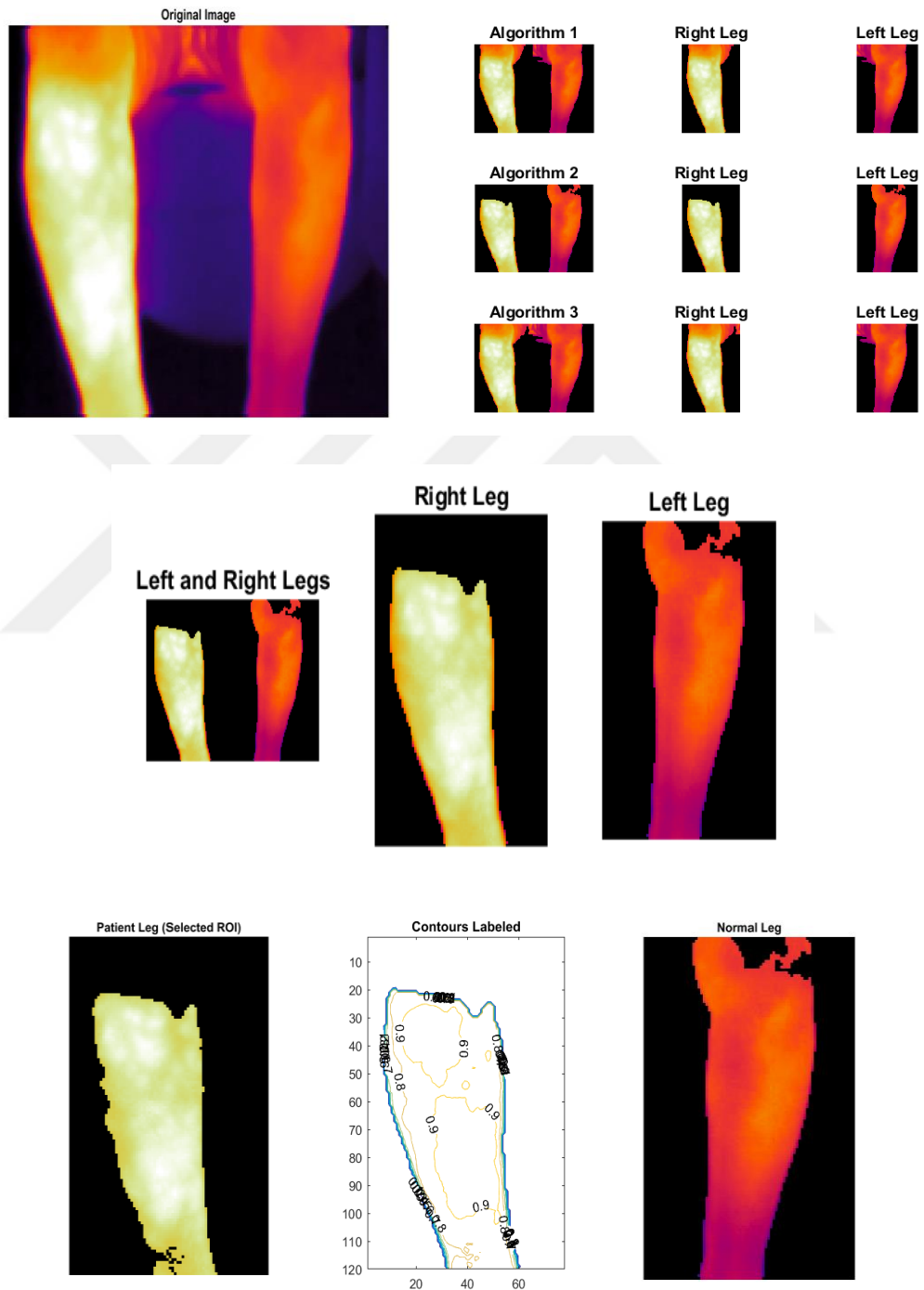
Figure A. 1 Resultant Images of the Developed Software (PATIENT)
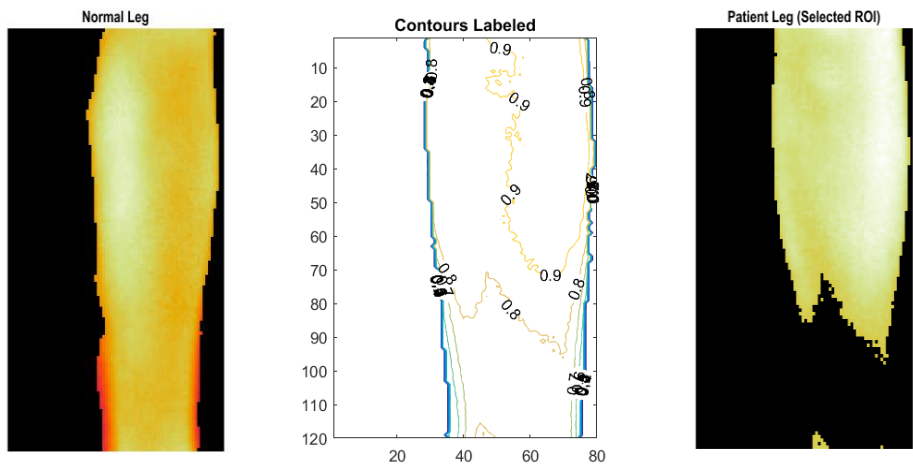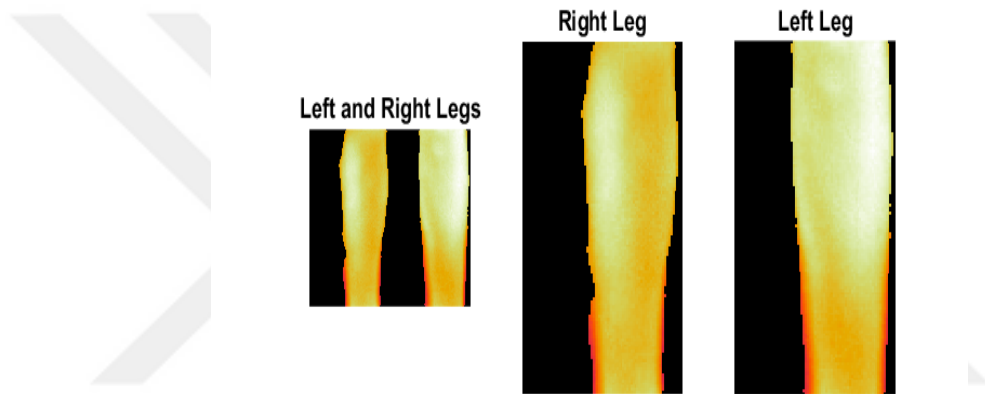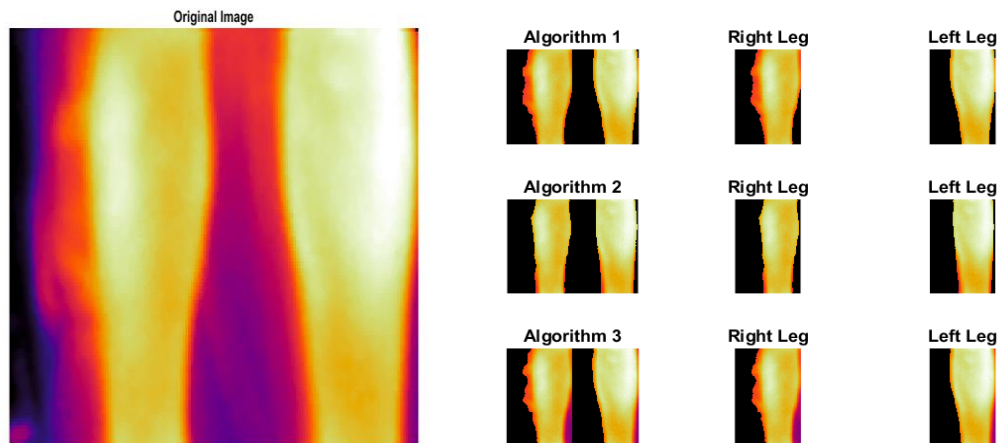
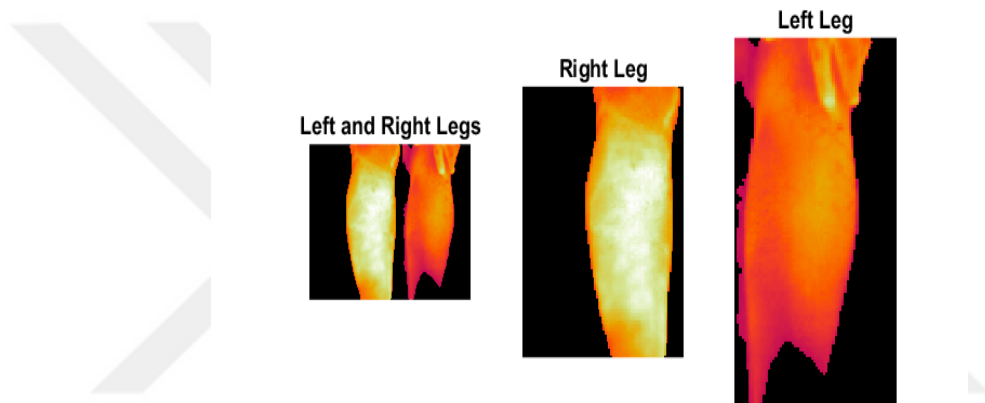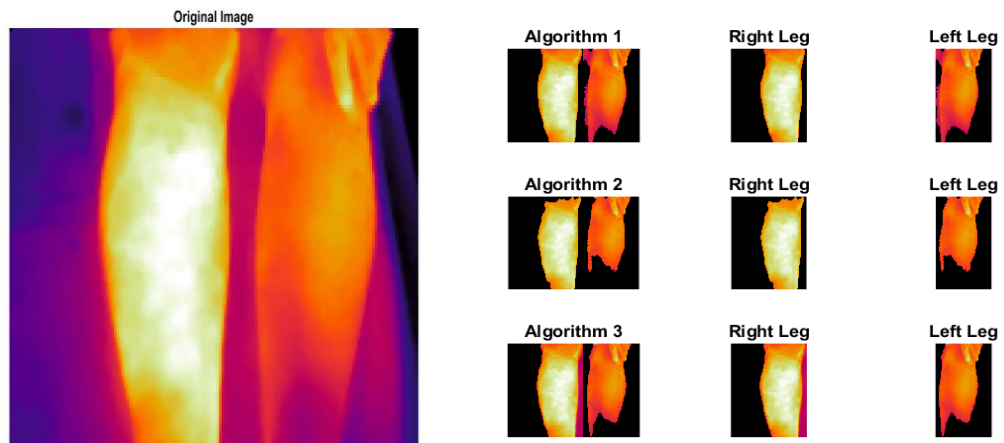**Figure A. 2** Resultant Images of the Developed Software (PATIENT)
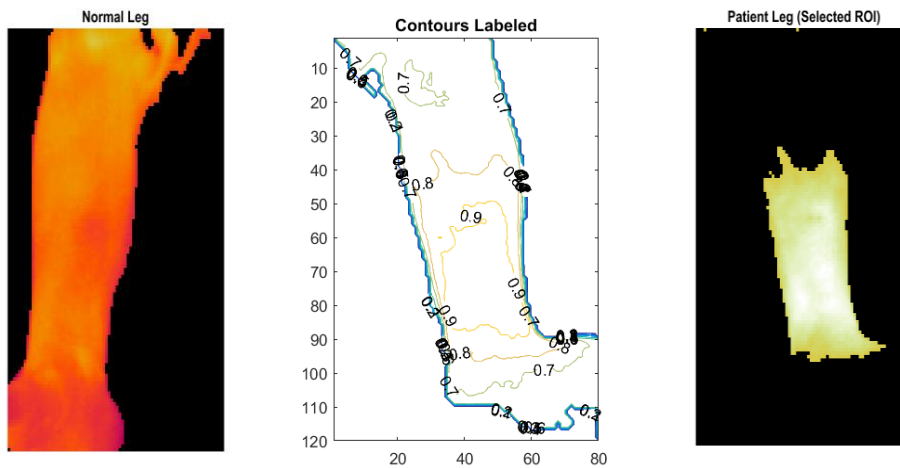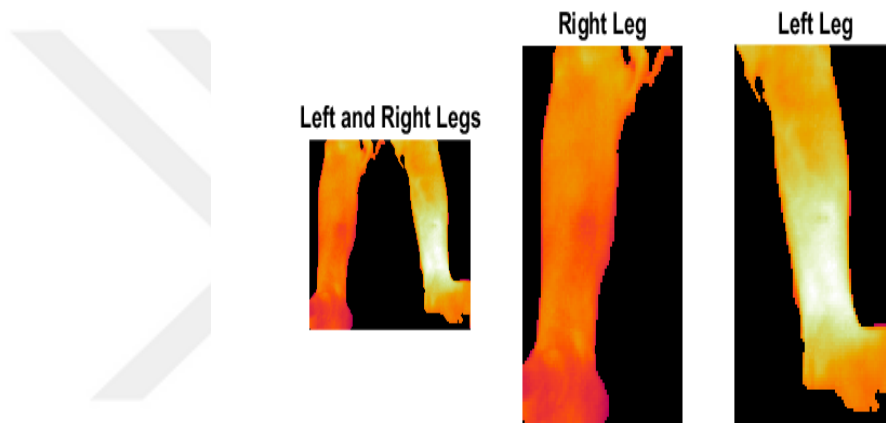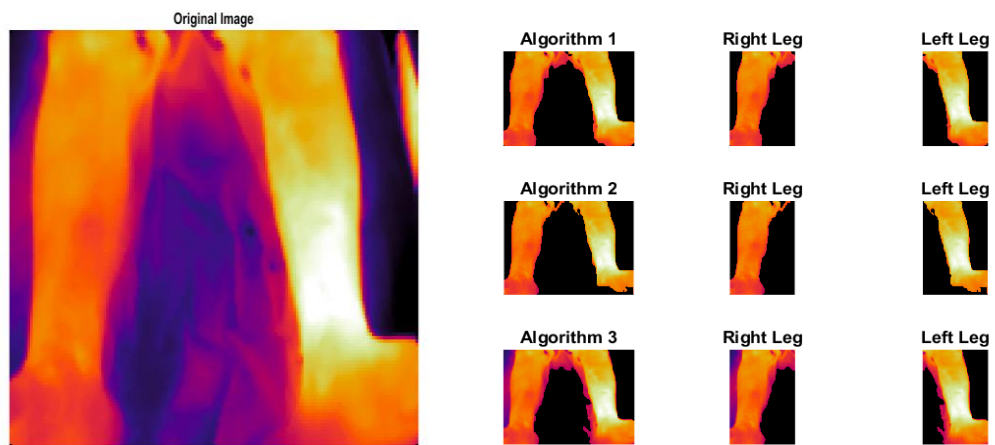
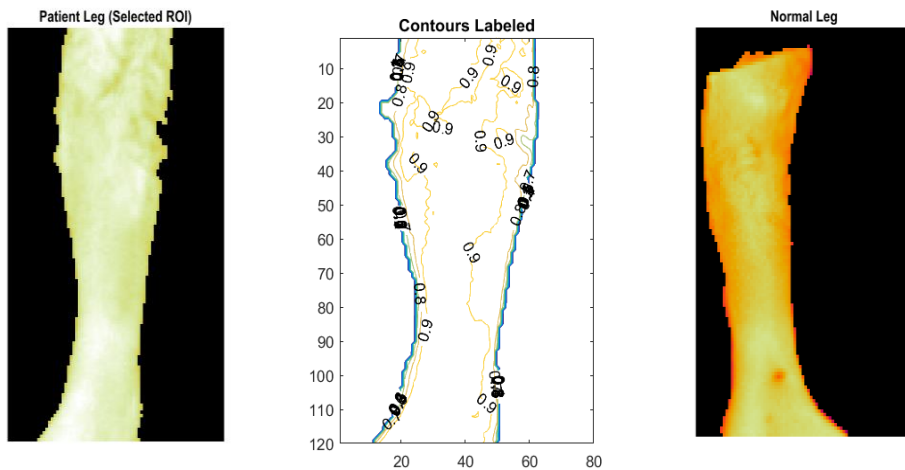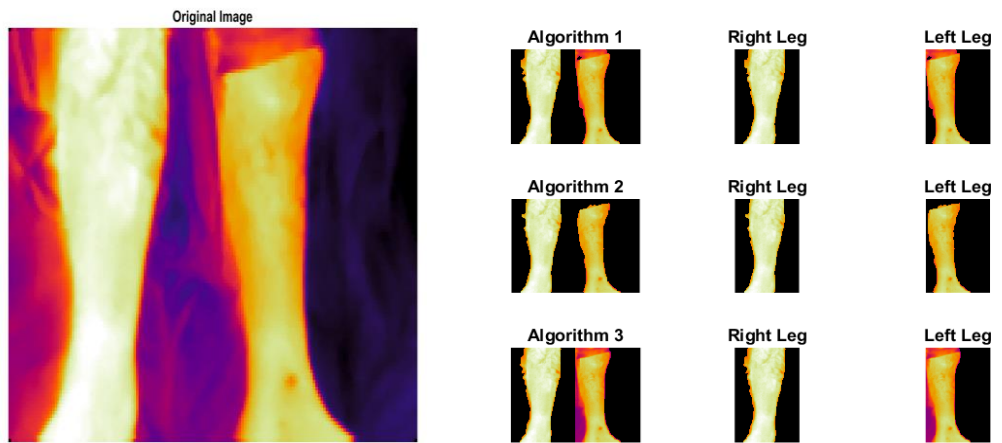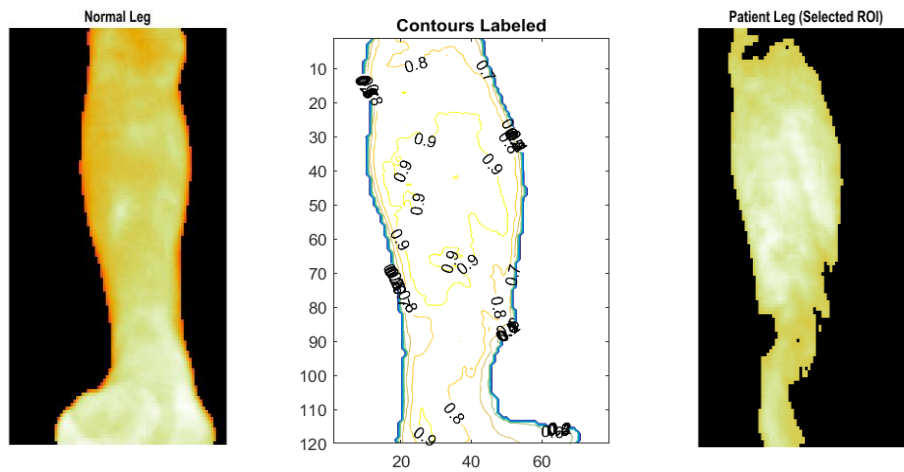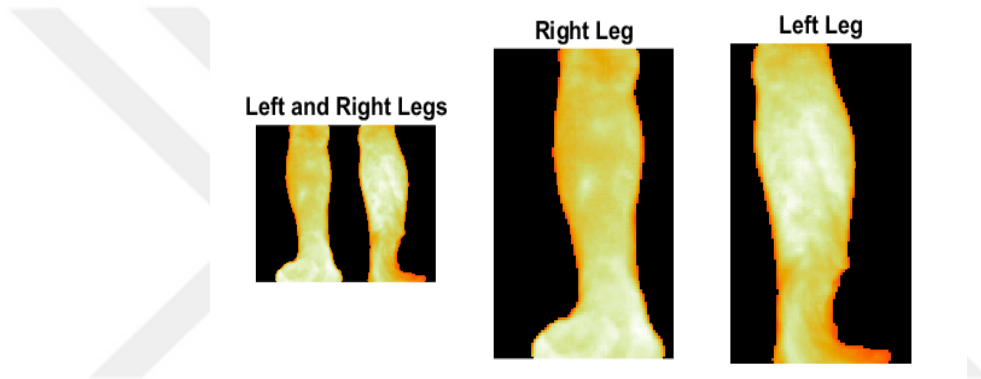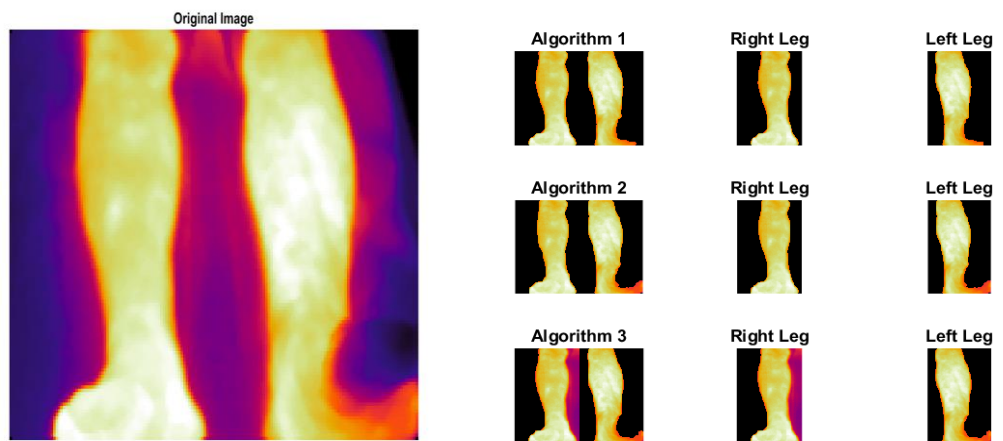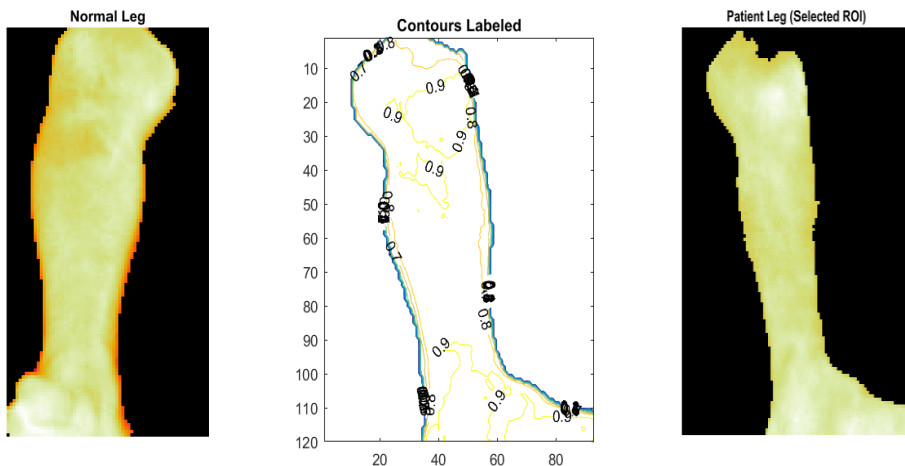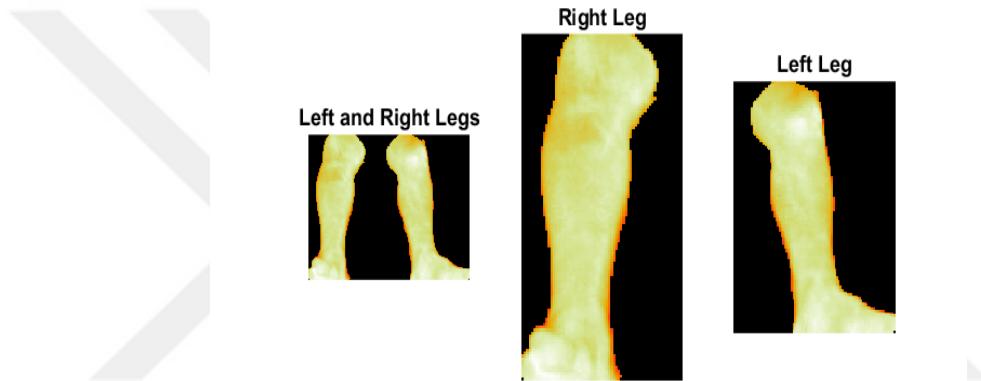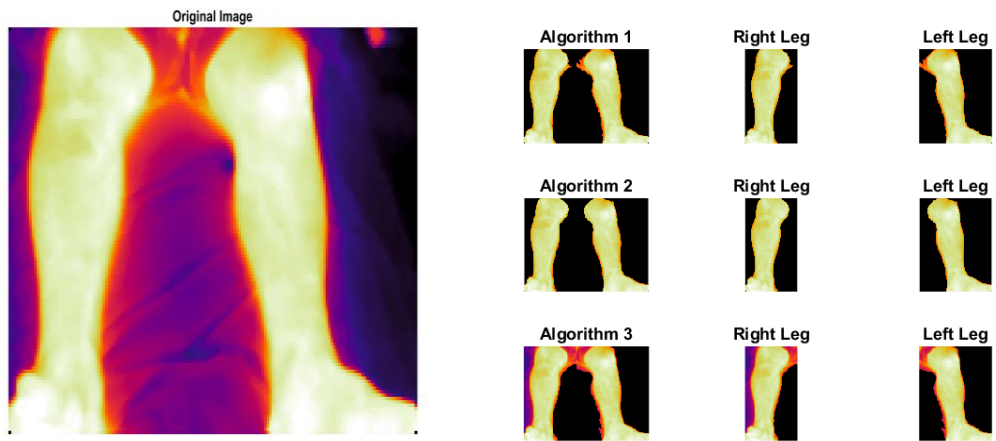**Figure A. 3** Resultant Images of the Developed Software (PATIENT)
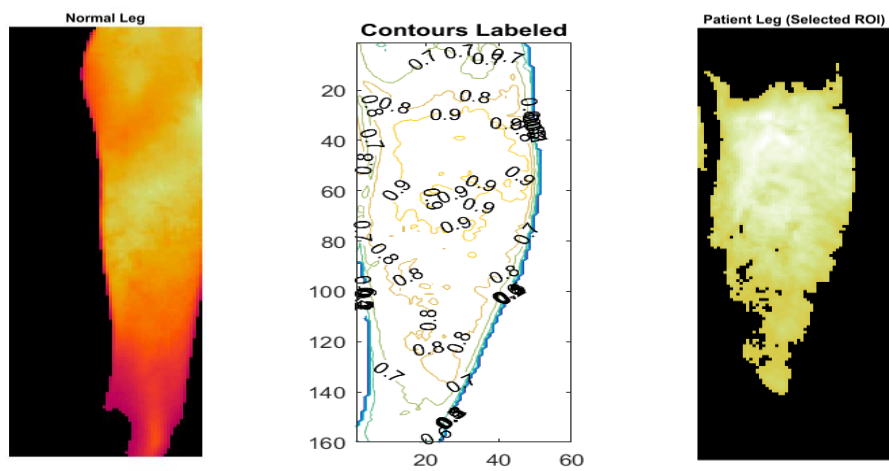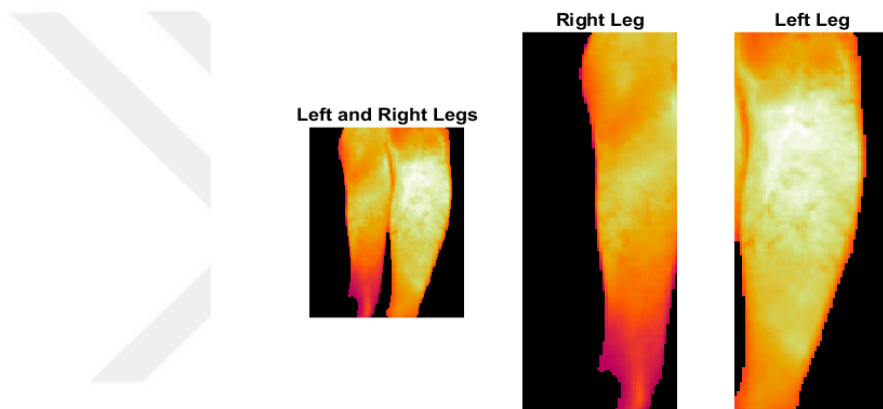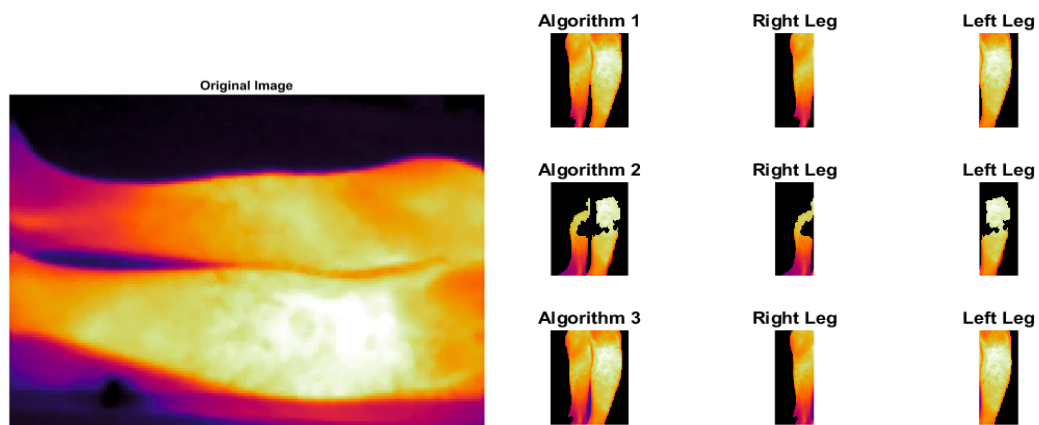
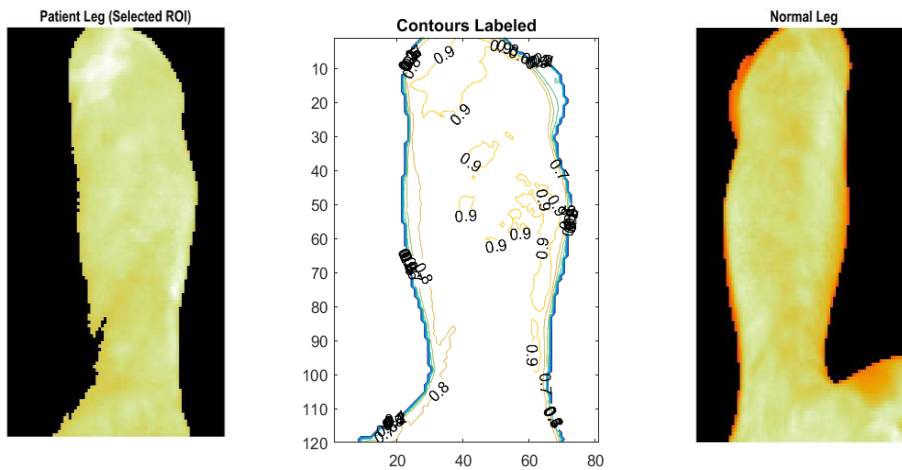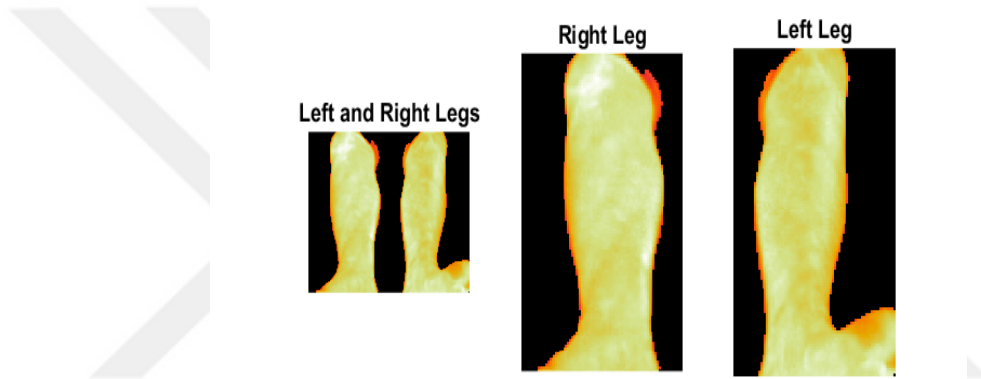**Figure A. 4** Resultant Images of the Developed Software (PATIENT)
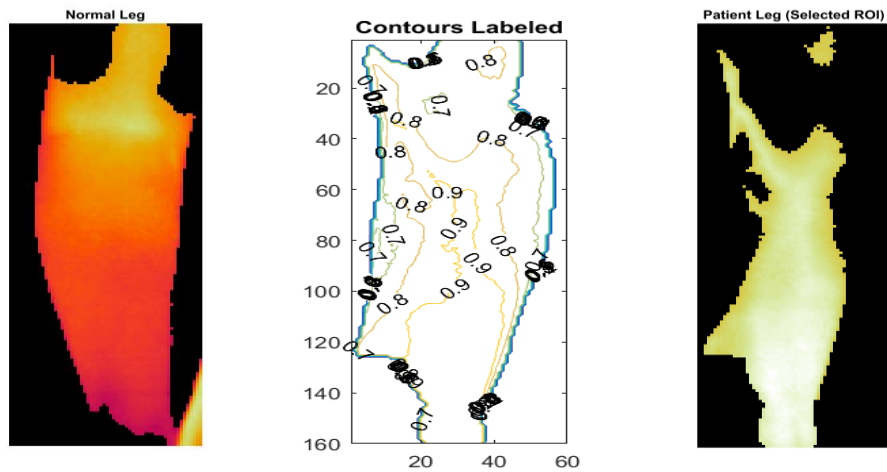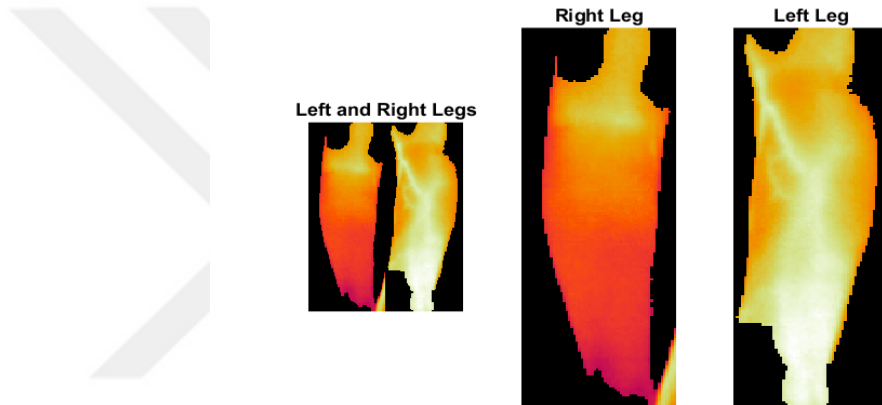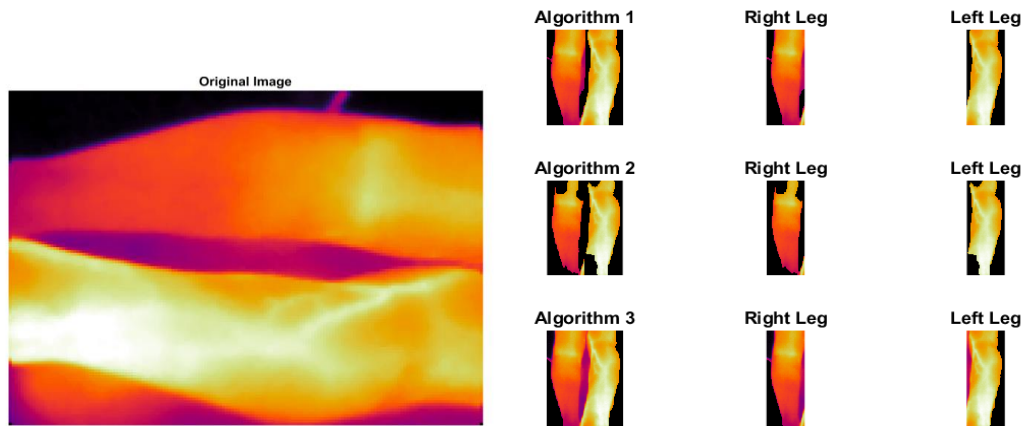
Figure A. 5 Resultant Images of the Developed Software (PATIENT)
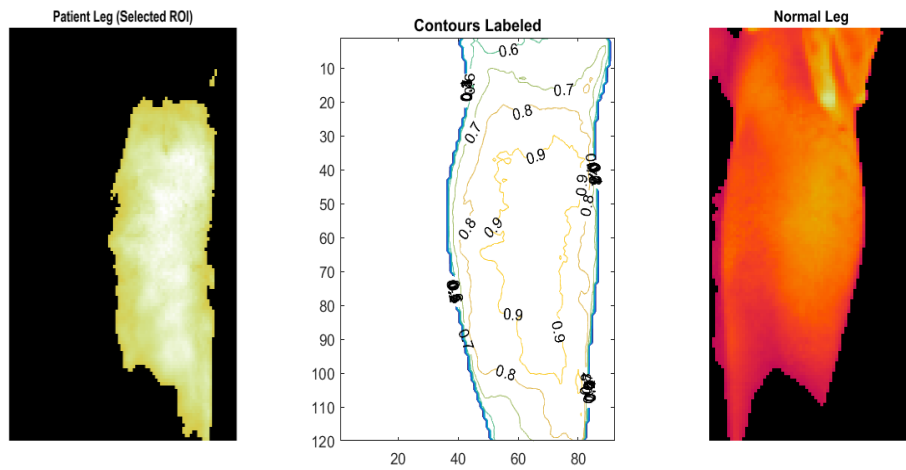
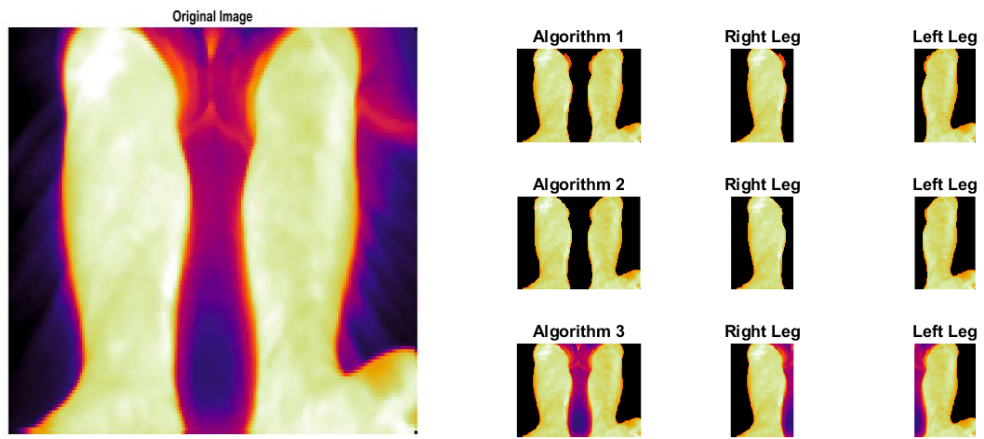**Figure A. 6** Resultant Images of the Developed Software (PATIENT)

Figure A. 7 Resultant Images of the Developed Software (PATIENT)

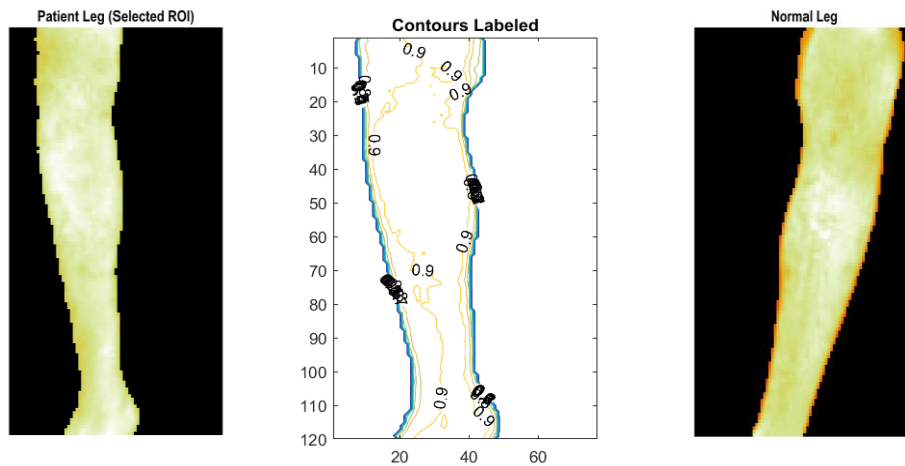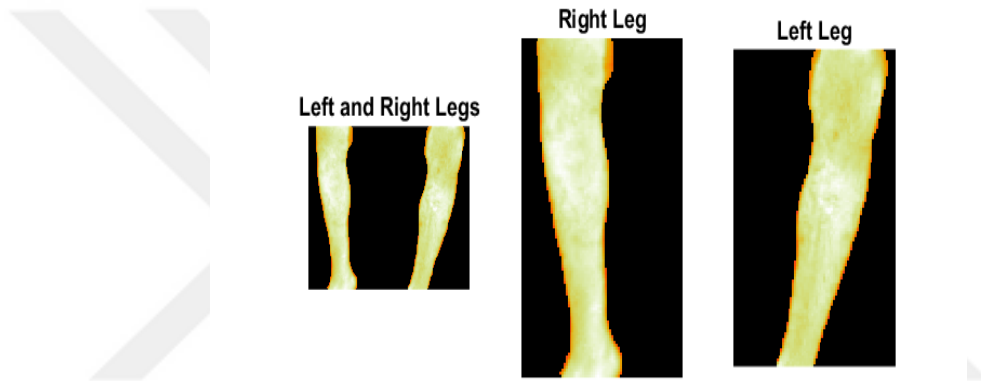**Figure A. 8** Resultant Images of the Developed Software (PATIENT)
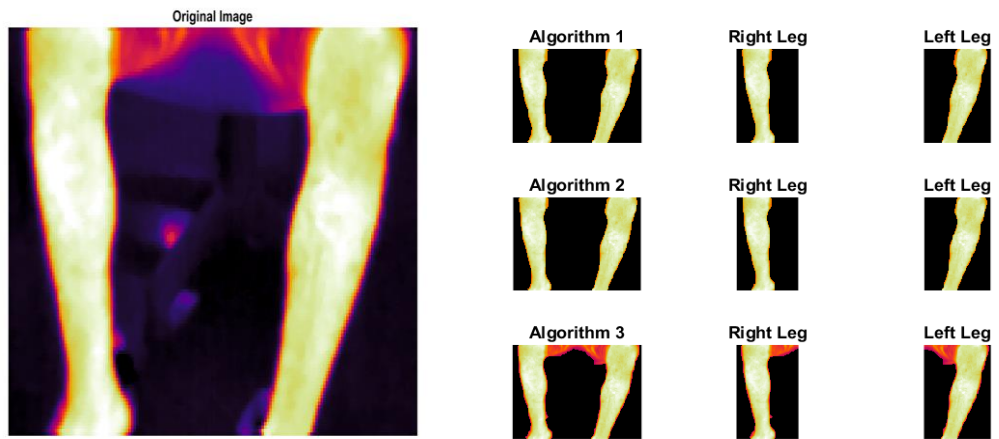
Figure A. 9 Resultant Images of the Developed Software (NORMAL)

Figure A. 10 Resultant Images of the Developed Software (NORMAL)

Figure A. 11 Resultant Images of the Developed Software (NORMAL)

CURRICULUM VITAE

1. Name Surname   **:** SEYDİ KAÇMAZ

2. Date of Birth   **:** 09/10/1986

3. Nationality   **:** Republic of Turkey

4. Education   **:**

Degree	University	Department	Year
Bachelor	Gaziantep University	Electrical-Electronics Engineering	2004-2009
Master	Gaziantep University	Electrical-Electronics Engineering / Computer Science	2009-2012
Doctorate	Gaziantep University	Electrical-Electronics Engineering / Computer Science	2012-2018

5. Academic Title: Research Assistant   (2009-2018)

Gaziantep University, Faculty of Engineering, Electrical-Electronics Department

6. Master Thesis

Adaptive fuzzy filterıng for artifact elimination in compressed images and videos

7. Publications

Kacmaz S., Ercelebi E., Zengin S., & Cindoruk S. (2017). The use of infrared thermal imaging in the diagnosis of deep vein thrombosis. *Infrared Physics & Technology*, *86*, 120-129.

Kaçmaz S., Erçelebi E., Cindoruk Ş., & Zengin S. (2016, October). Computer aided diagnosis of deep vein thrombosis using infrared thermal imaging. In *Medical Technologies National Congress (TIPTEKNO), 2016* (pp. 1-4). IEEE.

Kaçmaz S., Kayhan S. K., & Erçelebi E. (2012, April). A novel algorithm for blocking artifacts removal based on adaptive fuzzy filter in compressed images. In *Signal Processing and Communications Applications Conference (SIU), 2012 20th* (pp. 1-4). IEEE.

Cindoruk Ş., Zengin S., Eren Ş. H., Al B., Kaçmaz S., et al. Comparison of Wells score, D-dimer values, Infrared Camera Measurement, and Color Doppler Ultrasonography Performed by Emergency Physicians and Radiologists in Diagnosis of Deep Venous Thrombosis. In *XII.Ulusal Acil Tıp Kongresi, 3rd Intercontinental Emergency Medicine Congress*, 2016/5.